Seasonal and Interannual Variability of the marine carbonate system at the Ice Shelf in the Eastern Weddell Gyre and its sensitivity to future Ocean Acidification

Amy Weeber

Taught Masters

Thesis presented for the Degree of

Master of Science

Department of Oceanography

University of Cape Town

December 2012

UNIVERSITY OF CAPE TOWN
IYUNIVESITHI YASEKAPA • UNIVERSITEIT VAN KAAPSTAD

Abstract

Ocean Acidification through the uptake of anthropogenic CO_2 is resulting in a decrease in surface water carbonate ion concentration, a critical compound for marine calcifying organisms (Fabry et al., 2008; Orr et al., 2005). Natural seasonal variability is predicted to hasten the effects of Ocean Acidification in the Southern Ocean, resulting in possible surface water wintertime aragonite (the more soluble form of calcium carbonate) undersaturation ($\Omega_{arag} < 1$) south of the Antarctic Polar Front by the year 2030 (McNeil and Matear, 2008). An Ocean Acidification study was conducted to determine the seasonal and interannual variability in aragonite saturation state (Ω_{arag}) at the Antarctic ice shelf between 4°E and 14°W and in the Eastern Weddell Gyre, during the Austral summers of 2008/2009, 2009/2010, 2010/2011 and 2011/2012. This study shows that at the Antarctic ice shelf and in the Eastern Weddell Gyre (EWG), seasonal summertime phytoplankton blooms were a critical factor in the observed decrease in summer surface water CO_2 and the subsequent increase in summer surface water Ω_{arag}. The estimated Winter Water Ω_{arag} of 1.34 was increased during summer to above 1.5 in all years. Interannual variability in the timing of sea ice thaw influenced summertime primary production and thus surface water Ω_{arag}, where years with early sea ice thaw resulted in higher surface water Ω_{arag} than years with late sea ice thaw. Seasonal variability in summer surface water Total Alkalinity (TA) and Dissolved Inorganic Carbon (DIC), both of which control Ω_{arag}, was primarily influenced by variability in summer primary production and dilution from sea ice thaw. Interannual variability in Ω_{arag} was found to be higher at the ice shelf than in the EWG, highlighting the sensitivity of the ice shelf region to small seasonal variations. Aragonite-precipitating Thecosome Pteropods are prominent components of the Antarctic ecosystem, as both prey items and as predators, as well as being the major transporters of carbon from the surface into deeper waters (Comeau et al., 2010; Hunt et al., 2008). This study shows that at the ice shelf and in the EWG, surface water Ω_{arag} is currently favorable for the survival of Thecosome Pteropods, but that possibly by the middle of this century surface water Ω_{arag} will decrease below 1 during winter and early summer, resulting in the dissolution of aragonite shelled organisms. Seasonal summertime increase in Ω_{arag} may be sufficient to create favourable surface water aragonite conditions for Pteropods in current surface waters, however it is considered that this will not be the case by the end of this century.

Supervisors

Dr. Pedro M. S. Monteiro:

Coasts and Oceans, Natural Resource & the Environment,

Council for Scientific and Industrial Research (CSIR), South Africa

Dr. Howard Waldron:

Department of Oceanography,

University of Cape Town, South Africa

Acknowledgements

I am extremely grateful to have had Dr Pedro Monteiro as my supervisor. His constant support, knowledge and guidance made this thesis an enjoyable yet challenging project. I would like to thank Dr Howard Waldron for his encouragement and enthusiasm. Thanks to Dr Isabelle Ansorge for the Opportunity to Sail to Antarctica aboard the r/v SA Agulhas during which time I helped with the collection of the SANAE 51 dataset that I used in my thesis. I would also like to thank the science teams and the crew aboard the SANAE 48, 49, 50 and 51 cruises, for their continuous collection of accurate oceanographic data. Thank you to Luke Gregor for his great carbon advice, to Isabelle Giddy for draft corrections, to Dr Sandy Thomalla and Dr Sebastian Swart for cruise data and general helpfulness, and to my class mates for support and laughter.

Finally I would like to thank the Marine Research (Ma-Re) Institute, University of Cape Town and the National Research Foundation (NRF) for funding this research.

TABLE OF CONTENTS

1. Introduction

The oceans, covering approximately 70% of the earth's surface, play a large role in the regulation of our climate (Abbasi and Abbasi, 2011). They transport heat from the tropics polewards, drive the hydrological cycle and are home to thousands of species of fauna and flora. While some regions of the oceans reach depths of 6km it is only the thin surface layer that is in contact with the atmosphere. This surface ocean interacts with the atmosphere, exchanging heat, salt and gas. The flux of carbon dioxide (CO_2) gas between the atmosphere and the ocean surface is extremely important, as it balances earth's carbon cycle, creating an atmosphere that enables life, as we know it, to exist (Abbasi and Abbasi, 2011). Ice core records show that over at least the last 420 kyr atmospheric CO_2 levels have fluctuated between 280-300ppmv in accordance with the glacial cycles (Petit et al., 1999). The present-day level of atmospheric CO_2 is greater than any observed during the last 420 kyr (Petit et al., 1999) and probably in the last 2.1 million years (Hönisch et al., 2009), and is continuously increasing (IPCC, 2007). This increase in atmospheric CO_2 has been attributed to human activities such as the burning of fossil fuels, cement production and agriculture (Doney, 2006). Anthropogenic CO_2 increase is already altering the earth's climate and the oceans-processes known as global warming (Held and Soden, 2000) and ocean acidification (Doney et al., 2009).

From the time when anthropogenic CO_2 was first identified as a possible driver of climate change (Arrhenius, 1896; Callendar, 1938), the oceanic absorption of CO_2 has been seen as an increasingly important CO_2 sink. It is estimated that the oceans have taken up 50% of the anthropogenic CO_2 since the industrial revolution (Sabine et al., 2004), and that the present uptake is around 25-30% (Canadell et al., 2007; Takahashi et al., 2009). Much research has gone into understanding and quantifying this oceanic CO_2 sink in order to better calculate the rate of atmospheric CO_2 increase, and thus comprehend the magnitude of future climate change. This being the primary focus, the effect that the elevated oceanic CO_2 uptake would have on the oceans was neglected until fairly recently, when scientists began to recognise that the increase in surface ocean CO_2 could affect the ocean pH as well as the ocean carbonate ion concentration (Feely et al., 2004; Zeebe et al., 2008; Zeebe, 2012). Decreasing ocean pH and shifts in marine carbonate speciation as a result of increased CO_2 in sea water is known as "Ocean Acidification" (Caldiera and Wickett, 2003). As oceans absorb CO_2, the pH as

well as the concentration of carbonate ions [CO_3^{2-}] decrease due to the reaction of CO_2 with water. Since the industrial revolution, the pH of the ocean surface waters has decreased by approximately 0.1 (Caldeira and Wicket, 2003; Orr et al., 2005) and the carbonate saturation depth has shoaled by up to 200m in some areas of the Atlantic, Pacific and Indian oceans (Feely et al., 2004).

Today's surface oceans are saturated with calcium carbonate, but increasing anthropogenic CO_2 is likely to change this by the year 2050 (Orr et al., 2005) or sooner (McNeil and Matear, 2008). If the carbonate saturation depth reaches the surface, the surface waters will become undersaturated with respect to calcium carbonate , resulting in dissolution of the shells and skeletons of calcifying organisms such as corals coccolithophorids, formanifera and pteropods (Doney et al., 2009; Fabry et al., 2008). Coral reefs are important ecosystems in tropical regions, while coccolithophorids, formanifera and pteropods provide key links in the food chain between smaller organisms and larger plankton and transport carbon from the surface into the deep oceans through the carbonate pump (Fabry et al., 2008; Hunt et al., 2008; Rost and Riebesell, 2004).

The scale, timing and consequences of Ocean Acidification vary greatly between oceanic regions and hence it is important to study Ocean Acidification at a regional scale (Orr et al., 2005). High latitude regions are predicted to be the first to be affected by Ocean Acidification. This is because gas and calcium carbonate ($CaCO_3$) salts are more soluble in cold water and due to the fact that high latitude regions have higher Revelle factors, making them more sensitive to small changes in surface water CO_2 (Egleston et al., 2010; Sabine et al., 2004). Orr et al (2005) show that the surface waters in some regions of the Southern Ocean will likely become undersaturated with aragonite (the more soluble form of calcium carbonate) when the atmospheric CO_2 reaches 550ppmv (Intergovernmental Panel on Climate Change (IPCC) predictions mark this as occurring in the year 2050). McNeil and Matear (2008) demonstrate that when taking natural seasonality into account, Southern Ocean surface waters could experience wintertime aragonite undersaturation as early as 2030, under the IPCC IS92a atmospheric CO_2 increase scenario. Aragonite–precipitating Thecosome Pteropods are a vital part of the marine ecosystems of the Southern Ocean, the Arctic Ocean and the North Pacific Ocean (Armstrong et al., 2005; Hunt et al., 2008; Kobayashi., 1974). These molluscs produce aragonite shells, the sinking of which is important in the export of carbon from the surface waters due to the ballasting properties of $CaCO_3$ (Ziveri et al., 2007).

Pteropods will still be able to form aragonite shells as carbonate ions decrease due to calcifying organisms relying primarily on HCO_3^- or metabolically-produced CO_2 for calcification (Roleda et al., 2012), but they will likely experience dissolution of their aragonite shells as surface water aragonite becomes undersaturated (Fabry et al., 2008). The physiological effects of Ocean Acidification are predicted to affect ecosystems before carbonate concentrations become undersaturated (Fabry et al., 2008; Royal-Society, 2005). This is caused by calcifying organisms using a greater proportion of their energy for the process of calcification as carbonate concentration decreases, and thus neglecting growth and reproduction (Fabry et al., 2008). Ocean Acidification could lead to the northward migration or the decline of Southern Ocean pteropods in the next few decades as surface waters become undersaturated with aragonite, resulting in unknown implications for the Southern Ocean ecosystem (Fabry et al., 2008; McNeil and Matear, 2008). A better understanding of how the seasonal cycle in the Southern Ocean affects regional scale Ocean Acidification processes is vital as detrimental wintertime surface water carbon conditions may occur within the next few decades (McNeil and Matear, 2008).

With this in mind, the importance of understanding the processes that control ocean carbonate chemistry become increasingly important, especially in vulnerable regions such as the Southern Ocean (McNeil and Matear, 2008; Orr et al., 2005; Sabine et al., 2004; Thomalla et al., 2011). This study will aim to analyse the seasonal and interannual variability of summertime surface water Ocean Acidification at the Antarctic ice shelf and in the Eastern Weddell Gyre. Continuously recorded underway fugacity of carbon dioxide (fCO_2) data together with empirically calculated Total Alkalinity will be used to look at the present and future surface water [CO_3^{2-}], Ω_{arag} and pH of this region during the Austral summers of the years 2008/2009, 2009/2010, 2010/2011, 2011/2012. We will try to develop a more thorough understanding of how seasonality in primary production and surface water dilution through summer sea ice thaw affects surface water biogeochemistry and thus the Thecosome Pteropods and the ecosystem.

2. Literature Review

2.1 Carbon Dioxide

Carbon dioxide (CO_2) is possibly the most important substance in the biosphere, as it has facilitated the development of life on earth by serving as the source of carbon, the primary element of which all living beings are made (Revelle, 1985). Carbon dioxide is also essential in regulating earth's temperature, as together with water vapour, CO_2 absorbs and backscatters the suns radiation, which heats the earth to temperatures that allow for the existence of liquid water and of life. The pre-industrial carbon cycle was roughly in a steady state with the fluxes of carbon into and out of the atmosphere, oceans and terrestrial biosphere approximately in equilibrium (Siegenthaler and Sarmiento, 1993). The anthropogenic addition of CO_2 gas into the earth's atmosphere is believed to have begun around the year 1751 at the start of the fossil fuel era (Andres et al., 1999). This addition of CO_2, primarily through the burning of fossil fuels, disrupted the carbon balance resulting in an accumulation of CO_2 in the atmosphere. Since the industrial revolution there is no doubt that atmospheric CO_2 levels have increased (Held and Soden, 2000; Keeling et al., 1995), from a pre-industrial (pre-1800) level of around 280ppmv (Friedli et al., 1986) to a present-day CO_2 level of 392ppmv (Tans and Keeling, 2011).

Joseph Fourier (1768-1830) is believed to have been the first to discover that the earth's atmosphere acts like the gases in a "hothouse", trapping the thermal radiation while being transparent to solar radiation, and thus raising the earth's temperature (Revelle, 1985). Tyndall (1861) a few decades later, discovered that it was in fact trace gases such as water vapour and CO_2 that were responsible for the trapping of this infrared radiation and hence the heating of our planet. The possibility that human activities were increasing atmospheric CO_2 and that someday this CO_2 increase could cause warming of the earth, was proposed at the turn of the 19th century by Arrhenius (1896) and Callendar (1938).

"Few of those familiar with the natural heat exchanges of the atmosphere, which go into the making of our climates and weather, would be prepared to admit that the activities of man could have any influence upon phenomena of so vast a scale. In the following paper I hope to show that such influence is not only possible, but is actually occurring at the present time" Callendar (1938).

Increasing CO_2 levels and the future subsequent warming of the earth was initially viewed as being beneficial to mankind, as it would possibly increase the temperature in the northern regions of civilization enhancing the growth of favourable plants (Callendar, 1938). With progressively more studies on increasing anthropogenic CO_2, the resulting human induced heating of the earth became known as "Global Warming" (Held and Soden, 2000). Today, the consequences of global warming, are a great concern for our planet as well as for the survival of those who inhabit it. With the predicted CO_2 increase over the following century, model trajectories show that the pH as well as the concentration of carbonate ions [CO_3^{2-}] of the surface oceans are predicted to decrease (Orr et al., 2005). Global temperatures are likely to rise by up to 4°C by the year 2100 under an IPCC business-as-usual CO_2 emission scenario (Betts et al., 2011) resulting in a possible 0.5-2m rise in sea level (Nicholls et al., 2011) and in the warming of the oceans which has previously been observed to possibly have been the cause of a global decrease in phytoplankton biomass, as increased upper ocean stratification limits the upwelling of nutrients (Behrenfeld et al., 2006).

Not all of the anthropogenic CO_2 remains in the atmosphere, in fact more than half of it is absorbed by CO_2 sinks (Le Quéré et al., 2009). Both the oceans and the terrestrial biosphere are responsible for regulating the atmospheric CO_2 concentration, primarily through photosynthesis. Between 1958 and 2008 oceanic and terrestrial carbon sinks absorbed approximately 57% of the anthropogenic CO_2 emissions, with the remainder accumulating in the atmosphere (Le Quéré et al., 2009). Model studies by Canadell et al (2007) calculated the 2000-2006 oceanic and land CO_2 sink to account for 0.24 and 0.3 of the total anthropogenic emissions respectively. Over the past 50 years these important carbon sinks appear to have decreased by around 5% (Le Quéré et al., 2009) which could be due to a number of factors:

atmospheric CO_2 increase is faster than the rate at which the oceans and terrestrial biosphere are able to regulate it, the ocean and land CO_2 sinks are decreasing in efficiency in high CO_2 concentrations because of the decrease in carbonate ions in the oceans which buffer the oceanic pCO_2 and because CO_2 fertilization on land is limited, because the oceans and/or the land are changing due to climate variability, or lastly because atmospheric models have not considered all the possible CO_2 sinks (Le Quéré et al., 2009).

The importance of the oceans in the uptake and storage of anthropogenic CO_2 is unquestionable (Gloor et al., 2003; Sabine et al., 2004; Siegenthaler and Sarmiento, 1993). It is estimated that the present net global ocean CO_2 uptake is 1.5 to 2.2 Pg C yr^{-1} (Takahashi et al., 2009; Watson and Orr., 2003). This accounts for 20-30% of the annual CO_2 (8 Pg C yr^{-1}) that enters the atmosphere (Canadell et al., 2007; Sabine et al., 2004; Takahashi et al., 2009). Sabine et al (2004) show that without the oceans, atmospheric CO_2 concentrations would be 55ppm higher than they are today. Although there seems to be an agreement of a net oceanic uptake of 2 Pg C yr^{-1}, there is still much discrepancy about the mechanisms of CO_2 uptake, in which regions of the oceans the major oceanic CO_2 sinks exist (Takahashi et al., 2009), and how they may change in an unstable climate (Le Quéré et al., 2009).

To understand the factors influencing the oceanic CO_2 sink it is important to look at regional scale processes. The Southern Ocean (south of 30° S) CO_2 sink, accounted for 20%+ of the global oceanic CO_2 uptake flux in the year 1995 (Takahashi et al., 2002) and has been shown to be significant in the global oceanic CO_2 uptake (McNeil et al., 2007; Sabine et al., 2004; Schlitzer, 2002). Although recent studies indicate that the Southern Ocean is sensitive to climate change (Hoppema, 2004; Le Quéré et al., 2007; Lovenduski et al., 2007; McNeil and Matear, 2008; Orr et al., 2005), it is still a region around which there is much uncertainty and very little *in situ* data (Takahashi et al., 2009). Recent studies suggest that the Southern Ocean CO_2 sink may have weakened, possibly due to an increase in Southern Ocean winds as a result of climate change (Canadell et al., 2007; Le Quéré et al., 2007). Contradicting these studies, Hauck et al (2010) suggest a strengthening of the oceanic anthropogenic CO_2 sink in the Weddell Gyre of the Southern Ocean between 1992 and 2008, emphasising that within the Southern Ocean regionality is high. If the Southern Ocean CO_2 sink decreases and atmospheric CO_2 emissions continue to increase, the Southern Ocean may soon become a source rather than a sink of CO_2 to the atmosphere, causing atmospheric CO_2 levels to rise faster than climate models predict.

2.2 Carbon and the ocean

Now that it has been shown how the oceanic carbon concentration plays a vital role in the regulation of atmospheric CO_2, it is important to understand what controls the oceanic CO_2. The surface oceans are in direct contact with the atmosphere and are thus the connection between the deeper water carbon and atmospheric carbon (Sarmiento and Gruber, 2006). Together, the oceans and the organisms that inhabit them are a substantial carbon reservoir as they contain about 38000 Gt C (gigatonnes of carbon; 1 Gt C = 1015 grams), accounting for around 95% of all the carbon in the oceans, atmosphere and terrestrial biosphere (Royal-Society, 2005). Sigman and Boyle (2000) show that the deep ocean carbon reservoir is more than 25 times larger than that of the surface ocean and the atmosphere combined (Figure 1). The majority of this carbon is stored in the deep oceans as Dissolved Inorganic Carbon (DIC). The biological and physical carbon pumps are the mechanisms by which the carbon in the surface waters is transported, against its concentration gradient, down into the deeper ocean, where it can be stored for thousands of years.

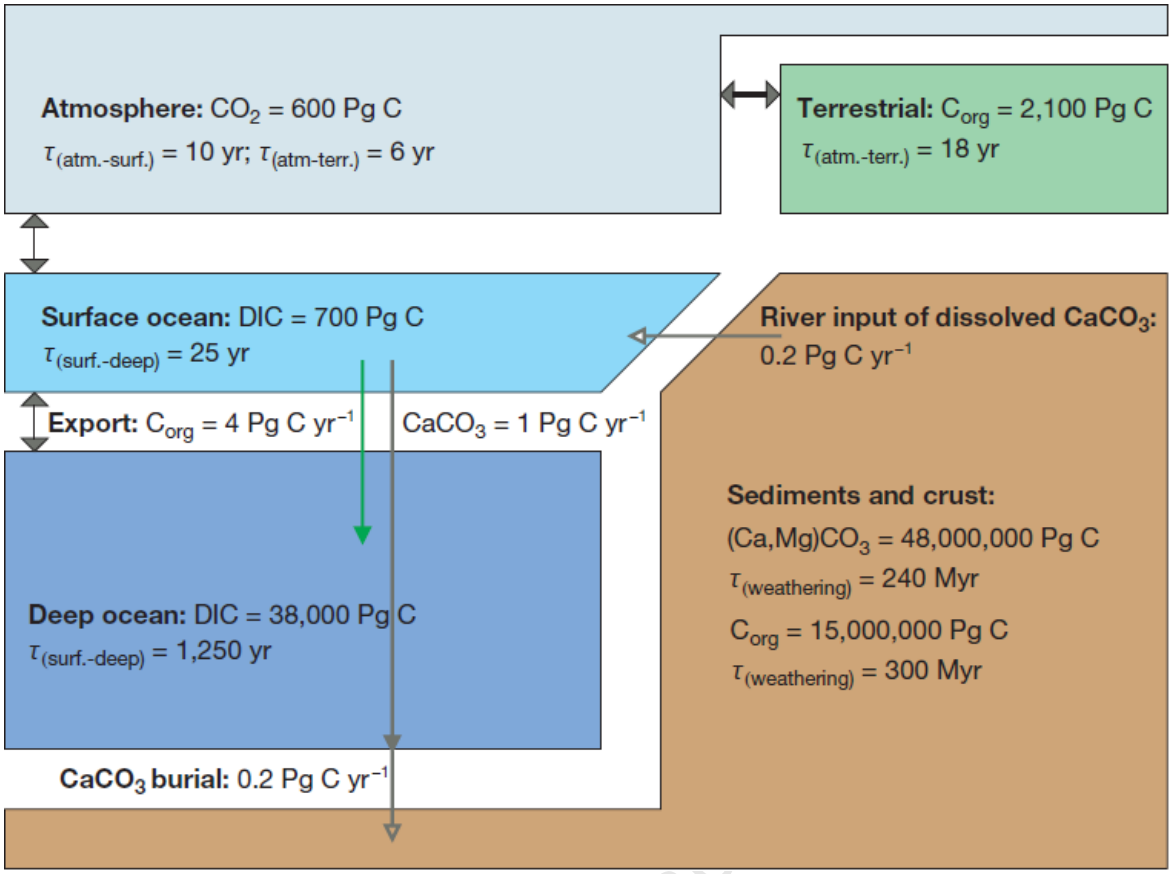

Figure 1. A simplifed view of the Holocene (pre-industrial) carbon cycle, taken from Sigman and Boyle (2000). Carbon that enters the oceans from exchange with the atmosphere on glacial/interglacial timescales is stored in a number of reservoirs (given in units of Pg C, or 1015 g C), as dissolved inorganic carbon (DIC), and organic carbon (C_{org}) and calcium carbonate ($CaCO_3$). A residence time (t, reservoir size divided by input or output) is given for each of the carbon reservoirs, which relates to the important exchange terms between reservoirs, indicated by double arrows. Relevant fluxes of C_{org} and $CaCO_3$ are shown by single arrows (Sigman and Boyle, 2000).

Once the CO_2 gas enters the ocean it dissolves in sea water, forming the more reactive aqueous CO_2. Unlike other gases that just dissolve in water, CO_2 reacts with water molecules to form carbonic acid (H_2CO_3) (Zeebe and Wolf-Gladrow, 2001). This acid then dissociates to form hydrogen ions (H^+) and bicarbonate ions (HCO^{3-}), which dissociate further to form carbonate ions (CO_3^{2-}). The following equations describe these chemical reactions:

$$CO_{2(aq)} + H_2O \overset{K_0}{\longleftrightarrow} H_2CO_3^* \qquad (eq.\,2.2.1)$$

$$H_2CO_3^* \overset{K_1}{\longleftrightarrow} H^+ + HCO_3^- \qquad (eq.\,2.2.2)$$

$$HCO_3^- \overset{K_2}{\longleftrightarrow} H^+ + CO_3^{2-} \qquad (eq.\ 2.2.3)$$

Where K_0, K_1 and K_2 are the equilibrium relationships between the different reactions and are dependent on the sea water temperature and salinity. Although it seems from these equations that the concentration of CO_3^{2-} ions increases as CO_2 is added, CO_3^{2-} is less stable than HCO_3^- and thus the reverse reaction is favoured for eq. 2.2.3. The increase in H^+ ions means that available CO_3^{2-} ions will be used up to create more HCO_3^-, resulting in an increase in HCO_3^- ions and a decrease in the available CO_3^{2-} ions. To describe the carbonate system, these equilibrium constants can be related to the concentrations of the carbonate and hydrogen ions present in the sea water by the following relationships:

$$K_0 = \frac{[H_2CO_3^*]}{pCO_2} \qquad (eq.\ 2.2.4)$$

$$K_1 = \frac{[H^+][HCO_3^-]}{[H_2CO_3^*]} \qquad (eq.\ 2.2.5)$$

$$K_2 = \frac{[H^+][CO_3^{2-}]}{[HCO_3^-]} \qquad (eq.\ 2.2.6)$$

The first equilibrium constant (K_0) is also known as the solubility coefficient of CO_2 in sea water and can be calculated by:

$$lnK_0 = A_1 + A_2\left(\frac{100}{T}\right) + A_3 \ln\left(\frac{T}{100}\right) + S\left[B_1 + B_2\left(\frac{T}{100}\right) + B_3\left(\frac{T}{100}\right)^2\right] \qquad (eq.\ 2.2.7)$$

Where A1, A2, A3, B1, B2 and B3 are constants with the units $mol.l^{-1}$ atm^{-1} (Weiss, 1974). The apparent dissociation constants (K_1 and K_2) can be calculated as in Mehrbach et al (1973).

Together, the dissolved carbon species in sea water are known as the Dissolved Inorganic Carbon (DIC). The relative proportions of each of these carbonate species (CO_2, H_2CO_3, HCO_3^- and CO_3^{2-}) control the pH of the sea water (Figure 2). The term pH describes the quantity of acid within a liquid and is defined by the following equation:

$$pH = -log_{10}[H^+] \qquad (eq.\,2.2.8)$$

The pH is the negative logarithm of the concentration of the hydrogen ions, which means that a 10-fold increase in hydrogen ion concentration will result in a pH decrease by one pH unit (Royal-Society, 2005). In water (H_2O) only a small amount of the H_2O molecules split up into H^+ and OH^- ions. The concentrations of these two ions in pure water are both 10^{-7} mol l^{-1} and hence pure water has a neutral pH of 7. Due to the presence of other ions in sea water, it has a slightly higher pH of around 8.2. The average surface sea water pH has decreased since preindustrial times by approximately 0.1 units, from about 8.21 to 8.10 (Royal-Society, 2005). With the predicted atmospheric increase in CO_2, the ocean pH is expected to fall by a further 0.3 to 0.4 pH units by the end of the century (Orr et al., 2005; McNeil and Matear, 2008). Looking at figure 2, this predicted decrease in pH would lead to an increase in the concentration of aqueous CO_2 and HCO_3^- ions and in a decrease in the concentration of CO_3^{2-} ions.

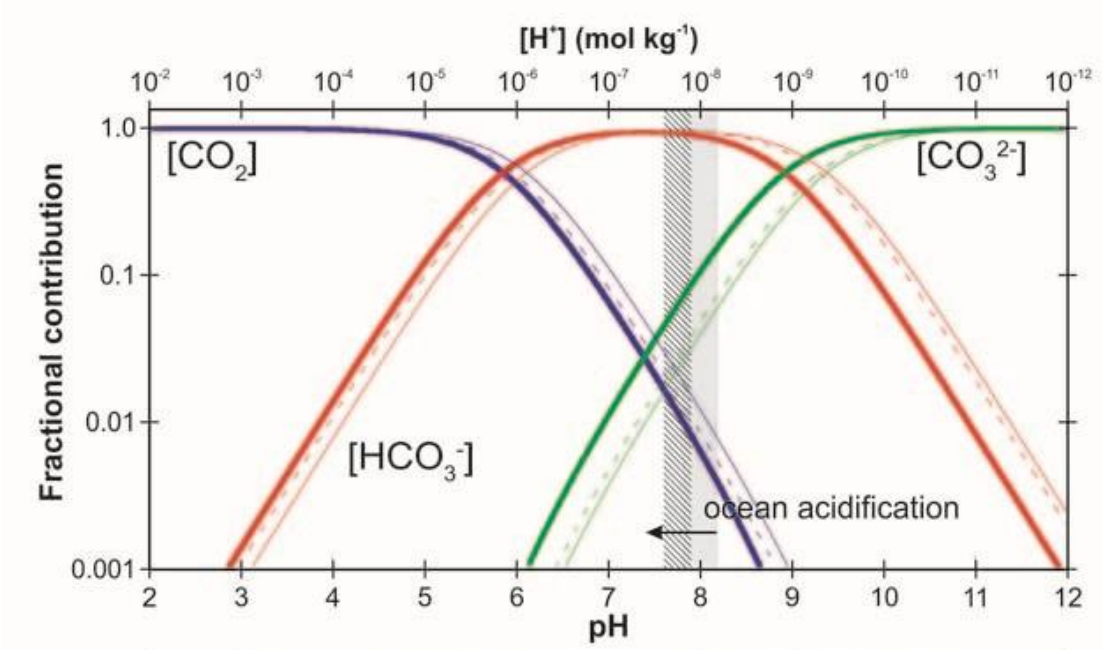

Figure 2: Bjerrum plot showing the relative proportions of $[HCO_3^-]$, $[CO_3^{2-}]$ and $[CO_2]$ to DIC in seawater under different temperature, salinity and pressure conditions (heavy curves are for S=35‰, T=25ºC, P=0bar, narrow curves are S=35, T=0ºC, P=0bar, dashed curves are S=35, T=0ºC, P=300bar), taken from and Ridgwell (2012). The shaded region reflecting the range of current day (annual average) ocean surface, and hashed lines reflect the corresponding projected year 2010 range (Barker and Ridgwell, 2012).

The net effect of increasing the concentration of CO_2 in sea water is an increase in the concentrations of H^+, H_2CO_3, HCO_3^- ions and a decrease in the concentration of CO_3^{2-} ions and in the pH. This occurs through the combining of the available CO_3^{2-} ions with increasing H^+ to further increase the HCO_3^- and thus decreasing the available CO_3^{2-} ions It is this decrease in carbonate ion concentration [CO_3^{2-}] that is of major concern for marine calcifying organisms that use carbonate ions in the formation of their skeletons and shells (Fabry et al., 2008). The formation and dissolution of one unit of calcium carbonate can be represented as:

$$\begin{array}{c} \text{Formation} \longrightarrow \\ [Ca^{2+}] + [CO_3^{2-}] \leftrightarrow CaCO_3 \\ \longleftarrow \text{Dissolution} \end{array} \qquad (eq.\,2.2.9)$$

As increasing amounts of CO_2 dissolve in the ocean and decrease the available [CO_3^{2-}] as explained above, this equation will move to the left, promoting the dissolution of carbonate minerals (Royal-Society, 2005). The dissolution of carbonate minerals increases the carbonate ions which combine with available H^+ ions to form bicarbonate and thus decrease [H^+], increasing the ocean pH (Royal-Society, 2005). This process plays an important role in slowing down the decrease in ocean pH as CO_2 levels rise, but is likely to decrease as the [CO_3^{2-}] decreases with increasing CO_2.

We now know that the oceans are alkaline and contain large amounts of dissolved carbon. The marine carbon species have thus far been described by five variables: pCO_2, H_2CO_3* (which includes both CO_2 and H_2CO_3 as they are often indistinguishable), HCO_3^- , CO_3^{2-} and H^+. Both the concentration of CO_2 and the pH of the ocean are commonly measured but are non conservative properties, changing with temperature, salinity and pressure (Sarmiento and Gruber, 2006). For this reason, two parameters have been defined that are conservative with respect to changes in state and can thus be used in ocean carbon models. These are DIC and Total Alkalinity (TA) and are defined by the following equations:

$$DIC = [H_2CO_3^*] + [HCO_3^-] + [CO_3^{2-}] \qquad (eq.\,2.2.10)$$

0.5% 88% 11%

$$TA = [HCO_3^-] + 2[CO_3^{2-}] + [B(OH)_4^-] + [OH^-] + [HPO_4^{2-}] + 2[PO_4^{3-}] + [H_3SiO_4^-] + [NH_3] + [HS^-] + \ldots - [H^+] - [HSO_4^-] - [HF] - [H_3PO_4] - [HNO_2] + \ldots \quad (eq.\ 2.2.11)$$

The three main forms of dissolved carbon present in sea water are: H_2CO_3*, HCO_3^- and CO_3^{2-} Together these carbon forms are known as DIC with bicarbonate being the most abundant form under current oceanic conditions (Fabry et al., 2008) (Figure 2).

DIC is a conservative property as during mixing and changes in temperature, salinity and pressure, DIC concentration remains constant (Wolf-Gladrow et al., 2007). The TA of sea water is much greater than the TA of fresh water and is defined as a measure of the excess of bases over acids (Dickson, 1981). In equation 2.2.11 which was modified from Dickson (1981) by Wolf-Gladrow et al (2007), [OH-] is the concentration of the hydroxide ion and $[B(OH)_4^-]$ is the concentration of the borate ion. Minor bases such as phosphate, silicate and sulphate usually contribute less than a percent to variations in alkalinity, and are therefore often neglected. Due to the minimal contribution of these ions to TA, it can be reasonably well approximated by:

$$TA \approx carbonate\ alkalinity = [HCO_3^-] + 2[CO_3^{2-}] \quad (eq.\ 2.2.13)$$

With an exchange of CO_2 between the atmosphere and the oceans there is a resulting change in DIC while TA remains constant (Figure 5). The concentration of carbonate and bicarbonate ions can be approximated by combining equations 2.2.12 and 2.2.13 and are reliable to about a 10% accuracy (Sarmiento and Gruber, 2006).

$$[CO_3^{2-}] \approx TA - DIC \quad (eq.\ 2.2.14)$$

$$[HCO_3^-] \approx 2 \cdot DIC - TA \quad (eq.\ 2.2.15)$$

These approximations will be useful when looking at the photosynthetic influences on Ocean Acidification processes, as photosynthesis decreases DIC, which in turn, increases [CO_3^{2-}]. Marine calcifying organisms need surface water carbonate ion concentrations to be supersaturated ([CO_3^{2-}] > 66µmol/kg so that their shells and skeletons do not dissolve. (Orr et al., 2005). This demonstrates the importance of DIC and TA in determining the carbonate ion concentration of the ocean, and shows that for an increase in TA, [CO_3^{2-}] will increase. The influences of temperature and salinity and of photosynthesis and calcification - the physical and biological carbon controls will now be considered.

2.2.1 Physical Processes

To consider the influences of temperature and salinity on sea water pCO_2, the solubility of CO_2 in sea water (Weiss, 1974) and the apparent dissociation constants of carbonic acid in sea water (Mehrbach, 1973) need to be considered (Takahashi et al., 1993). The CO_2 solubility (K_0) is strongly dependant on temperature (equation 7) due to gases being more soluble in colder water. From Takahashi et al (1993) changes in pCO_2 with temperature can be calculated:

$$\frac{1}{pCO_2}\frac{\partial pCO_2}{\partial T} = \partial ln\frac{pCO_2}{\partial T} = 0.04231\ C^{-1} \qquad (eq.\ 2.2.1.1)$$

This equation shows the sensitivity of pCO_2 to changes in temperature. With every 16°C increase in temperature, the pCO_2 in the surface waters of the ocean doubles. Due to this temperature effect, the pCO_2 increases (decreases) with a warming (cooling) of the water. The effect of temperature on oceanic pCO_2 is often a controlling factor in oligotrophic regions where the lack of nutrients limits photosynthesis (Takahashi et al., 1993). In these regions, winter cooling decreases the surface water pCO_2 while summer heating increases it, with the biological drawdown of CO_2 having little effect. In nutrient rich waters such as the Southern Ocean, the North Atlantic and the North Pacific, summer heating results in the formation of a stable surface layer, which facilitates the development of phytoplankton blooms and thus the decrease in pCO_2 (Takahashi et al., 1993) and subsequent increase in [CO_3^{2-}]. In these regions the summer photosynthetic uptake of CO_2 is usually greater than the pCO_2 increase due to warming, resulting in the effect of temperature not playing a large role in variations in surface water [CO_3^{2-}]. Furthermore, due to gas being more soluble in colder water, polar

oceans with low sea surface temperatures absorb more gas than subtropical oceans, making them sensitive to small variations in anthropogenic CO_2 (Egleston et al., 2010).

The influence of salinity on the pCO_2 is less significant than the influence of temperature on pCO_2, as salinity is relatively constant throughout the oceans. For a salinity increase of 1 salinity unit, the oceanic pCO_2 will increase by approximately 9µatm (Sarmiento and Gruber, 2006). The variation in oceanic salinity is approximately 7, whereas the oceanic variation in temperature is 30° C, and thus salinity plays a much less important role in controlling pCO_2 than temperature.

2.2.2 Biological Processes

The biological production of organic material and carbonate minerals together with their subsequent death and sinking were called the "biological carbon pumps" by Volk and Hoffert (1985). These pumps act to transport carbon against its concentration gradient from the surface waters into the deep oceans where it can be stored for 1000's of years. Most of the sinking organic material and carbonate minerals are remineralised by heterotrophic organisms in the upper water layers, returning DIC and nutrients to the surface waters. Only a small percentage of the organic carbon and minerals sink below the thermocline before they are remineralised. Some of this carbon is remineralised in the deeper layers and a small amount is stored in the deep oceans as DIC. These important processes create a DIC gradient, with lower DIC at the surface and higher DIC at depth.

The first and most important biological process that influences the ocean DIC is photosynthesis. This can only take place in the upper, sunlight layers of the ocean as photosynthesis is light dependant. Photosynthesis occurs through primary production which is the uptake of CO_2 and nutrients to form organic matter, from which all organisms on earth are made. The five major elements necessary for photosynthesis are C, O, N, H and P (Redfield, 1963)). The concentrations of C, O and H are usually sufficiently high so that they are never a limiting factor for photosynthesis. Elements that can sometimes result in the limitation of photosynthesis are referred to as nutrients. Depending on their relative concentrations in organisms, nutrients can be divided into macronutrients (N and P) and micronutrients (trace elements), (Sarmiento and Gruber, 2006). Both macronutrients and micronutrients are essential for photosynthesis and the lack of any one can limit or even

prevent biological production. The commonly used formula to describe marine photosynthesis uses the balance coefficients of A. C. Redfield who was one of the first scientists to work out the relative proportions of each nutrient necessary for photosynthesis (Redfield, 1963).

$$106CO_2 + 16NO_3^- + PO_4^{3-} + 78H_2O + 18H^+ \leftrightarrow C_{106}H_{175}O_{42}N_{16}P + 138O_2 \quad (eq.\ 2.2.2.1)$$

The reverse process is known as respiration, which is the breakdown of organic compounds which consumes oxygen and forms CO_2 and nutrients, increasing the concentration of DIC. Nutrient stoichiometry is often used in biogeochemistry to estimate the utilisation of one nutrient from another. The Redfield nutrient ratios are still commonly used, although there have been studies since then questioning their accuracy (for example: Anderson and Sarmiento, 1994; Giddy et al., 2012; Takahashi et al., 1985). Anderson and Sarmiento (1994) examined the nutrient changes due to biological activity between 400 and 4000m in the South Atlantic, Indian and Pacific oceans, where they found the general C:N:P ratio (in the absence of denitrification) to be 117:16:1. The Redfield N:P ratio of 16 is an average approximation for diverse oceanic phytoplankton assemblages that have a variety of growth strategies and oceanic conditions (Arrigo, 2005). Arrigo (2005) show how phytoplankton have three different growth strategies which influence their N:P ratios, none of which were found to be 16. This must be considered when using nitrate concentrations to estimate primary production.

Photosynthesis is central to the marine carbon cycle as it enables the conversion of DIC into organic carbon in the surface layers of the ocean. The organic carbon or soft tissue pump results in the net uptake of CO_2 and nutrients in the euphotic zone and the subsequent sinking of carbon in the form of Particulate Organic Carbon (POC). Without this biological uptake and transport of nutrients and carbon, the nutrient and carbon concentration in the oceans would be almost constant throughout the ocean.

Photosynthesis decreases DIC in the surface waters while respiration increases DIC. Photosynthesis also affects TA through the utilisation of free protons (Figure 5). The formation of 1 mol of organic matter results in a 1 mol decrease in DIC and a 0.14 mol

(16/117) increase in TA (from the N/C ratios of Anderson and Sarmiento, 1994). Most of the protons during photosynthesis are used to convert nitrate to organic nitrogen. This increase in TA as a result of nitrate uptake can be accounted for by subtracting the value of nitrate that was utilised during photosynthesis, from TA, as a 1 mol decrease in nitrate results in a 1mol increase in TA (Goldman and Brewer, 1980). Thus, the organic carbon pump causes a decrease in DIC and an increase in TA at the surface, and an increase in DIC and a decrease in TA in the deeper waters through the remineralization of organic matter.

The second biological process which influences oceanic DIC is the formation and dissolution of calcium carbonate minerals. The formation of calcite and aragonite minerals occurs in the upper layers of the ocean due to the three main groups of calcifying organisms: coccolithophorids, foraminifera and Thecosome pteropods. Coccolithophorids are a group of phytoplankton that form an outer armour of $CaCO_3$ plates called coccoliths (). These plates are formed inside the organism and can be replaced as frequently as once every 15 minutes. Currently, coccolithophorids are responsible for approximately a third of the total marine calcium carbonate formation (Iglesias-Rodriguez et al., 2008) and are abundant in the North Atlantic and North Pacific oceans as well as in many coastal and shelf regions (Iglesias-Rodriguez et al., 2002). Foraminifera and pteropods are zooplanktonic organisms that form a major link in the marine food chain by consuming smaller planktonic species while being prey for animals. Foraminifera make $CaCO_3$ skeletons from the mineral calcite, and have been shown to be responsible for between 23-56% of the total open marine $CaCO_3$ flux (Schiebel, 2002). Pteropods are the main aragonite calcifying organisms in the Southern Ocean, influencing the density biomass and trophic structure of the Antarctic ecosystem (Hunt et al., 2008). These molluscs are important as both prey items for larger zooplankton, pelagic fish and some sea birds and as consumers of the smaller plankton and crustaceans. They also contribute > 50% to the carbonate flux south of the Polar Front due to the rapid sinking of their $CaCO_3$ shells (Hunt et al., 2008). The ballasting properties of their shells make them significant contributors to the organic carbon flux (Hunt et al., 2008). Very few studies have been done on the life cycles of pteropods, especially the Southern Ocean species. It is believed that they are protandrous hermaphrodites that survive for 1-2 years producing two generations per life cycle. Pteropods are key organisms in the Southern Ocean and their ability to survive increasing CO_2 and decreasing $[CO_3^{2-}]$ predicted for this century is of great concern. Their possible northward migration or decline will likely impact the Southern Ocean ecosystem as well as the oceanic carbon uptake (Honjo, 2004; Hunt et al., 2008). Aragonite is

approximately 50% less stable than calcite (Mucci, 1983), suggesting that aragonite calcifiers (such as the pteropods) will be the first to be affected by ocean acidification. Marine calcifying organisms form their calcium carbonate skeletons and shells according to the following equation:

$$Ca^{2+} + 2HCO_3^- \rightarrow CO_2 + CaCO_3 + H_2O \qquad (eq.\ 2.2.2.2)$$

The formation and dissolution of calcium carbonate changes DIC and TA by 1 and 2 units respectively (Figure 5). Calcifying organisms form calcium carbonate in the surface waters, decreasing DIC and TA in a 1:2 ratio. When these organisms die, they sink and are mostly dissolved in the water column which increases DIC and TA in the deeper waters. The formation of $CaCO_3$ and its subsequent sinking and dissolution, transports DIC and TA from the surface waters downwards, a process known as the carbonate pump (Sarmiento and Gruber, 2006). The carbonate pump therefore results in an increase in the surface water concentration of aqueous CO_2, and for this reason has also been termed the Carbonate counter pump (Figure 3) (Rost and Riebesell, 2004). The relative strengths of the organic carbon and the carbonate pumps have a large influence on the atmosphere-ocean CO_2 flux. This ratio of particulate inorganic carbon to organic carbon in exported biogenic matter is known as the *rain ratio* (Rost and Riebesell, 2004). A *rain ratio* of above 1 indicates that calcification is greater than photosynthesis, which will result in decreased $[CO_3^{2-}]$, and the opposite is true for a *rain ratio* of less than 1, where increased photosynthesis will increase the $[CO_3^{2-}]$.

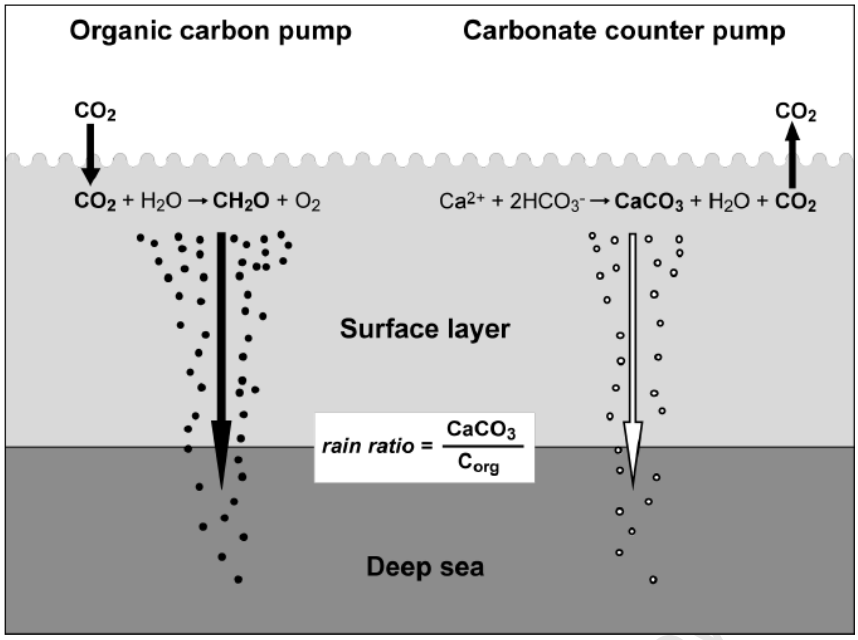

Figure 3. Schematic to show the oceanic biological carbon pumps: the organic carbon pump which decreases CO2 in the surface water and transports it to depths and the calcium carbonate pump which releases CO2 into the ocean surface layers. The relative strengths of these two processes (*rain ratio*) largely determine the biologically mediated ocean atmosphere CO2 exchange (Rost and Riebesell, 2004).

2.2.3 Carbonate saturation state

The calcium carbonate saturation state (Ω) is dependent on the measured ion concentrations of Ca^{2+} and CO_3^{2-} as well as their concentrations in equilibrium with the mineral calcium carbonate (Royal-Society, 2005)). The product of the concentrations of these ions in their saturated state is known as the calcium carbonate stoichiometric solubility product ($K_{sp}^{CaCO_3}$), (Mucci, 1983), which can be calculated by:

$$K_{sp}^{CaCO_3} = [CO_3^{2-}]_{sat}[Ca^{2+}]_{sat} \qquad (eq.\ 2.2.3.1)$$

where $[CO_3^{2-}]_{sat}$ and $[Ca^{2+}]_{sat}$ are the equilibrium concentrations of carbonate and calcium. The solubility product for aragonite and calcite differ due to the chemical structure of the calcium carbonate crystals, resulting in aragonite being 50% more soluble than calcite. The solubility product is dependent on temperature and salinity (Millero et al., 2006) and can be

calculated at a pressure of 1atmosphere as in Sarmiento and Gruber (2006) using the equations of Mucci (1983):

$$\ln K_{sp}^{aragonite} = -395.9180 + \frac{6685.097}{T} + 71.595\ \ln(T) - 0.17959 \cdot T + \left(-0.157481 + \frac{202.938}{T} + 0.0039780 \cdot T\right) S^{1/2} - 0.23067 \cdot S + 0.0136808 \cdot S^{3/2} \quad (eq.\ 2.2.3.2)$$

$$\ln K_{sp}^{calcite} = -395.8293 + \frac{6537.773}{T} + 71.595\ \ln(T) - 0.17959 \cdot T + \left(-1.79838 + \frac{410.64}{T} + 0.0065453 \cdot T\right) S^{1/2} - 0.17755 \cdot S + 0.0094979 \cdot S^{3/2} \quad (eq.\ 2.2.3.3)$$

where K_{sp} is in (mol/kg^2), T is the temperature in Kelvin and S is the salinity in psu. From these equations it can be seen that the solubility product increases as salinity increases. With an increase in salinity, the ionic strength of the solution is increased, causing a subsequent decrease in the ion activity coefficients of the calcium and the carbonate ions (Mucci, 1983). Interestingly, the solubilities of calcite and aragonite decrease with increasing temperature, causing them to be more soluble in colder, deep water and in high latitude regions where surface waters are colder (Sarmiento and Gruber 2006). The saturation state is dependent on the solubility product and is defined as the product of solutes over the product of solutes at saturation (the solubility product). It is a measure of how saturated the water is with respect to calcium carbonate.

$$\Omega = \frac{[CO_3^{2-}][Ca^{2+}]}{K_{sp}^{CaCO_3}} \quad (eq.\ 2.2.3.4)$$

where $[CO_3^{2-}]$ and $[Ca^{2+}]$ are the observed concentrations of carbonate and calcium ions. The concentrations of CO_3^{2-} and Ca^{2+} can be calculated from measurements of DIC and TA, but are also dependent on the water temperature and salinity (Mehrbach et al., 1973). As $[Ca^{2+}]$ is abundant in sea water, and varies much less than the $[CO_3^{2-}]$, for conceptual purposes $[Ca^{2+}]$ can be approximated to be constant. The saturation state can thus be simplified to:

$$\Omega \approx \frac{[CO_3^{2-}]}{[CO_3^{2-}]_{sat}} \qquad (eq.\ 2.2.3.5)$$

This is a useful simplification as it is just the observed calcite concentration over the saturated calcite concentration, where the observed calcite concentration can be approximated by the concentrations of DIC and TA (equation 2.2.14). Water is assumed to be supersaturated with respect to calcium carbonate when $\Omega > 1$ and undersaturated when $\Omega < 1$. The solubility of calcium carbonate increases with decreasing temperature and increasing pressure (Royal-Society, 2005). This means that at a certain depth where $\Omega = 1$ (the isocline) calcium carbonate formation will equal dissolution, and below this depth calcium carbonate will dissolve. There are two views on calcification chemistry that are explained in Roleda et al (2012). One is that calcifying organisms are not reliant on $\Omega > 1$ for calcification as they are able to use HCO_3^{2-} or CO_2 for calcification (Nicol 1960; Raven, 2011) and the other is that calcifiers rely on CO_3^{2-} ions and therefore require $\Omega > 1$ for calcification. Should the first view be correct, calcifiers may be able to calcify in waters where $\Omega < 1$, but they will likely begin to experience shell dissolution (Bednarsek et al., 2012) and will thus still be affected by undersaturated waters.

The calcite and aragonite isoclines vary extensively throughout the ocean. The calcite isocline is found at around depths of 4500m in the North Atlantic and above 1000m in the North Pacific, while the aragonite isocline can be up to 1000m shallower (Sarmiento and Gruber, 2006). In the North Pacific the aragonite saturation horizon almost reaches the surface.

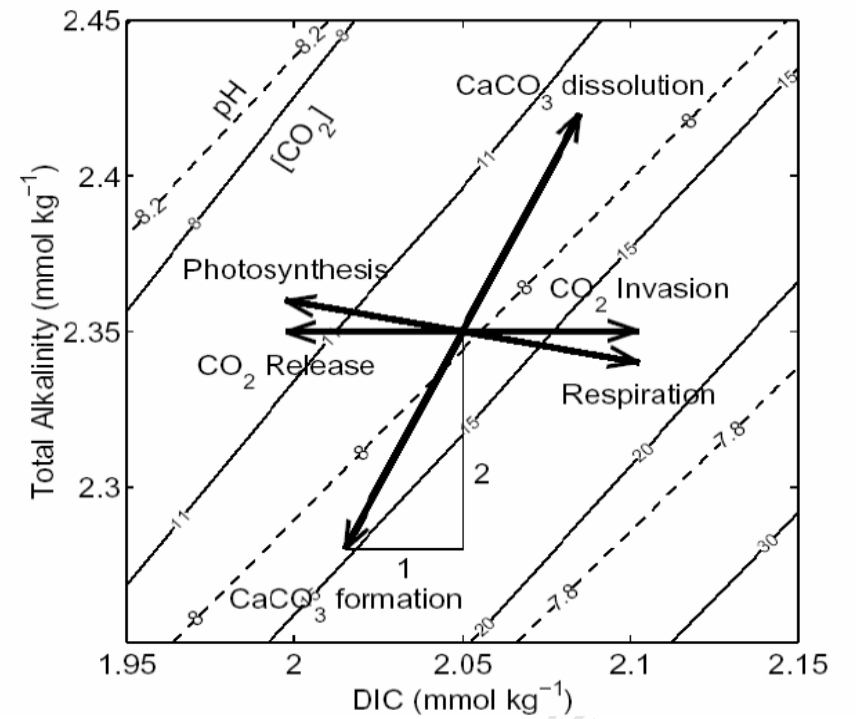

Figure 5. Effects of various processes on DIC and TA (arrows), taken from Zeebe and Wolf-Gladrow (2001). Solid and dashed lines indicate levels of constant dissolved CO_2 in µmol kg^{-1} and pH respectively as a function of dissolved inorganic carbon (DIC) and total alkalinity (TA).

Surface water DIC and TA and hence [CO_3^{2-}] are controlled by the air-sea flux of CO_2, photosynthesis/respiration, calcification/dissolution, dilution from fresh water inputs, and upwelling processes, where deeper waters have higher DIC and TA. There is agreement between studies that the high latitude Southern Ocean is particularly vulnerable to climate change as it has below freezing water temperatures (Schröder and Fahrbach, 1999), high Revelle factors (Sabine et al., 2004) and upwelling DIC rich waters (Deacon, 1979; Orsi et al., 1993). Combined with increasing atmospheric pCO_2, the surface waters of the Southern Ocean will likely become undersaturated with calcium carbonate between 2030-2050 (McNeil and Matear, 2008; Orr et al., 2005). This may result in a decline in Southern Ocean pteropods, their northward migration and ultimately in their decline (Hunt et al., 2008). A decrease in these zooplankton species will have significant ecological impacts as the trophic structure of this ecosystem as well as the Southern Ocean CO_2 uptake will be affected (Hunt et al., 2008).

2.2.4 The Revelle Factor

Revelle and Suess (1957) showed how the increase in the pCO_2 of sea water is about 10 times higher than the increase in total CO_2 when CO_2 is added. This affect was attributed to the "buffer" capacity of the ocean which has since been termed the Revelle Factor after Roger Revelle. The Revelle or "buffer" Factor quantifies the sensitivity of CO_2, H^+, and aragonite and carbonate saturation state (Ω) to changes in DIC and TA (Egleston et al., 2010). Due to the Revelle Factor, changes in oceanic pCO_2 are dependent on the absolute values of DIC and TA and can be approximated as in Sarmiento and Gruber (2006) by:

$$\gamma DIC \approx \frac{3 \cdot TA \cdot DIC - 2 \cdot DIC^2}{(2 \cdot DIC - TA)(TA - DIC)} \qquad (eq.\,2.2.4.\,1)$$

where γDIC is the Revelle factor. The ability of the oceans to take up excess CO_2 is inversely proportional to the Revelle Factor, so regions with low Revelle Factors have high uptake capacity, while regions with a high Revelle Factor have a low uptake capacity (Sabine et al., 2004). The global variation in the surface oceans buffering capacity can be seen in figure 4. High latitude regions where Revelle Factors are high are more susceptible to small variations in CO_2, as a small increase in DIC will result in a substantial increase in pCO_2. The opposite can be said for low latitude regions with lower Revelle factors, where large changes in DIC result in small changes in the pCO_2. Current Revelle Factors have increased by approximately one unit since the industrial revolution (Sabine et al, 2004), suggesting that as excess CO_2 increases the DIC of the surface oceans, the oceans buffering capacity will decrease, increasing the oceans sensitivity to local variability in DIC during this century (Egleston et al., 2010).

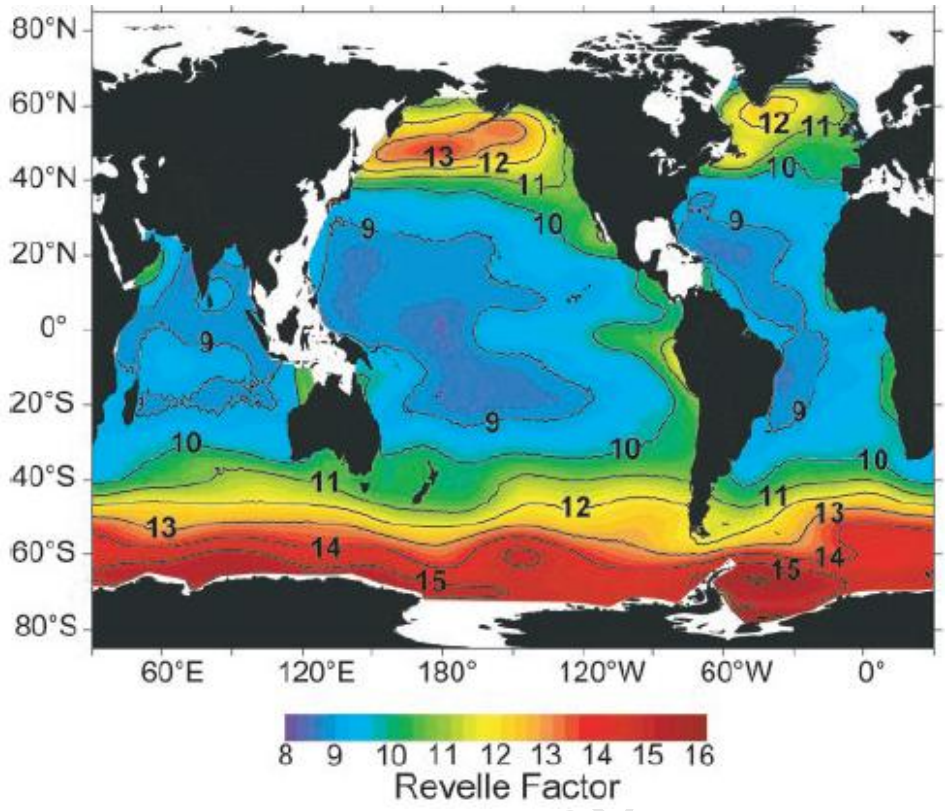

Figure 4. Map of the 1994 distribution of Revelle factor, (*dP*CO2/*d*DIC)/ (*P*CO2/DIC), averaged for the upper 50m of the water column (Sabine et al, 2004).

2.3 Seasonality

Productivity and hence carbon dynamics in much of the Southern Ocean, especially the seasonal ice zone (MIZ) are characterised by a strong seasonal cycle (Thomalla et al., 2011). The seasonal cycle influences ocean productivity, as it links climate forcing to the ecosystem response (Thomalla et al., 2011). The seasonality of the Southern Ocean was investigated by Gordon (1981), in which he explained that both summer heating as well as the upwelling of warm, sub-surface water are the major mechanisms that cause the sea ice to melt, resulting in the subsequent formation of a stratified upper water column, alleviating light limitation and facilitating phytoplankton blooms. Within the Southern Ocean variability in the seasonal cycle has been observed (Thomalla et al., 2011), which in turn causes variability in marine productivity and in the surface water [CO_3^{2-}]. It is therefore crucial to understand the regional dynamics of the seasonal cycle and how it influences surface water biogeochemistry,

especially in the Southern Ocean where seasonality is predicted to amplify the effects of Ocean Acidification (McNeil and Matear, 2008).

In the Southern Ocean, sea ice surrounds the Antarctic continent during winter. Surface waters begin to freeze in March, with sea ice reaching a maximum extent by September and then rapidly melting during December (Kimura and Wakatsuchi, 2011; Maykut, 1984). This creates a strong seasonal cycle where, during winter, strong winds result in Ekman transport and in the upwelling of Circumpolar Deep Water (CDW) that is capped by sea ice, limiting gas exchange. Summer heating melts the sea ice, decreasing the salinity and increasing the temperature of the surface water (Gordon, 1981). This has been shown to result in the Southern Ocean being a winter source and a summer sink region for atmospheric CO_2 (Takahashi, 1993). The timing of summer bloom initiation is critical in the Marginal Ice Zone (MIZ) of the Southern Ocean, where bloom initiation during the first two weeks of December is optimal (Thomalla et al., 2011). The seasonal cycle has also been shown to influence the calcite saturation of the Southern Ocean waters, where increased DIC during winter will likely hasten surface water aragonite undersaturation (McNeil and Matear, 2008).

2.4 The Weddell Gyre

The Weddell Sea circulation is characterised by the elongate cyclonic Weddell Gyre (Carmack and Foster, 1977; Deacon, 1979). The Weddell Gyre (WG) is bound on the north by the Scotia Ridge, on the south by the Antarctic continent, on the west by the Antarctic Peninsula and extends eastward to between 20° and 30° E (Figure 6) (Carmack and Foster, 1977; Orsi et al., 1993). At around 58°S, the WG flows eastward, with the southern extent of the Antarctic Circumpolar Current (ACC). At around 20° E the flow turns southwards, towards Antarctica, forming the lesser structured eastern limb of the Weddell Gyre (Orsi et al., 1993). The gyre then joins the westward flowing Antarctic Coastal Current until around 27° to 30°W where the current splits, one branch flowing south-westwards towards the Filchner and Ronne Ice Shelves, and the other branch following the western boundary of the Antarctic Continent (Orsi et al., 1993). The Weddell Gyre transports salt and heat from the Antarctic Circumpolar Current to the Antarctic continental shelves.

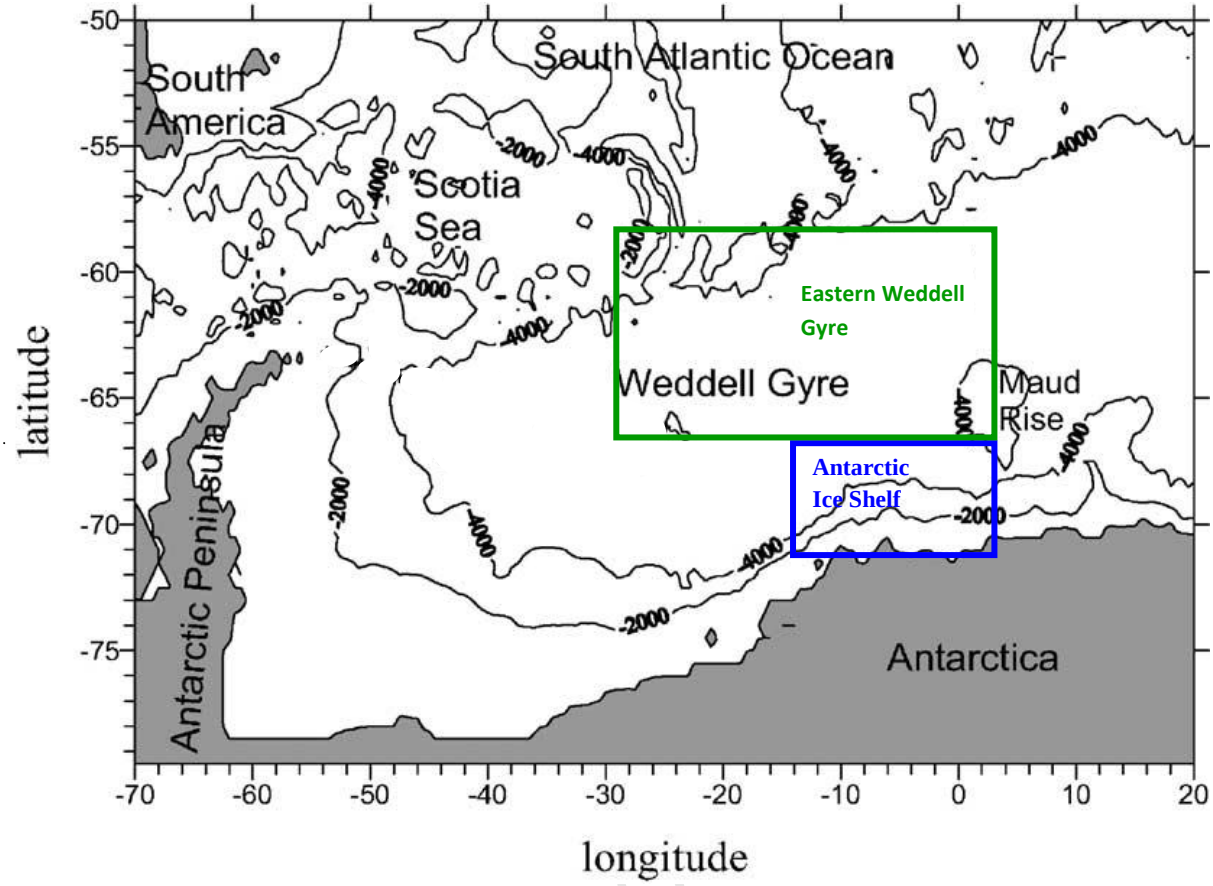

Figure 6. Map of the Weddell Gyre and neighbouring areas adapted from Hoppema et al (2002). The study regions are shown in blue (Ice shelf region) and green (Weddell open ocean region).

2.4.1 Water masses

There are four major water masses within the Weddell Sea that are classified according to their thermohaline properties. These water masses as defined by Orsi et al (1993) are: Surface waters, Circumpolar Deep Water (CDW), Weddell Sea Deep Water (WSDW) and Weddell Sea Bottom Water (WSBW). With the exception of CDW, all of the other water masses are formed locally within the Weddell Sea. Salty, warm, DIC-rich CDW is advected into the eastern section of the WG (Deacon, 1979; Orsi et al., 1993). This CDW is a mixture of North Atlantic Deep Water, from which it receives its high salinity values, and deep waters from the Indian and the Pacific Oceans, giving CDW its characteristic low oxygen and high DIC concentrations (Schmitz, 1995; Whitworth and Nowling, 1987). After entering the WG, CDW is referred to as Warm Deep Water (WDW) by Carmack and Foster (1975a), or as Weddell Deep Water (WDW) by Gordon and Huber (1995). The WDW represents the

warmest (t > 0.2°C) and one of the saltiest (S >34.6) water masses within the WG and is found between 200-800m depth (Orsi et al 1993). This warm water travels south-westwards with the gyre circulation and is modified through mixing with surrounding waters masses as it upwells within the gyre, becoming Modified Warm Deep Water (MWDW) (Whitworth and Nowling, 1987; Orsi et al., 1993). The dominant winds above the WG result in divergent Ekman transport of the surface waters and in the upwelling of WDW at the centre of the gyre (Gordon et al., 1981). WDW is a source of heat and salt to the icy waters of the WG, acting to melt sea ice and increase the salinity and the DIC of the surface water layers (Gordon et al., 1984).

The seasonally-driven surface waters of the WG are fresher and colder than the WDW below as a result of air-sea and sea-ice interactions (Orsi et al., 1993). The surface layers (up to depths of 200 to 300m) of the WG show strong seasonality and consist of Summer Surface Water (SSW), Winter Water (WW) and Ice Shelf Waters (ISW), (Carmack and Foster, 1975a; Carmack 1977; Schröder and Fahrbach, 1999). During summer, the surface waters of the WG are warmed 1° to 4° C above freezing and diluted by fresh water from sea ice melt. This forms a warmer, fresher and hence less dense layer of water capping the cold, saltier WW with a strong, seasonal halocline, increasing the stratification of the upper water column (Carmack and Foster, 1975a; Jones et al., 2010). The formation of this fresh surface layer creates vertical stability, providing a well-illuminated environment allowing for the growth of phytoplankton (Smith and Nelson, 1986). Hoppema et al (1995) suggest that it is the stability of the water column through sea ice melt rather than the temperature increase that is the pivotal factor for the initiation of phytoplankton growth during summer. The formation of sea ice as well as deep overturning during winter results in thermohaline convection, and in the formation of WW which lies below the seasonal pycnocline (Mosby, 1934; Carmack and Foster, 1975; Carmack and Foster 1977). WW water is well mixed as a result of winter storms and is characterised by a virtually isothermal temperature minimum layer in the water column (Jones et al., 2010). Brine rejection during sea ice formation slightly increases the salinity of WW. This water type is variable as its properties are dependent on the extent of the previous winter's ice-formation and minimum temperatures. Foster and Carmack (1976b) defined WW as the surface water with temperatures of -1.8 to -1.6°C and salinities of 34.64-34.68psu. The winter mixed layer as characterised by Gordon and Huber (1984), has a mean salinity and temperature of 34.287psu and -1.844°C respectively, with an average thickness

of 108m. Jones et al (2010) and Geibert et al (2010) identify the winter mixed layer that marks the remnant of WW as the depth where the potential temperature is at a minimum, below the warmer surface layer. Much of the WG is covered by ice during winter, prohibiting the surface waters from interacting with the atmosphere (Bakker et al, 1997), which suggests that the WW below the ice will contain its winter properties unless influenced by sub-surface waters.

2.5 Empirical data

The under-sampling of much of the oceanic surface waters with respect to carbon (Monteiro et al., 2010) has resulted in the use of empirically calculated oceanic carbonate parameters (eg. Millero et al., 1998; Lee et al., 2006; McNeil and Matear, 2008; Lenton et al., 2012). The distribution of TA in the oceans has been shown to follow that of salinity as they are both mainly affected by the addition or removal of fresh water, and hence the ratio of TA to salinity is almost constant (Millero et al., 1998). Millero et al (1998) were the first to estimate salinity normalised TA from SST data, which has since been shown to be subject to error due to the method of salinity normalisation (Friis et al., 2003). Lee et al (2006) using 5692 data points derived regional correlations of TA with sea surface temperature (SST) and salinity (SSS). They found that a second-order polynomial model provided the most accurate results with the use of specific constants depending on which oceanic region is being studied. For the Southern Ocean where 33 < SSS < 36 the following equation has been derived:

$$TA = 2305 + 52.48(SSS - 35) + 2.85(SSS - 35)^2 - 0.49(SST - 20) + 0.086(SST - 20)^2 \quad \text{(eq. 2.5.1)}$$

Lenton et al (2012) used more than 4.4 million observations of SST and SSS to reconstruct surface water TA values for different regions of the world's oceans using the equations of Lee et al (2006). They found acceptable comparisons between calculated and observed TA for many oceanic regions, especially in the Southern Ocean. Empirical studies are important as they provide a means of predicting the possible effects of anthropogenic CO_2 increase on the oceanic absorption of CO_2 (Lenton et al., 2012) as well as on the seasonal variability in the calcium carbonate saturation state of our oceans, especially in the light of climate change (McNeil and Matear, 2008).

2.6 Aims and key questions

- What controls the seasonal and interannual variability in surface water carbonate ion concentration at the Eastern Weddell Gyre ice shelf?

The Southern Ocean summer photosynthetic drawdown of CO_2, facilitated by the formation of a stratified surface layer of ice melt water has been noted by previous studies (Takahashi et al., 1993; Sabine and Key, 1998; Hoppema, 2004; Bakker et al., 2008), and is the primary mechanism by which summer surface water aragonite saturation state (Ω_{arag}) is increased from its minimum winter value (McNeil and Matear 2008). McNeil and Matear (2008) propose that understanding how seasonality affects Ocean Acidification processes in the Southern Ocean south of the Polar Front is vital, as the timing of detrimental carbonate conditions may be dramatically changed. We aim to analyse the primary processes that influence the seasonal cycle of Ω_{arag}, as well as the processes that cause interannual variability in surface water Ω_{arag} at the Eastern Weddell Gyre ice shelf.

Continuous *in situ* surface water fCO_2, salinity and temperature data, collected during the early and late Austral summers of 2008/2009, 2009/2010, 2010/2011 and 2011/2012 aboard the r/v SA Agulhas, will be used to calculate surface water Total Alkalinity, using the algorithm of Lee et al (2006). Surface water Dissolved Inorganic Carbon, Revelle Factor, carbonate ion concentration, calcite and aragonite saturation state, and pH using the CO2Sys programme (Lewis and Wallace, 1998), with constants K_1 and K_2 from Mehrbach et al (1973) refit by Dickson and Millero (1987). The seasonal and interannual variability in these carbon parameters will be analysed to determine the current controls on the surface water marine carbonate system at the Eastern Weddell Gyre ice shelf.

- Ecosystem implications of Ocean Acidification

Decreasing surface water carbonate ion concentrations [CO_3^{2-}] will likely affect the ice shelf and Eastern Weddell Gyre (EWG) ecosystems before aragonite undersaturation is reached and Thecosome Pteropod aragonite shells begin to dissolve (Fabry et al., 2008; Orr et al.,

2005; Bednarsek et al., 2012). This is as a result of the increased energy needed for calcifying organisms to calcify as [CO_3^{2-}] decreases, resulting in a likely decrease in growth and reproductive success, with unknown ecosystem implications. Pteropods are key organisms in the Antarctic ecosystem (Hunt et al., 2008) and it is therefore vital to understand how variations in the seasonal cycle affect surface water [CO_3^{2-}] and thus the pteropods.

- Will the Southern Ocean Thecosome Pteropods survive this century?

The periodic aragonite undersaturation ($\Omega_{arag} < 1$) of Southern Ocean surface waters is predicted to occur by the middle of this century (Orr et al., 2005) or sooner (McNeil and Matear, 2008). Increasing anthropogenic CO_2 increases the DIC of surface waters, making them increasingly sensitive to local variations in Dissolved Inorganic Carbon and Total Alkalinity especially in high latitude oceans (Egleston et al., 2010), suggesting that regional scale Ocean Acidification studies are important. Whether or not the Thecosome Pteropods will survive this century largely depends on seasonal primary production and how it may change in a changing climate. Here we analyse three future ice shelf seasonal ice thaw scenarios: Early sea ice thaw, Late sea ice thaw and "Normal" sea ice thaw. Surface water fCO_2 is increased by 160µatm (predicted for the middle of this century) and is doubled (predicted for the end of this century) and subsequent possible ecosystem implications are investigated.

3. Methods

Data were collected during the 2008/2009, 2009/2010, 2010/2011 and 2011/2012 SANAE cruises, aboard the polar supply and research ship, SA Agulhas. All four cruises had the same general cruise track, although their dates and coordinates differed slightly (Table 1). The r/v SA Agulhas left Cape Town during December and sailed along the GoodHope line to Antarctica, arriving at the Antarctic ice shelf between 0-10°W in late December/early January. The r/v SA Agulhas remained at the Antarctic ice shelf for a period of up to two weeks (ice station 1). The r/v SA Agulhas then left the Antarctic ice shelf in January, sailing through the Weddell Sea to South Georgia Island (northward leg of the Buoy Run). The r/v SA Agulhas returned to the Antarctica ice shelf (0-10°W) during late January/February (Southward leg of the Buoy Run) where it remained for two to four weeks, completing the second ice station samples. During all years the r/v SA Agulhas left Antarctica during February to sail back along the GoodHope line to Cape Town.

Continuous underway surface data was collected during all four cruises, while underway surface station data was collected during SANAE 49, 50 and 51. Underway UCTDs were deployed during the SANAE 49, 50 and 51 cruises when there were ice free conditions that allowed for a safe retrieval of the UCTD probe. The only temporal data sets collected during the SANAE cruises were time series collected along the Antarctic Ice Shelf during the first and second ice stations.

Table 1. Dates of the legs of the four SANAE cruises, with leg 1 from cape town to Antarctica, leg 2 at the Antarctic ice shelf, leg 3 from Antarctica to South Georgia Island, leg 4 from South Georgia Island to Antarctica, leg five t the Antarctic ice shelf and leg six from Antarctica to Cape Town.

Cruise	leg 1	leg 2	leg 3	leg 4	leg 5	leg 6
SANAE 48 (2008-2009)	23 Dec-4 Jan	5-25 Jan	26 Jan-1 Feb	2 Feb-9 Feb	10-20 Feb	21 Feb-5 Mar
SANAE 49 (2009-2010)	9-22 Dec	1-16 Jan	16-24 Jan	25 Jan-2 Feb	2-13 Feb	13-23 Feb
SANAE 50 (2010-2011)	8-19 Dec	20-31 Dec	1-10 Jan	10-20 Jan	21 Jan-1 Feb	5-16 Feb
SANAE 51 (2011-2012)	10-24 Dec	25 Dec-3 Jan	4-15 Jan	16-24 Jan	24 Jan-8 Feb	23Feb-2 Mar

The data that will be analysed in this study was collected during legs 2, 3, 4 and 5 of all the SANAE cruises. Legs 1 and 6 will not be analysed during this study. Although legs 3 and 4 extend all the way to South Georgia Island (54.5°S 37°W), the data north of 58°S will not be investigated in this study as the boundary between the Weddell Gyre and the Antarctic Circumpolar Current lies at approximately 58°S. The four Cruise tracks showing the data for this study can be seen in figure 9. This data was separated into two data sets: Ice Shelf (IS) data which was collected between 71-68°S 4°E-14°E and Eastern Weddell Gyre (EWG) data collected between 68-58°S 4°E-30°W (Figure 9).

3.1 Station sampling

Discrete underway station samples were collected every 4 hours, increasing to every 2 hours in frontal regions during the northward and southward legs of the SANAE 50 and SANAE 51 Buoy Run. Measurements of surface water Total Alkalinity (TA), Dissolved Inorganic Carbon (DIC), salinity, nutrients and chlorophyll *a* fluorescence were collected at these stations, but unfortunately the TA and DIC data collected during SANAE 51 will not be used as the CRM's differed by approximately 20µmol/kg at the beginning and the end of each sample run, suggesting inaccurate values. Water was collected from the uncontaminated underway surface sea water lab supply (from the Fe fish) or from the uncontaminated underway supply in the engine room, when sea ice limited the deployment of the Fe fish. Salinity, DIC and TA were all analysed on board. Nutrients were analysed on board during the SANAE 50 cruise while for SANAE 51 water was stored in nutrient vials and immediately frozen. These vials were then thawed and analysed back in the laboratory.

High resolution vertical profiles of potential temperature and salinity were obtained on the downcast of conductivity, temperature, depth (CTD) sensor (SeaBird 911plus). CTD casts were conducted at the Antarctic ice shelf during leg 2 of SANAE 49, 50 and 51 and leg 5 of SANAE 50 and 51. Ice shelf CTD's were deployed twice a day at approximately mid-day and mid-night during SANAE 51. During SANAE 50 ice shelf CTDs were deployed daily at 8pm. All ice shelf CTDs were deployed to the maximum depth of the sea floor of approximately 250-400m. A line of CTDs was also completed during the Buoy Run to South Georgia Island within the EWG on legs 3 and 4 during SANAE 49 and on leg 4 during SANAE 50. During the Buoy Run on SANAE 49, CTD's were deployed to 500m depth at

9:00 and 21:00 hours daily. The SANAE 50 Buoy Run CTDs were deployed every 2 hours to a depth of 500m. TA, DIC, salinity, nutrient and chlorophyll *a* fluorescence data were collected from a sampling carousel of 24 x 12 litre Niskin bottles attached to the CTD and closed at varying depths during the upward cast. The bottles were closed at depths as to best capture surface features such as the thermocline and the chlorophyll *a* maximum. An auxiliary fluorometer sensor attached to the CTD measured vertical chlorophyll *a* fluorescence which was later compared to the chlorophyll *a* fluorescence measured from the CTD bottle samples.

The UCTD is an underway CTD probe that allows for the collection of temperature and salinity profiles from the surface up to depths of 400m. This instrument was deployed approximately every 2 hours on the Buoy Run when there were ice free waters, during the SANAE 49, 50 and 51 cruises. During the SANAE 50 cruise, CTD stations were conducted every 2 hours on the southward leg of the Buoy Run which were alternated with the UCTD stations. The conductivity cell was damaged on the SANAE 49 cruise and thus SANAE 49 contains no UCTD salinity data. The UCTD data for SANAE 51 was unfortunately unavailable for this study. CTD and UCTD data was used to calculate MLD at the ice shelf and along the Buoy Run transect as well as to investigate sub-surface waters.

3.2 Continuous surface measurements of fCO_2, SST, salinity and chlorophyll *a* fluorescence

Fugacity of carbon dioxide (fCO_2) was determined quasi-continuously in surface water and in the marine atmosphere with an underway, General Oceanics equibrator-based system with a Li-COR LI-7000 infra-red gas analyser, designed after Wanninkhof and Thoning (1993) and described by Pierrot et al, (2009). Four reference gases of known CO_2 partial pressure (pCO_2) were used: 0.00, 357.32, 377.8 and 427.83ppm, which were provided and cross-calibrated to international standards by the GAW station at Cape Point. Once every six hours the instrument cycle returned to these gases followed by atmospheric measurements. Sea water was drawn from about 5m depth at the ships keel, while marine air was continuously pumped from the crow's nest. The sea water was directed into a chamber (the equilibrator) where the CO_2 in the water equilibrates with the gas in the headspace of the chamber (Pierrot et al,

2009). This gas was then pumped through a non-dispersive infrared analyser which instantaneously measures the CO_2 mole fraction (xCO_2) of the gas. Regularly, atmospheric air was pumped through the analyser and its CO_2 mole fraction was determined.

Ancillary instruments logged onto the underway pCO_2 analyser include a GPS and atmospheric pressure probe situated 5m above the Licor and equilibrator in a deck housing, intake temperature near the keel at 5m Depth, a Turner 10-AU fluorometer, a Fluke digital thermometer to measure the equilibrator temperature, a differential barometer to record the equilibrator pressure relative to atmospheric pressure, and an Idronaut multisensor that measures the sea surface temperature and the surface water salinity. The Idronaut multisensory was fitted with an oxygen optode which measured surface oxygen concentrations. This data supplied a surface time series of fCO_2, Sea Surface Temperature (SST), sea surface salinity (SSS) and chlorophyll *a* fluorescence at the Antarctic ice shelf during all four cruises.

3.3 Data

For the construction of figures MATLAB R2011a, version 7.12.0.635 was used.

3.3.1 Station sampling and nutrients

Where salinity was available the potential density was calculated from vertical profiles of potential temperature and salinity. The Mixed Layer Depth (MLD) was calculated using CTD and UCTD profiles, as the depth where the potential density exceeded that measured at 10m by 0.03 kg m^{-3}. When salinity was not available the MLD was calculated as the depth where the temperature exceeded that measured at 10m by 0.2 °C as in Thomalla et al (2011).

WW within the Weddell Gyre has been characterised by previous studies as the winter mixed layer where the potential temperature is at a minimum, below the warmer surface layer (Jones et al., 2010; Geibert et al., 2010). To identify WW during this study, all CTD data collected during SANAE 50 where TA and DIC were measured was used. This included two ice shelf CTDs during leg 2 and all the Buoy Run CTDs collected during leg 4. The winter mixed layer where temperature was at a minimum was identified for all 25 CTD casts. WW was

found between 50 and 180m at all CTD stations (Table 2). The measured water properties of the winter mixed layer were then averaged to get an accurate representation of the mean temperature, salinity, nutrients, TA and DIC of WW. This data was then used to calculate WW fCO_2, carbonate ion concentration [CO_3^{2-}], Revelle Factor, pH, calcium carbonate saturation state (Ω_{car}) and aragonite saturation state (Ω_{arag}), (Table 3) using the CO2Sys programme (Lewis and Wallace, 1998), with constants K_1 and K_2 from Mehrbach et al, 1973 refit by Dickson and Millero (1987). As the CTDs during SANAE 50 were the only CTDs where TA and DIC were accurately measured (Table 3), these WW properties have been assumed to be the WW properties for the last four years during which the SANAE 48, 49, 50 and 51 research cruises took place.

The salinity used in this study is practical salinity which is measured in psu and therefore does not have units. The new Thermodynamic Equation of State (TEOS-10) uses absolute salinity in g/kg (IOC, 2010) which was not used in this study. Salinity samples collected from the uncontaminated underway lab supply and from selected depths during the CTD casts on SANAE 50 and SANAE 51, were stored in 250 ml salinity bottles and analysed *in situ* using a Guildline Portasal 8410A portable salinometer unit. During SANAE 50 over 400 salinity samples were analysed continuously throughout the cruise, while during SANAE 51 240 salinity samples were analysed during three discrete sessions towards the end of the cruise, due to a limited number of sea-water standards. The measured salinity samples were then used to test the accuracy of the Idronaut underway conductivity sensor. The times of the underway stations and of the surface CTD samples taken at 5m during the CTD upcast were matched to the underway data to get comparable salinity data points. The underway data was also averaged to the nearest 10 and 20 values at the times of the stations and the CTDs to check if this changed the relationship. When the station salinity values were plotted against the continuous salinity values, the ones averaged to the nearest 10 and to the nearest 20 points showed R^2 values slightly lower than those from the values chosen by matching the station times.

SANAE 50 Idronaut underway salinity compared well to the Portasal salinity for legs 3 and 4 with $R^2 = 0.99$ (Figure 7a). During legs 2 and 5 there were no Portasal salinity measurements so the CTD salinity values at 5m depth were compared to the Idronaut underway salinity values. The Idronaut underway salinities were very similar to the CTD salinities during leg 2, with $R^2 = 0.99$. For leg 5 the Idronaut underway salinity values were approximately 0.16

higher than the CTD salinities and this bias in the leg 5 Idronaut underway salinity data has been corrected for.

During the SANAE 51 cruise, sea ice trapped in the sea water intake disrupted the underway water flow causing air bubbles to get into the underway Idronaut salinity sensor during leg 2. This made the underway Idronaut salinity data questionable during legs 2, 3 and 4 of SANAE 51. To correct for this the Portasal salinity values for legs 3 and 4 were interpolated with latitude using MATLAB R2011a, to obtain a continuous underway salinity dataset (Figure 7b,c). A two hourly running mean was calculated for the Idronaut underway salinity values during leg 4 where Portasal salinity values showed similar patters to Idronaut underway salinity values. There did not appear to be a regular offset between the Idronaut and the Portasal salinity, and therefore the interpolated Portasal salinity values have been used for all Buoy Run stations, rather than the Idronaut underway salinity. Unfortunately due to a lack of salinity bottles there were no Portasal salinity samples for the SANAE 51 ice station CTDs and thus there is no salinity data for leg 2. The air bubbles in the Idronaut underway sensor seemed to be gone by leg 5 and the underway salinity values looked to be accurate, ranging from 33.88 to 34.35psu. The Idronaut underway salinity values for SANAE 48 and SANAE 49 seemed to be accurate as they ranged between 33.04-34.18 and 32.9-34.32 respectively.

Nitrate (NO_3) and silicate (SiO_4) were determined using the Lachat QuikChem 8500 series 2 Flow Injection Analyser (FIA). For Nitrate the 31-107-04-1-E method was used while the 31-114-27-1-D method was used for silicate. The FIA was used on board the r/v SA Agulhas during the SANAE 50 cruise, while for SANAE 51 the nutrient vials were frozen and analysed in the University of Cape Town's Oceanography lab after the cruise. Phosphate (PO_4) was determined manually according to the method described in Grasshoff et al (1983).

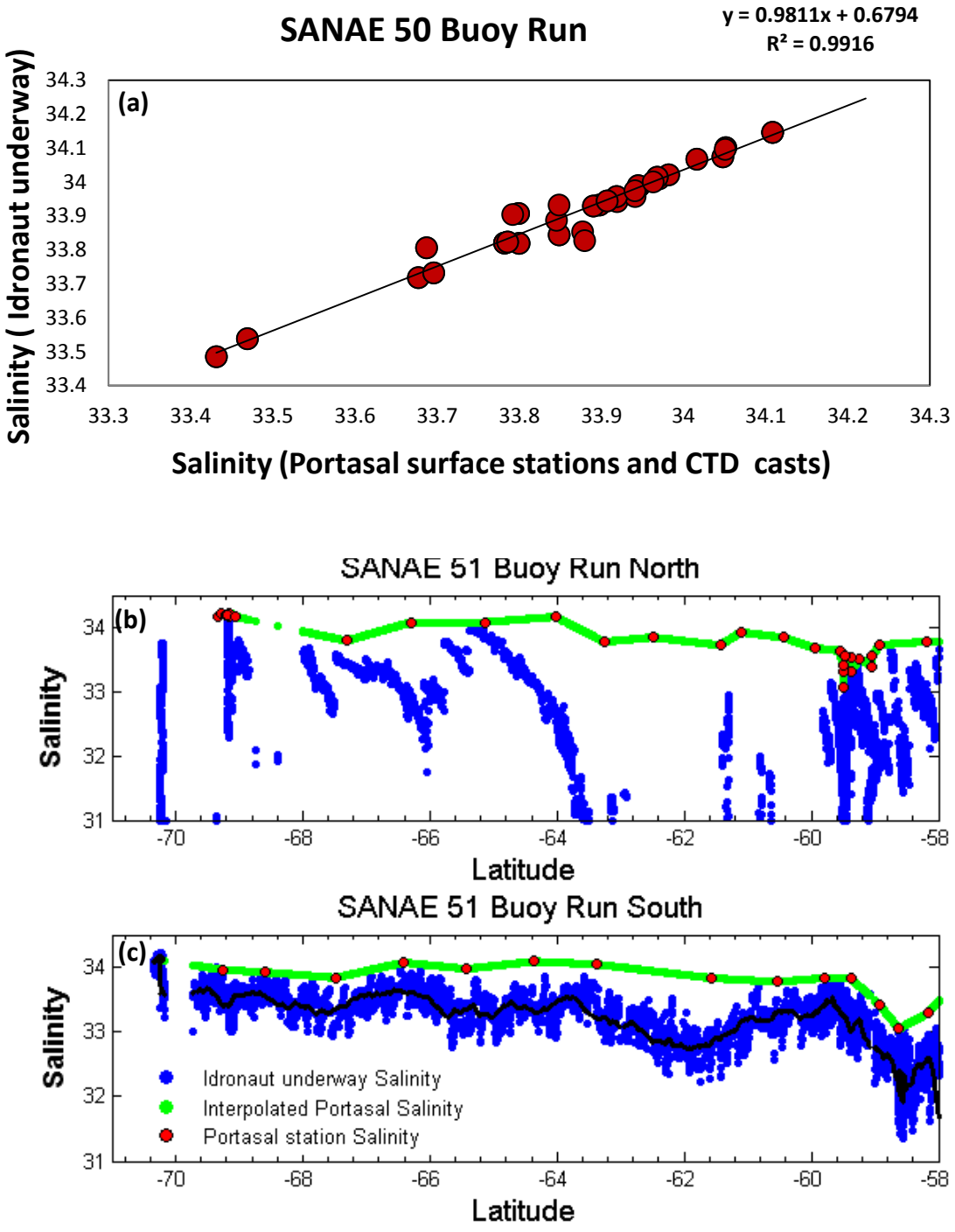

Figure 7. **(a)** Comparison between the Idronaut underway salinity data and the Portasal discrete salinity samples during the northward and southward legs of the SANAE 50 Buoy Run for both underway stations as well as surface CTD samples. Comparison between the SANAE 51 Idronaut continuous underway salinity data, the Portasal discrete salinity samples and the interpolated Portasal discrete salinity samples during **(b)** the northward leg and **(c)** the southward leg of the Buoy Run, with black points showing the 2 hourly running mean of the Idronaut salinity data.

3.3.2 Underway pCO_2 system

The LICOR analyser measures the xCO_2 of the equilibrator gas which is in equilibrium with the xCO_2 of the water. The air measured inside the analyser is dry whereas the air inside the equilibrator is assumed to be at 100% humidity, thus the water vapour pressure is used to correct the measured dry mole fraction (Pierrot et al., 2009):

$$(pCO_2)^{wet}_{equT} = (xCO_2)^{dry}_{equT} [P_{equ} - pH_2O(SSS, equT)] \qquad \text{(eq. 3.3.2.1)}$$

Where $(xCO_2)^{dry}_{equT}$ is the CO_2 mole fraction measured by the gas analyzer, the pH_2O is the water vapour pressure at the salinity of the sea surface and at the equilibrator temperature (equT), and the P_{equ} is the pressure inside the equilibrator. Salinity is needed to calculate the water vapour pressure (Weiss and Price 1980). During SANAE 51 where the underway Idronaut salinity was shown to be inaccurate, the interpolated Portasal salinity values were used to calculate the pH_2O for legs 3 and 4. For legs 2 and 5 where Portsal salinity data was not available, the underway Idronaut salinity was used and thus this fCO_2 data during leg 2 should be viewed with caution. For the other cruises the underway Idronaut salinity values seemed to be accurate except during leg 5 of SANAE 50 where a bias of 0.16psu was corrected for.

The fugacity of CO_2 (fCO_2) was determined through correction of the partial pressure of CO_2 (pCO_2) for non-ideal behaviour (Weiss, 1974). There was found to be a slight difference between the intake temperature and the equilibrator temperature for all four cruises. The average temperature differences were 1.39°C, 1.79°C, 1.05°C and 0.68°C for SANAE 48, 49, 50 and 51 respectively. To correct for this temperature difference, the empirical temperature dependence method of Takahashi et al (1993) was used, where SST is the sea surface temperature:

$$(fCO_2)^{wet}_{SST} = (fCO_2)^{wet}_{equT} \, exp\{0.0423(SST - equT)\} \qquad (eq. 3.3.2.2)$$

Surface water fCO_2, SSS, SST and chlorophyll *a* fluorescence data from the underway system were co-located to the station data as well as to the CTD casts. This was done as in Jones et al (2010), by matching the times of the stations and of the surface CTD sample taken at 5m during the CTD upcast to the underway data. In icy waters the underway data system

was periodically blocked by ice trapped in the sea water intake and thus there are gaps in the data. Chlorophyll *a* fluorescence data periodically showed a strong diurnal cycle which is indicative of fluorescence quenching, a decrease in the fluorescence quantum yield that is commonly observed in the daytime when solar radiation is at its maximum (Sackmann et al., 2008; Frajka-Williams et al., 2009). Fluorescence quenching was highest when conditions were calm, with higher productivity and a stratified upper water column (eg. SANAE 51, leg 2, Figure 8a). To correct for this daytime fluorescence quenching the night time data (10pm to 2am) was averaged and then interpolated to get an estimate of chlorophyll a fluorescence during the study, from which phytoplankton blooms can be identified.

3.3.3 Total alkalinity and dissolved inorganic carbon

Samples for the determination of total dissolved inorganic carbon (DIC) and total alkalinity (TA) concentrations were collected during the underway surface stations as well as from the uncontaminated Niskin bottles at a multitude of depths during CTD casts during the SANAE 50 cruise. Ship based analysis samples were stored in 500 ml bottles with 200 µL of 50 % HgCl (Mercuric Chloride) solution. These samples were analysed *in situ* using the Marianda Versatile Instrument for the determination of total inorganic carbon and titration alkalinity (VINDTA 3C). VINDTA determines the TA by potentiometric titration and from the same sample measures the DIC coulometrically. Certified Reference Materials (CRM's) were run before and after each batch and every fifth sample was run as a duplicate to determine the accuracy and the reproducibility of the VINDTA. Once the nutrient data was processed, raw TA and DIC data were post-calibrated using the MATLAB script (VINDTA_CALCALK) by van Hoven. Accuracy of the TA data was 6µmol/kg and the accuracy of the DIC data was 5µmol/kg.

Surface TA and DIC were normalised to the salinity of Winter Water (WW), in order to correct for effects of dilution, as was done by Jones et al (2010). The salinity correction method proposed by Friis et al (2003) was used, as it is the recommended method if the salinity range of the data is large. The natural slope of the SANE 50 TA and DIC data when plotted against salinity was used to find the x intercept ($TA_{S=0}$ and $DIC_{S=0}$). Both TA and DIC showed a positive salinity relationship, with $TA_{S=0}$ = 176µmol/kg and $DIC_{S=0}$ = 708µmol/kg. These are similar to the values used in Jones et al (2010), where they used $TA_{S=0}$ = 269µmol/kg and $DIC_{S=0}$ = 966µmol/kg. The equation of Friis et al (2011) were then used to

calculate salinity normalised TA (nTA) and salinity normalised DIC (nDIC), where S is the observed salinity and S_{ref} is the salinity of Winter Water, found in this study to be 34.33psu (Table 2)

$$\boldsymbol{nTA = \frac{TA_{obs} - TA_{S=0}}{S} \cdot S_{ref} + TA_{S=0}} \qquad \text{(eq. 3.3.3.1)}$$

A similar equation was used to calculate nDIC.

3.3.4 Empirically calculated carbon data

An optimal second order polynomial fitting TA data to sea surface salinity (SSS) and sea surface temperature (SST) was created for each ocean basin by Lee et al (2006). In this study the equation of Lee et al (2006) with the constants suggested for the Southern Ocean region was used to empirically calculate surface water TA (see eq. 2.6.1). First the continuous SSS and SST data from the underway pCO_2 analyser was checked against the surface station, surface CTD and surface UCTD data for SANAE 49, 50 and SANAE 51, where data was available (see section 3.1)

The corrected SSS and SST data were then used to empirically calculate surface water TA for legs 2, 3, 4 and 5 of all four SANAE cruises. To determine the accuracy of the calculated total alkalinity, the TA calculated from SSS and SST during the SANAE 50 Buoy Run were compared to the *in situ* station and surface CTD measured TA from the VINDTA potentiometric titration. This was done as in Jones et al (2010), by matching the times of the stations and of the surface CTD samples taken at 5m during the CTD upcast, to the continuous surface underway data. The underway data was also averaged to the nearest 10 and 20 values at the times of the stations and the CTDs to check if this changed the relationship. When the calculated TA was plotted against the measured TA, the ones averaged to the nearest 10 and to the nearest 20 points showed R^2 values slightly lower than the ones chosen by matching the station times. Due to this the continuous data points chosen by matching the station times have been used to compare the calculated TA to the measured TA (Figure 8). Calculated TA compared well to underway station data, but not as well to the surface CTD data. This could be due to the fact that while the CTD is being deployed the ship

remains stationary for approximately 45 minutes, and thus the surface water is mixed with deeper water.

Calculated total alkalinity and the continuous underway fCO_2 data were then used to calculate the remaining carbonate parameters necessary for an Ocean Acidification study using the CO2Sys programme (Lewis and Wallace, 1998), with constants K_1 and K_2 from Mehrbach et al, 1973 refit by Dickson and Millero (1987). Thus data sets of continuous surface water DIC, pH, Revelle Factor, carbonate ion concentration, calcite saturation state (Ω_{car}) and aragonite saturation state (Ω_{arag}) were calculated for legs 2, 3, 4 and 5 of the SANAE 48, 49, 50 and 51 cruises.

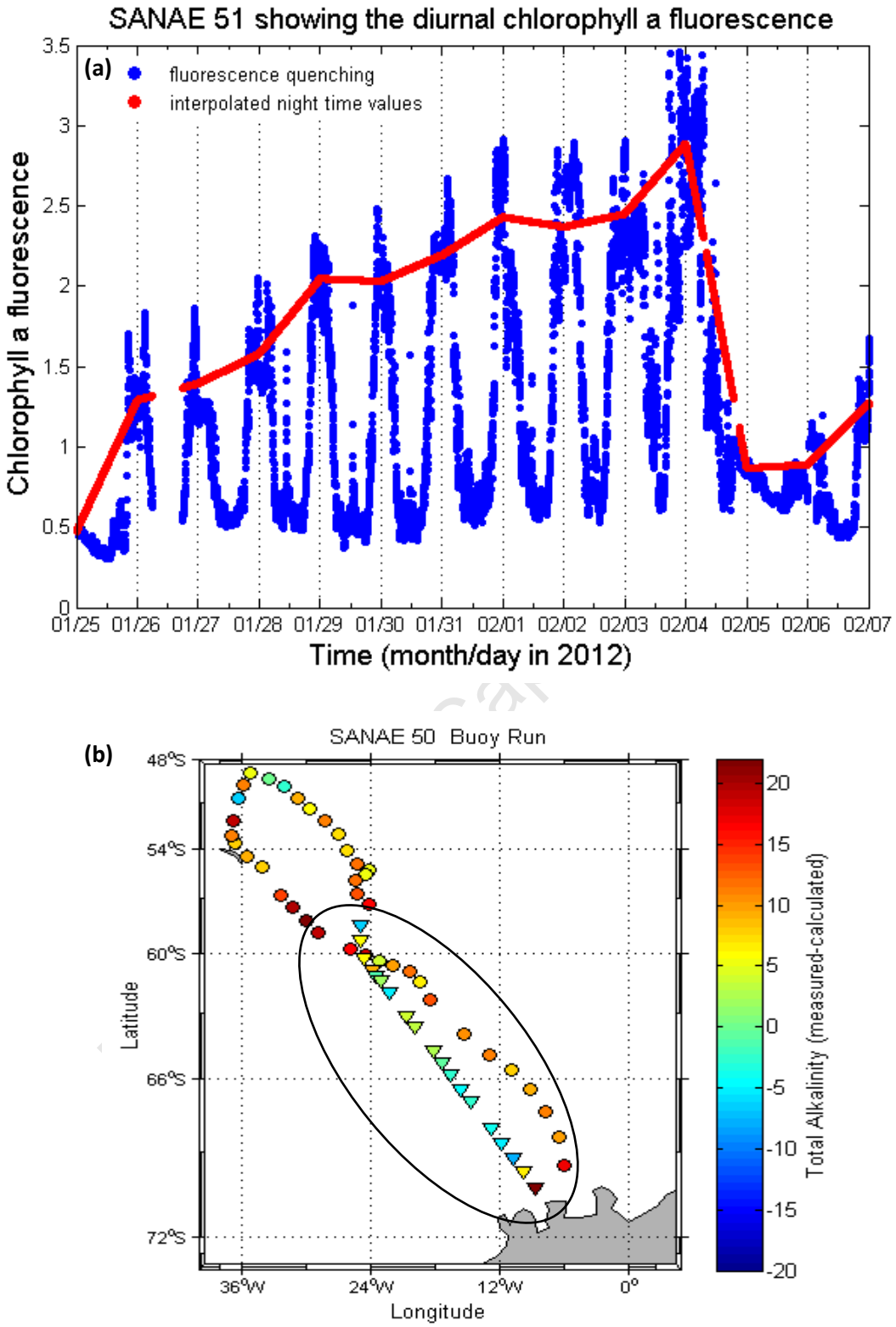

Figure 8. (a) Chlorophyll *a* fluorescence showing the daytime fluorescence quenching in blue and the interpolated night time averaged fluorescence in red, with the grid lines indicating mid night, and **(b)** calculated Total Alkalinity minus measured Total Alkalinity for all Buoy Run station (circles) and surface CTD (triangles) data during the SANAE 50 Buoy Run, with data points collected in the study area circled in black.

Table 2. Station, winter mixed layer depth (WMLD, m), temperature (°C), salinity, nitrate (NO_3, μmol kg−1), silicate (SiO_4, μmol kg−1) and phosphate (PO_4, μmol kg−1) of WW, represented by the winter mixed layer, for all SANAE 50 Ice Shelf and Buoy Run CTDs where TA and DIC were measured.

Station	Latitude	Longitude	WMLD	Temperature	Salinity	NO_3	SiO_4	PO_4
Leg2 CTD 1	-70.27	-8.00	300	-1.72	34.34	27.79	123.52	1.99
Leg2 CTD 8	-69.80	-2.60	200	-1.91	34.25	33.31	102.99	2.39
Leg4 CTD 131	-58.50	-24.95	100	-1.23	34.25	26.28	110.28	1.82
Leg4 CTD 133	-59.33	-24.97	100	-1.37	34.31	28.38	111.43	1.82
Leg4 CTD 136	-60.28	-24.64	100	-1.31	34.08	26.08	102.29	1.76
Leg4 CTD 136	-60.28	-24.64	100	-1.31	34.06	26.08	102.29	1.76
Leg4 CTD 138	-60.87	-23.84	100	-0.84	34.10	22.43	77.95	1.68
Leg4 CTD 139	-61.15	-23.46	80	-1.67	34.25	24.94	116.74	1.83
Leg4 CTD 140	-61.43	-23.07	80	-1.53	34.37	26.27	117.00	1.95
Leg4 CTD 142	-62.00	-22.29	100	-1.59	34.41	20.42	128.47	2.16
Leg4 CTD 142	-62.00	-22.29	100	-1.59	34.41	19.79	123.89	1.89
Leg4 CTD 144	-62.57	-21.49	50	-1.65	34.31	22.63	117.49	1.83
Leg4 CTD 146	-63.13	-20.68	80	-1.69	34.41	21.66	119.64	1.92
Leg4 CTD 148	-63.69	-19.86	80	-1.69	34.41	18.70	122.98	2.13
Leg4 CTD 150	-64.23	-19.03	100	-1.68	34.38	21.10	96.41	2.02
Leg4 CTD 152	-64.78	-18.19	80	-1.76	34.40	21.92	98.43	1.86
Leg4 CTD 154	-65.31	-17.37	100	-1.78	34.38	17.95	104.64	1.93
Leg4 CTD 156	-65.85	-16.51	80	-1.79	34.36	19.01	102.58	1.86
Leg4 CTD 158	-66.44	-15.56	70	-1.79	34.36	20.12	106.72	1.95
Leg4 CTD 160	-66.98	-14.64	80	-1.82	34.43	21.23	108.95	1.89
Leg4 CTD 162	-67.54	-13.70	70	-1.49	34.42	26.73	92.59	1.77
Leg4 CTD 164	-68.07	-12.78	85	-1.64	34.42	28.07	103.78	1.89
Leg4 CTD 166	-68.63	-11.77	60	-1.60	34.34	26.03	106.13	1.86
Leg4 CTD 168	-69.19	-10.77	55	-1.53	34.35	26.62	115.86	1.87
Leg4 CTD 172	-70.29	-8.68	180	-1.68	34.41	27.28	102.90	1.96
Mean WW			101±53	-1.59±0.23	34.33±0.11	24.03±3.83	108.64±11.43	1.91±0.15

Table 3. Station, measured total alkalinity (TA, µmol/kg), measured dissolved inorganic carbon (DIC, µmol/ kg), calculated pH, fCO_2 (µatm), carbonate ion concentration (CO_3^{2-}, µmol/kg), Revelle Factor (Revelle), Ω_{car} (calcium carbonate saturation state) and Ω_{arag} (aragonite saturation state) of WW, represented by the winter mixed layer, for all SANAE 50 Ice Shelf and Buoy Run CTDs where TA and DIC were measured. Station positions and winter mixed layer depths are shown in table 2 above.

Station	DIC	TA	pH	fCO_2	CO_3^{2-}	Revelle	Ω_{car}	Ω_{arag}
Leg2 CTD 1	2201.74	2334.69	8.09	330.01	98.19	15.17	2.22	1.39
Leg2 CTD 8	2214.46	2325.78	8.04	379.40	86.51	16.20	2.00	1.25
Leg4 CTD 131	2209.22	2307.23	7.99	426.87	79.92	16.72	1.88	1.18
Leg4 CTD 133	2208.60	2326.07	8.05	372.31	90.40	15.84	2.13	1.34
Leg4 CTD 136	2183.08	2314.03	8.09	334.49	97.59	15.19	2.30	1.45
Leg4 CTD 136	2181.81	2312.34	8.09	334.88	97.33	15.21	2.30	1.44
Leg4 CTD 138	2192.13	2312.87	8.05	366.29	92.45	15.66	2.18	1.37
Leg4 CTD 139	2198.65	2323.27	8.08	348.03	94.06	15.50	2.23	1.40
Leg4 CTD 140	2205.98	2332.07	8.07	350.04	95.02	15.45	2.25	1.41
Leg4 CTD 142	2218.50	2334.31	8.04	377.20	89.29	15.95	2.10	1.32
Leg4 CTD 142	2217.13	2334.12	8.05	373.14	90.10	15.88	2.12	1.33
Leg4 CTD 144	2198.60	2319.12	8.06	358.41	91.81	15.67	2.19	1.37
Leg4 CTD 146	2210.85	2309.49	8.00	418.72	80.01	16.69	1.89	1.19
Leg4 CTD 148	2206.41	2326.23	8.06	362.86	91.29	15.73	2.16	1.36
Leg4 CTD 150	2213.37	2325.08	8.04	382.78	87.20	16.13	2.05	1.29
Leg4 CTD 152	2210.80	2324.59	8.04	375.66	88.37	16.02	2.09	1.31
Leg4 CTD 154	2209.95	2329.52	8.06	361.07	91.42	15.77	2.15	1.35
Leg4 CTD 156	2207.34	2324.03	8.05	367.02	89.86	15.89	2.13	1.34
Leg4 CTD 158	2203.97	2326.96	8.07	351.93	93.24	15.60	2.21	1.39
Leg4 CTD 160	2210.38	2326.39	8.05	369.64	89.46	15.92	2.12	1.33
Leg4 CTD 162	2214.26	2323.56	8.03	392.68	86.20	16.22	2.04	1.28
Leg4 CTD 164	2218.31	2322.30	8.01	405.70	83.18	16.48	1.97	1.23
Leg4 CTD 166	2208.74	2323.35	8.05	375.73	88.83	15.97	2.11	1.33
Leg4 CTD 168	2211.19	2319.72	8.03	393.66	85.51	16.24	2.03	1.28
Leg4 CTD 172	2211.66	2348.62	8.10	325.36	101.20	15.03	2.34	1.47
Mean WW	2206.69±9.61	2324.23±9.01	8.05±0.03	369.36±25.75	90.34±5.3	15.85±0.45	2.13±0.12	1.34±0.07

3.4 Future predictions of surface water carbonate ion, Ω_{arag} and pH

Surface water fCO_2 was increased from its current value in 10µatm increments and used in the CO2Sys programme (Lewis and Wallace, 1998), with constants K_1 and K_2 from Mehrbach et al, 1973 refit by Dickson and Millero (1987) with surface water TA, SST, SSS and nutrients remaining unchanged from their present conditions, to calculate possible future ocean $[CO_3^{2-}]$, Ω_{arag} and pH. When surface water fCO_2 was increased by 160µatm, the calculated Ω_{arag} fell below the level of aragonite saturation (Ω_{arag}=1) at some point during all four of the cruises. An atmospheric fCO_2 increase of 160µatm is predicted to occur by the year 2054 according to the IS92a atmospheric CO_2 increase scenario (IPCC (2007). Although there is disequilibrium between the increase in atmospheric CO_2 and surface ocean CO_2 (McNeil and Matear, 2008), for the scope of this study we have assumed that surface water CO_2 will increase at a similar rate to atmospheric CO_2. While this is not very accurate, it will give us some idea of the timing of surface water aragonite undersaturation. Thus the first future ocean fCO_2 increase sensitivity test that will be investigated during this study is when surface ocean fCO_2 increased by 160µatm, resulting in the periodic aragonite undersaturation of the Antarctic ice shelf and Weddell Gyre surface waters.

A second future ocean carbonate predictions was conducted by doubling the surface water fCO_2 while again leaving TA, SST and SSS unchanged. The CO2Sys programme was again used to calculate $[CO_3^{2-}]$ and pH using the doubled fCO_2 and unchanged TA, SST and SSS, as was done in Orr et al (2005). A sensitivity test was conducted to determine the effects on variability in temperature and salinity on Ω, using the WW estimations (see tables 2 and 3). When temperature was increased from -2 to 2°C, Ω_{arag} increased, on average, by 0.02, approximately 2.4% of the summer seasonal increase in Ω_{arag}. Salinity was increased from 33 to 34.5 psu, resulting in a mean decrease in Ω_{arag} of 0.01, approximately 1.2% of the summer seasonal increase in Ω_{arag} This suggests that photosynthesis and dilution have a much greater effect on Ω_{arag} than the variability in temperature and salinity observed during this study.

4. Results

The Southern Ocean Carbon-Climate Observatory programme (SOCCO) has conducted underway observation cruises from South Africa to Antarctica since 2008 aboard the polar supply and research ship, SA Agulhas. During these cruises, continuous underway surface measurements, UCTD and CTD measurements of ocean carbon (fCO_2, TA, DIC), temperature, salinity and nutrients at the Antarctic Ice Shelf (IS) between 71-68°S 2°E-14°W and within the Eastern Weddell Gyre (EWG) were recorded. Not all of the data collected in the EWG will be used during this study, only the data between 68-58°S 2°E-31°W (Figure 9). The northern extent of this study was chosen to be 58°S as the southern boundary of the Weddell Gyre lies at 58°S, north of which is the Antarctic Circumpolar Current. The cruise leg dates for SANAE 48, 49, 50 and 51 are shown in table 1 and their chronology is summarised in the diagram below. The r/v SA Agulhas sailed from Cape Town (CT) to Antarctica, to South Georgia Island (S.Georgia), back to Antarctica and then to Cape Town (CT) during all four SANAE cruises.

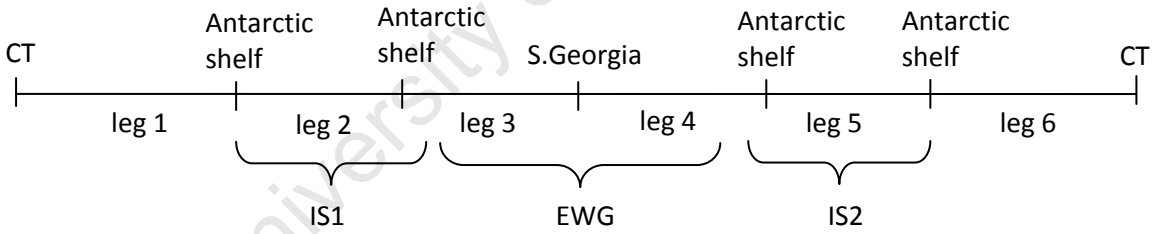

Austral summer sea surface temperature (SST), surface water salinity (SSS), fCO_2, TA, DIC, carbonate ion concentration [CO_3^{2-}], Revelle Factor, aragonite saturation state (Ω_{arag}) and pH, are investigated for the Austral summers in 2008/2009, 2009/2010, 2010/2011 and 2011/2012. The data will be analysed as follows for all years: Ice Shelf 1 (IS1) is the data collected south of 68°S during leg 2 and the beginning of leg 3 at the ice shelf in the vicinity of 4°E-14°W. The Eastern Weddell Gyre (EWG) data is the data collected between 68-58°S on legs 3 and 4, during the transects to and from South Georgia Island. Ice Shelf 2 (IS2) is the data collected south of 68°S during the last part of leg 4 and leg 5 at the ice shelf in the vicinity of 4°E-14°W (see diagram above). IS1 and IS2 will be analysed as a temporal sequence at the ice shelf, separately from the EWG.

The importance of summer primary production and surface water dilution from summer sea ice melt on the seasonal and interannual variability of Ω_{arag} will be analysed for IS1 and IS2. The influence of interannual variability in the timing of sea ice thaw on surface water properties is examined for the ice shelf region, to understand the controlling mechanisms behind variability in surface water $\Omega_{arag.}$ The progression of surface water biogeochemical properties from early summer water during December and early January to late summer water during late January and February will be analysed. The EWG data was only collected during a 2-3 week period in January of all years, and the seasonal dynamics of the marine carbonate system in the EWG could therefore not be fully resolved. Winter water (WW) sampled from SANAE 50 CTDs was used as a proxy for winter surface water during all years. Surface water $[CO_3^{2-}]$ and Ω_{arag} are averaged into weekly bins for the IS and for the EWG, and the interannual variability of the marine carbonate system at the ice shelf and in the EWG is investigated. All years showed freshening of the surface water during January as summer progressed (Figures 11a,16a,21a,26a) and as sea ice melted-but there were important differences in the phasing of the seasonal cycle of ice melt.

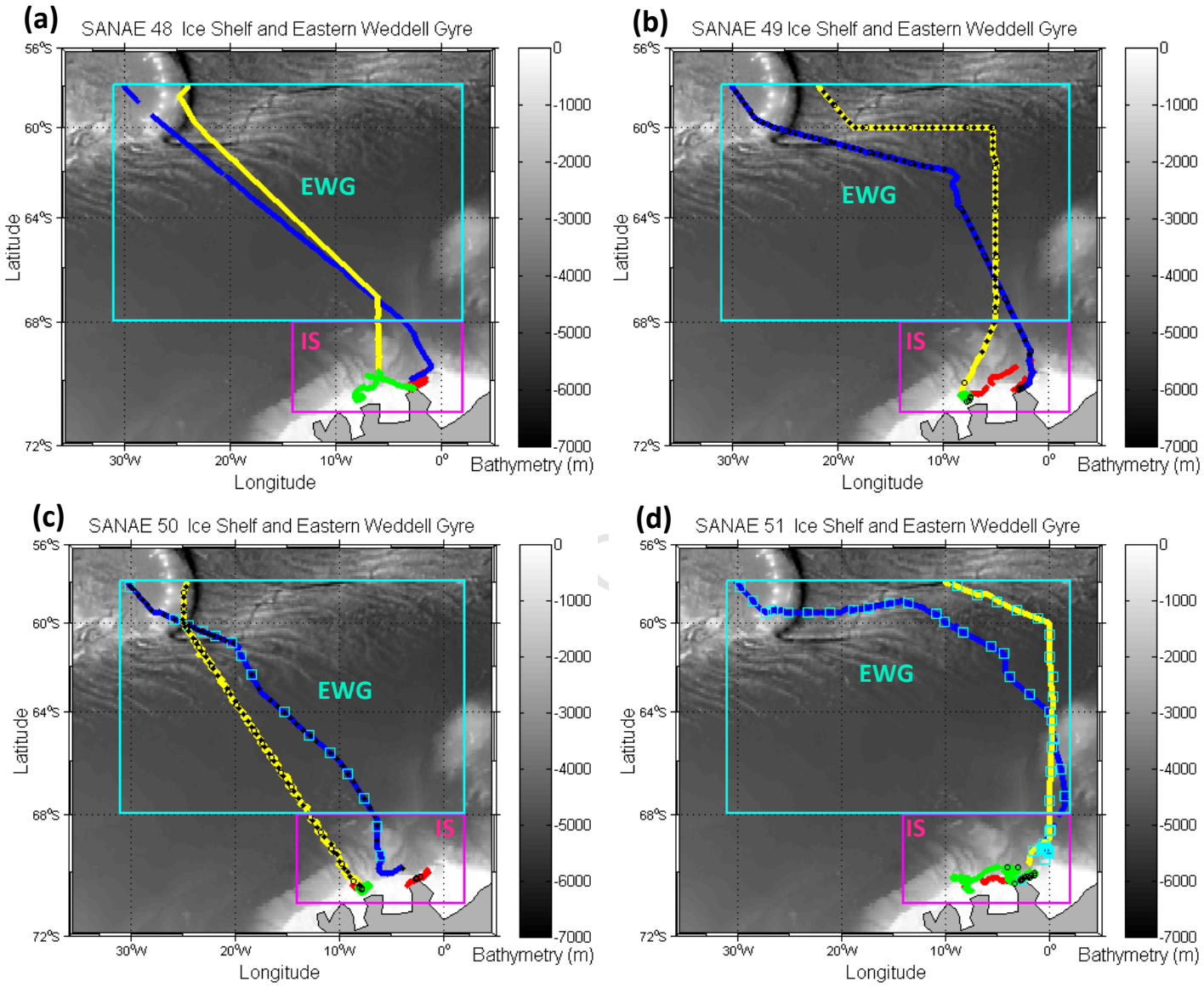

Figure 9. Map showing the cruise track for of SANAE 58 **(a)**, SANAE 49 **(b)**, SANAE 50 **(c)** and SANAE 51 **(d)** using a combination of continuous underway data, CTD, UCTD and nutrient stations collected aboard the polar supply and research vessel, SA Agulhas. Continuous underway data for legs 2 (red), 3 (blue), 4 (yellow) and 5 (green) between 71-68°S and 2°E-31°W are shown with the gaps due to the underway machine being blocked by sea ice. Also plotted are CTD stations (black circles), UCTD stations (black dots) and underway nutrient stations (cyan squares). The Eastern Weddell Gyre (EWG) and the Ice Shelf (IS) study regions are marked by the cyan and pink squares respectively. Regional bathymetry (ETOPO2) is overlaid for the region.

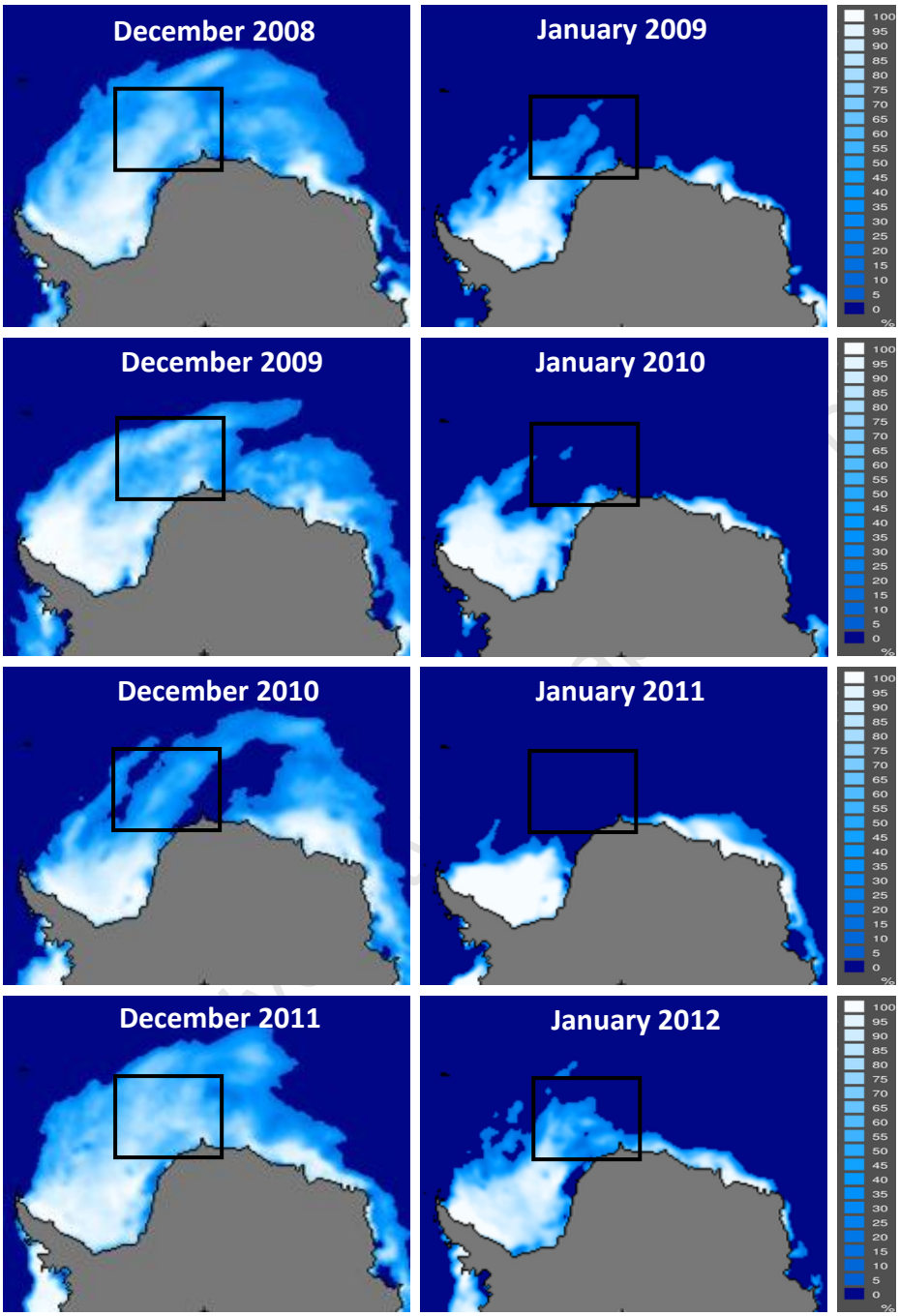

Early sea ice melt at the ice shelf

Late sea ice melt in the EWG

"Normal" sea ice melt at the ice shelf

"Normal" sea ice melt in the EWG

Early sea ice melt at the ice shelf

Early sea ice melt in the EWG

Late sea ice melt at the ice shelf

Late sea ice melt in the EWG

Figure 10. Monthly Sea Ice Concentration Images obtained from the National Snow & Ice Data Centre (NSIDC) for the Southern Hemisphere for December (2008, 2009, 2010, 2011) and for January (2009, 2010, 2011, 2012), (Fetterer et al., 2002, updated 2009). The study region is shown by the black square and the phasing of sea ice melt during each year is stated on the right of the figure. Early or late is relative to a mid-December sea ice thaw which is optimal for bloom initiation (Thomalla et al., 2011).

4.1 Surface water temperature, salinity and carbonate parameters

The surface water characteristics during all four years were influenced by the variability in the phasing of the seasonal sea ice thaw. To understand the intra-annual and interannual differences in the surface water properties, the timing of sea ice melt during December and January needed to be considered. The two first order mechanisms that change TA and DIC that will be analysed in this study are primary production and dilution. Primary production decreases DIC and TA in a ratio of 117:-16 (Anderson and Sarmiento, 1994) due to the uptake of CO_2 which decreases DIC, and the uptake of NO_3^- during photosynthesis which decreases H^+ ions in the surrounding water therefore increasing TA. The effects of photosynthesis on TA could not be quantified in this study as there was not sufficient nitrate data. The second order processes that affect TA and DIC are air-sea exchange of CO_2, calcification and the formation and dissolution of ikaite (Jones et al., 2010), which will not be emphasised in this study although they are important to the high latitude carbon cycle.

Surface water properties at the ice shelf during each summer cruise are described in the following and their variability is examined in detail in the discussion. Surface water properties in EWG are not looked at in detail due to the lack of temporal data, but their mean values are compared to the ice shelf seasonal cycle.

4.1.1 SANAE 48

SANAE 48 was around 2 weeks late with respect to the other four SOCCO cruises. The r/v SA Agulhas arrived at the Antarctic ice shelf on the 8th January 2009 and left the ice shelf on the 20th February 2009 to return to Cape Town. In both December 2008 and January 2009 sea ice melted early at the ice shelf relative to the summers of 2010 and 2012 (Figure 10). In the EWG the opposite was seen, where sea ice melt was relatively late.

The surface water in the ice shelf became fresher as summer progressed and sea ice melted, fluctuating between 33.00 and 34.10psu (Figure 11a). Winter Water (WW) sea surface salinity (SSS) was estimated to be 34.33±0.11psu which suggests that by the time IS1 was conducted, sea ice melt had formed a layer of fresher Summer Surface Water (SSW) above the denser WW. SST ranged between -2.00 and 0.60°C for all regions except for some areas during IS2 where the SST went below -2°C (Figure 11b). We feel that it is important to note

at this point in the thesis that water with SST's of below -2°C is likely supercooled water, as the freezing point for this region with salinities between 33 and 34.4 is -1.88°C (Bakker et al, 2008). A recent study by Shi et al (2011) found supercooled water (water with temperatures below freezing point) in Prydz Bay, Antarctica, where water temperatures ranged between -2.14 and -1.96°C, up to 0.16°C below the *in situ* freezing point. They conclude that the supercooled water formed in a cavity below the ice shelf where very cold waters are found (around -2°C) and where its density was decreased by the addition of ice melt water from the base of the sea ice. Through upwelling processes or by the melting of the sea ice above this cold water, its upper boundary is removed and it rises rapidly as it is less dense than the surrounding water. Once the temperature of this cold water reaches the *in situ* freezing point, supercooling takes place (Shi et al., 2011). As supercooled water is not key to our study, this will not be discussed further in the discussion.

Surface water fCO_2 was undersaturated (below the mean atmospheric fCO_2 of 376µatm) during both ice shelf periods ranging between 180 and 350µatm, with lower fCO_2 values correlating to elevated chlorophyll *a* fluorescence (Figure 11c). Although no statistics was done on the data, from visually inspecting the data it could be seen that fCO_2 and chlorophyll a fluorescence were correlated, as during periods when chlorophyll a was high, fCO_2 was usually undersaturated. Chlorophyll *a* fluorescence was highest during late January and early February, after which it decreased, with fCO_2 remaining below 350µatm.

Table 4. Mean values of sea surface salinity (SSS, psu), sea surface temperature (SSS, °C) and fCO_2 (µatm) for the first ice station (IS1), the second ice station (IS2) and the Eastern Weddell Gyre (EWG) during SANAE 48.

	Mean values for IS1			Mean values for IS2			Mean values for EWG		
Cruise	SSS	SST	fCO_2	SSS	SST	fCO_2	SSS	SST	fCO_2
SANAE 48	33.68	-1.02	231.0±26	33.48	-1.96	241.9±19	33.90	-0.93	335.9±20

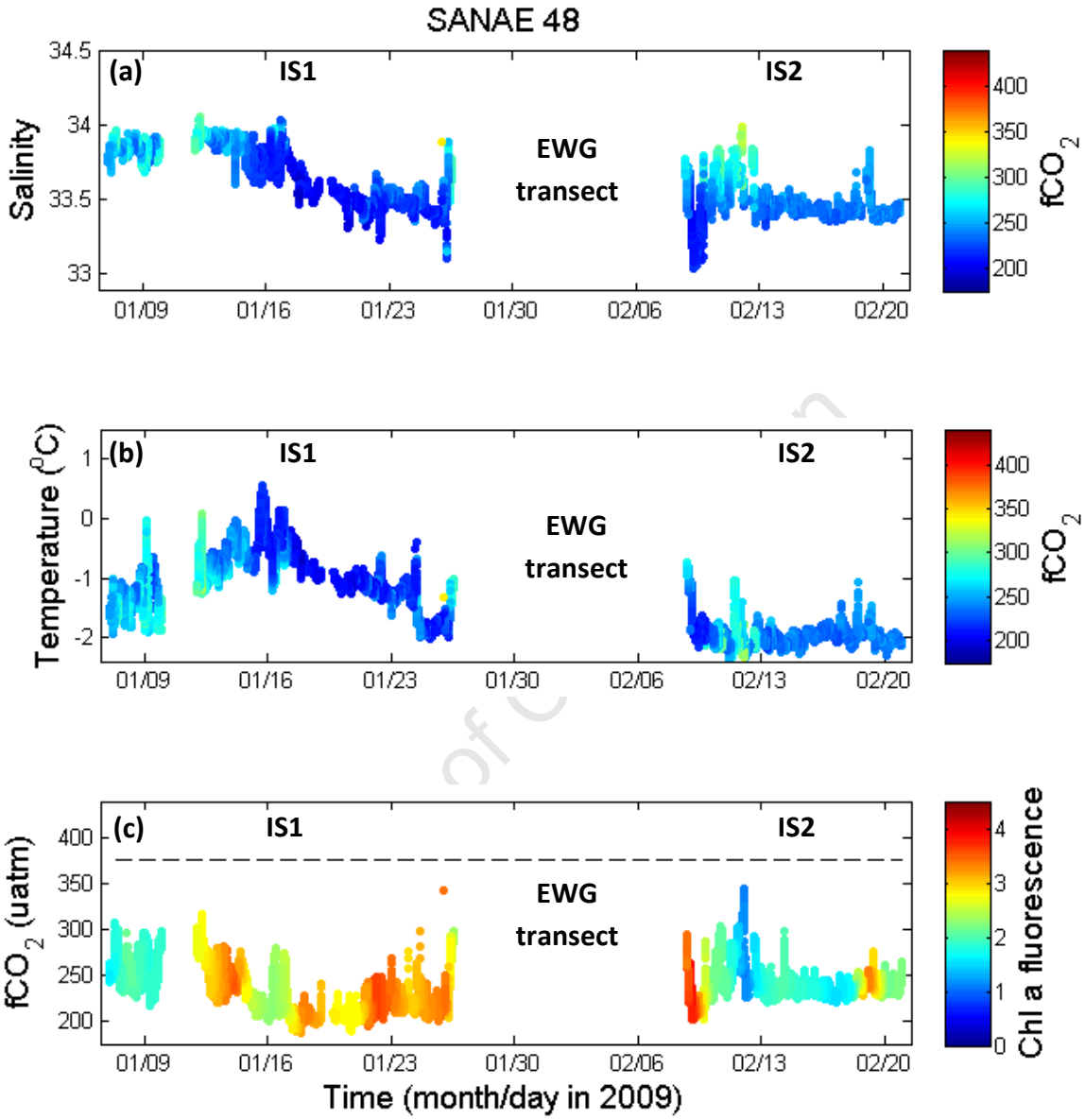

Figure 11. (a) Sea surface salinity with fCO_2 in colour, **(b)** Sea surface temperature with fCO_2 in colour and **(c)** Sea surface fCO_2 with Chlorophyll a fluorescence in colour and with mean atmospheric fCO_2 of 376µtm shown by the dashed black line, during SANAE 48 IS1 and IS2, with the gap due to spatial data collected in the EWG from the 26th January to 8th February 2009.

TA at IS1 and IS2 ranged between 2270-2306µmol/kg and 2264-2311µmol/kg respectively (Figure 12a). A slight decreasing trend was seen in TA from early January to February due to sea ice melt, diluting the surface water and decreasing SSS as summer progressed, with a mean TA during IS1 of 2289.3µmol/kg and during IS2 of 2284µmol/kg (Table 5). Ice shelf DIC decreased from early January to late January during IS1, with a mean concentration of 2105.8µmol/kg, after which it increased slightly during IS2 in February most likely due to the ingasing of atmospheric CO_2 (Table 5). DIC at the ice shelf was almost always below 2150µmol/kg, dropping below 2100µmol/kg between 15th and 23rd January 2009 when chlorophyll *a* fluorescence was high and fCO_2 was below 250µatm (Figure 11c,12b). [CO_3^{2-}] increased initially during IS1 after which it decreased, with mean values of 130.1 and 119.8µmol/kg during IS1 and IS2 respectively (Table 5). [CO_3^{2-}] was supersaturated during IS1 and IS2, reaching a maximum of 154µmol/kg on the 18th January and never decreasing below 100µatm (Figure 12c). The Revelle Factor ranged between 11.5 and 15 during both ice stations, with the exception of a higher peak on the 12th February (Figure 13a), increasing from early to mid-January and then decreasing slightly. Ω_{arag} was > 1, fluctuating between 1.5 and 2.5 during IS1 and IS2 (Figure 13b), with a mean value during IS1 and IS2 of 1.97 and 1.91 respectively (Table 5). Surface water pH was above 8.1 during both ice stations, decreasing slightly from IS1 to IS2 with a mean value of 8.24 and 8.22 respectively (Figure 13c).

Mean surface water fCO_2 at both IS1 and IS2 was almost 100µatm lower than the mean fCO_2 recorded in the EWG where sea ice melt was late (Table 4). In the EWG, the mean TA and DIC were higher than at the mean TA and DIC at the ice shelf, while the mean [CO_3^{2-}] and Ω_{arag} were both lower than the mean [CO_3^{2-}] and Ω_{arag} at the ice shelf (Table 5).

All available ice shelf surface data was averaged to get a monthly average TA and DIC for January and February, with winter conditions estimated from SANAE 50 CTD's (Table 3), (Figure 14a). In the EWG data was collected only during January and thus a mean summer TA and DIC was calculated. The seasonal evolution of Ω_{arag} at the ice shelf shows that Ω_{arag} increases from winter (Ω_{arag}=1.34) to January (Ω_{arag}=1.97), with a decrease in both TA and DIC. Ω_{arag} decreased slightly from January to February when DIC increased likely due to the ingasing of atmospheric CO_2 and TA decreased through dilution from sea ice melt (Figure 14a). Salinity normalised TA (nTA) and DIC (nDIC) show the seasonal evolution of Ω_{arag} at the ice shelf in the absence of dilution, which decreases both TA and DIC (Figure 14b). Without the effects of dilution, Ω_{arag} reaches a maximum in January of approximately 2.4.

The effects of photosynthesis on TA could not be investigated as there was not sufficient nitrate data. The uptake of NO_3^- during photosynthesis decreases the H^+ ions in the surrounding water, increasing the TA, which is likely the cause of the increase in nTA as nDIC is decreased as seen in figure 14b.The influence of dilution on Ω_{arag} was much higher at the ice shelf than in the EWG (Figure 14).

Table 5. Mean values of total alkalinity (TA, µmol/kg),dissolved inorganic carbon (DIC, µmol/kg) carbonate ion concentration (CO_3^{2-}) and aragonite saturation state (Ω_{arag}) for the first ice station (IS1), the second ice station (IS2) and the Eastern Weddell Gyre (EWG) during SANAE 48.

	Mean values for IS1				Mean values for IS2				Mean values for EWG			
Cruise	TA	DIC	CO_3^{2-}	Ω_{arag}	TA	DIC	CO_3^{2-}	Ω_{arag}	TA	DIC	CO_3^{2-}	Ω_{arag}
SANAE 48	2289.3	2105.8	130.1	1.97	2284.0	2117.1	119.8	1.91	2298.9	2170.6	98.2	1.48

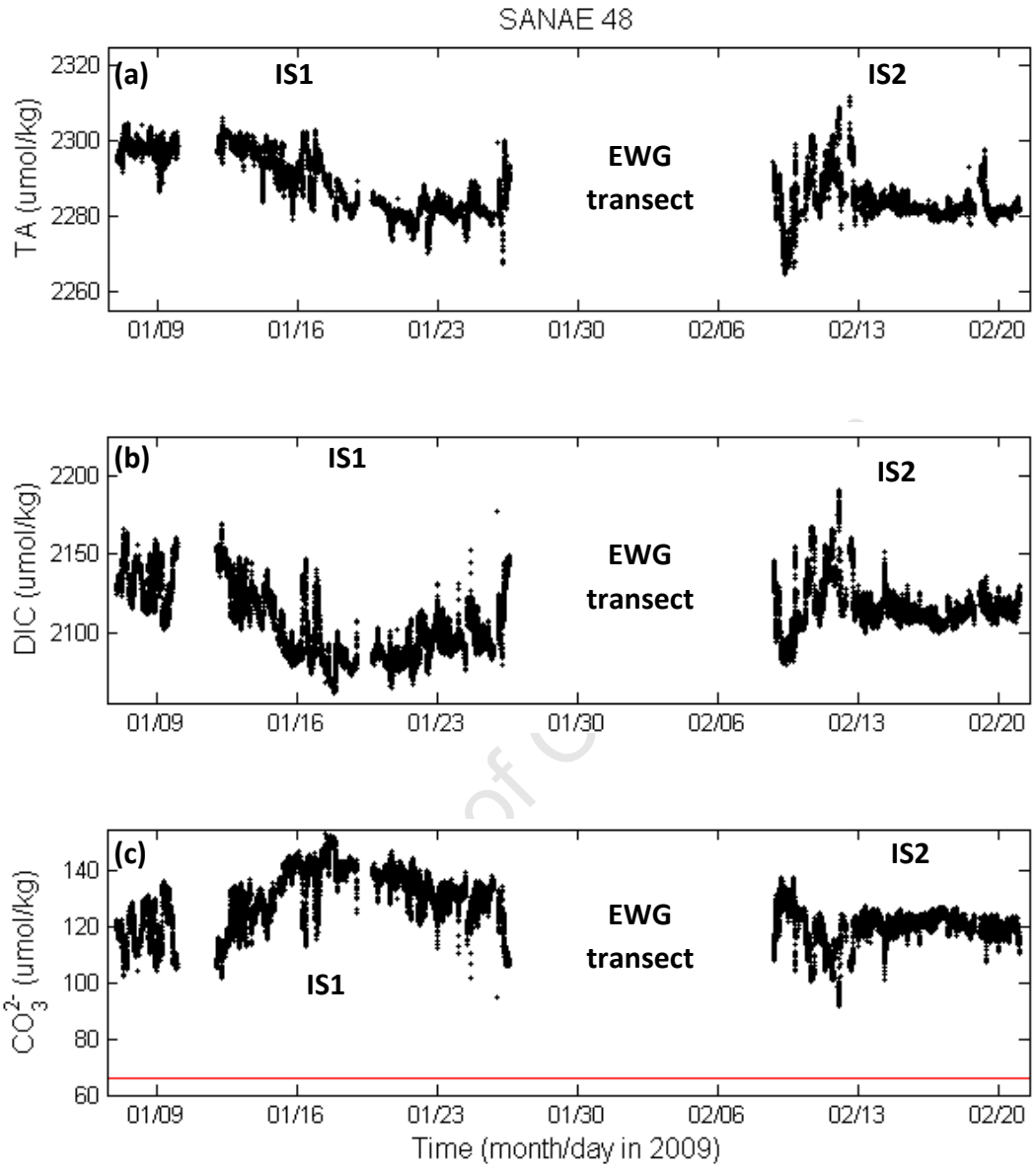

Figure 12. (a) Total alkalinity (TA), **(b)** dissolved inorganic carbon (DIC), **(c)** carbonate ion concentration (CO_3^{2-}) with a red line indicating the carbonate ion concentration below which aragonite becomes undersaturated (66µmol/kg), during SANAE 48 IS1 and IS2, with the gap due to spatial data collected in the EWG from the 26th January to 8th February 2009. The seasonality in CO_3^{2-} concentration can be seen **(c)** reaching a maximum during mid-January when DIC was at a minimum.

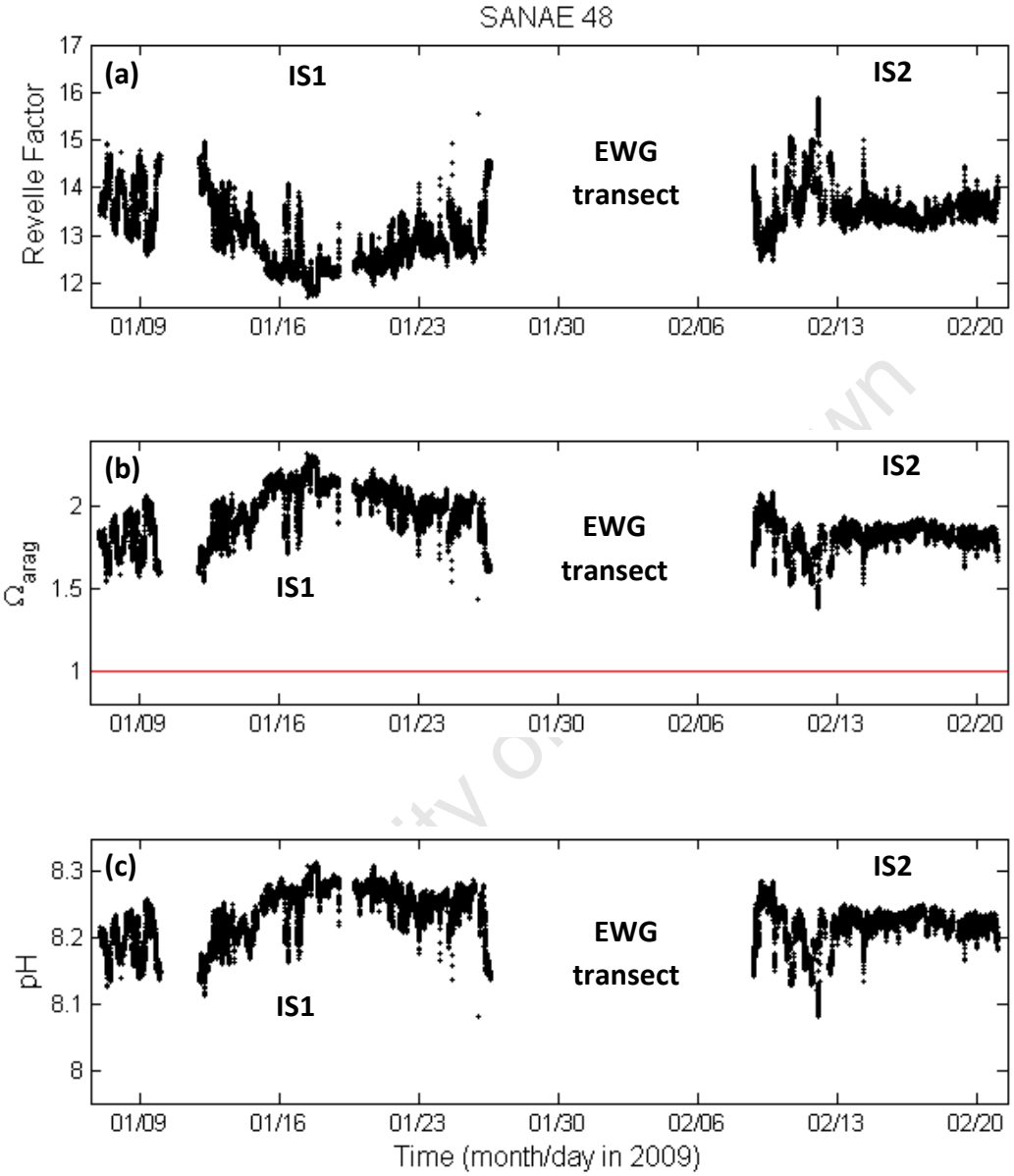

c

Figure 13. (a) Revelle Factor, **(b)** aragonite saturation state (Ω_{arag}) with a red line indicating the aragonite saturation horizon (Ω_{arag}=1), **(c)** pH, during SANAE 48 IS1 and IS2, with the gap due to spatial data collected in the EWG from the 26th January to 8th February 2009.

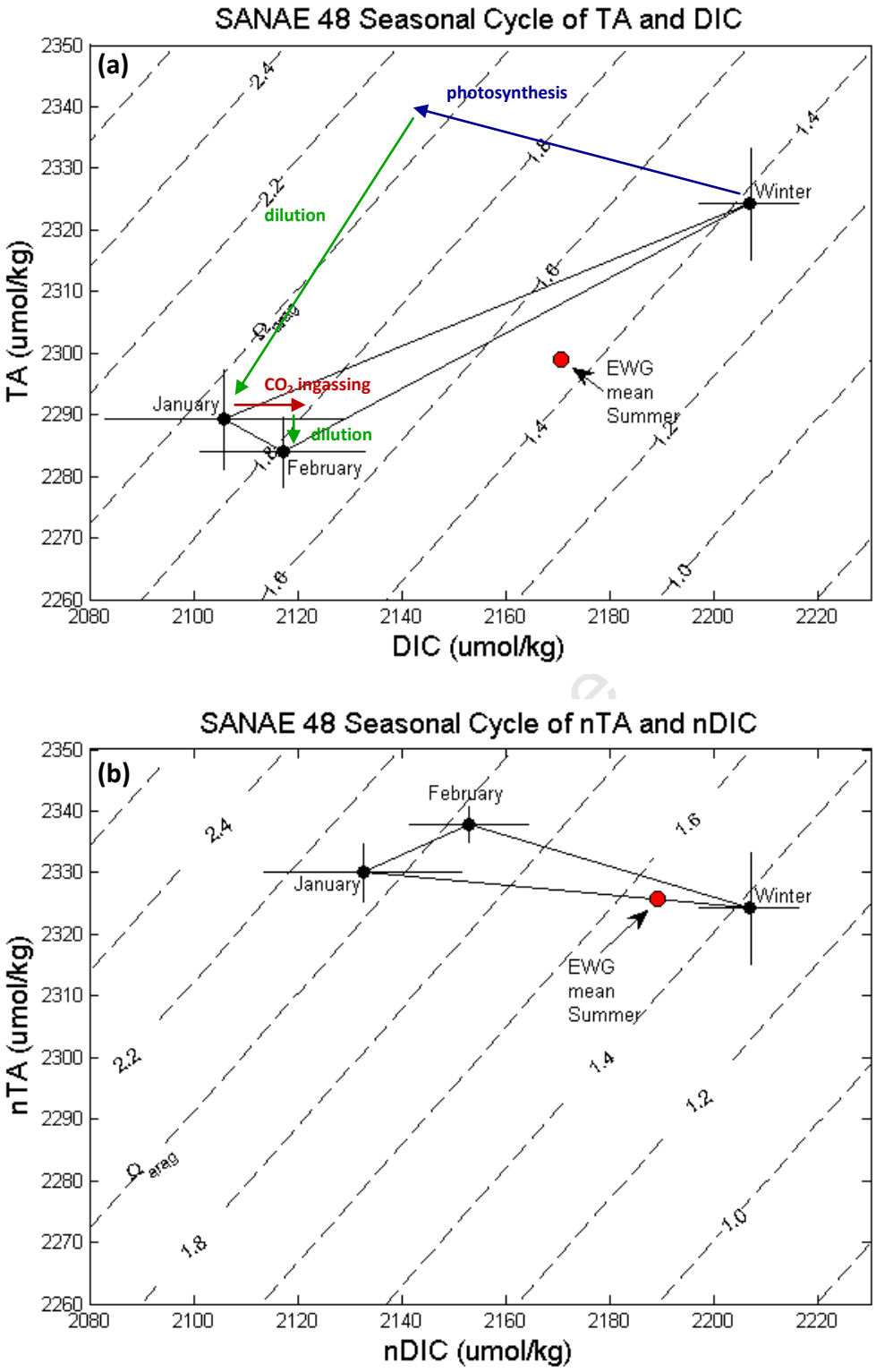

Figure 14. Seasonal evolution of **(a)** mean January 2009 and February 2009 total alkalinity (TA) and dissolved inorganic carbon (DIC) at the ice shelf with vectors indicating various processes that altered TA and DIC, as inferred from the salinity normalised TA (nTA) and salinity normalised DIC (nDIC) below, with the mean summer EWG TA and DIC shown in red and **(b)** mean January 2009 and February 2009 nTA and nDIC at the ice shelf with the mean summer EWG nTA and nDIC shown in red. Winter surface water conditions have been estimated from SANAE 50 CTDs, contours show aragonite saturation state (Ω_{arag}) at -1°C and 33.86psu.

4.1.2 SANAE 49

Ice shelf data collection during SANAE 49 began on the 2nd January 2010, a week earlier than the SANAE 48 cruise. The timing of sea ice melt at the ice shelf was similar to the previous year, with slightly later sea ice thaw along the Antarctic ice shelf between 5°E and 15°S, where IS1 and IS2 took place, and earlier sea ice thaw in the EWG (Figure 10). In comparison to the other three years, the timing of sea ice melt at the ice shelf and in the EWG during December 2009 and January 2010 (SANAE 49) is approximated as the 'normal' situation. CTD and UCTD data was only available during IS1 and in the EWG and has been plotted on the same scales as used for SANAE 50 and 51 to see the interannual variability in the underlying water properties. The Mixed Layer Depth (MLD) is shown on the CTD and UCTD contour plots to get an idea of the water column stratification, which is important in Marginal Ice Zones (MIZ) in relieving light limitation and facilitating phytoplankton blooms (Smith and Nelson, 1986).

Surface water during IS1 was saltier than in the previous year, with an average SSS of 33.85psu (Table 6). From 1st-9th January the SSS fluctuated around the relatively high value of 34.1 (which is close to 34.2, the salinity of WW), after which it dropped to 33.5psu and then varied between 33.5 and 33.3psu during the remainder of IS1 (Figure 15a). During IS2, SSS was low, with a mean value of 33.14psu (Table 6). SST was low during the first week of IS1 and during IS2, fluctuating between -1.8 and -0.5°C (Figure 15b). SST increased to 1°C on the 9th January 2010 after which it varied between -1.9 and 1°C. During both IS1 and IS2 the fCO_2 was predominantly undersaturated, with the exception of a four day period during January where fCO_2 increased above the mean atmospheric value of 376µatm (Figure 15c). Between the 11th and 15th of January during IS1, fCO_2 increased to 440µatm coinciding with a deepening of the MLD and very low chlorophyll *a* fluorescence (Figures 15c,16a).

Table 6. Mean values of sea surface salinity (SSS, psu), sea surface temperature (SSS, °C) and fCO_2 (µatm) for the first ice station (IS1), the second ice station (IS2) and the Eastern Weddell Gyre (EWG) during SANAE 48 and 49.

	Mean values for IS1			Mean values for IS2			Mean values for EWG		
Cruise	SSS	SST	fCO_2	SSS	SST	fCO_2	SSS	SST	fCO_2
SANAE 48	33.68	-1.02	231.0±26	33.48	-1.96	241.9±19	33.90	-0.93	335.9±20
SANAE 49	33.85	-1.16	322.8±22	33.14	-0.99	293.9±25	33.89	0.50	315.2±46

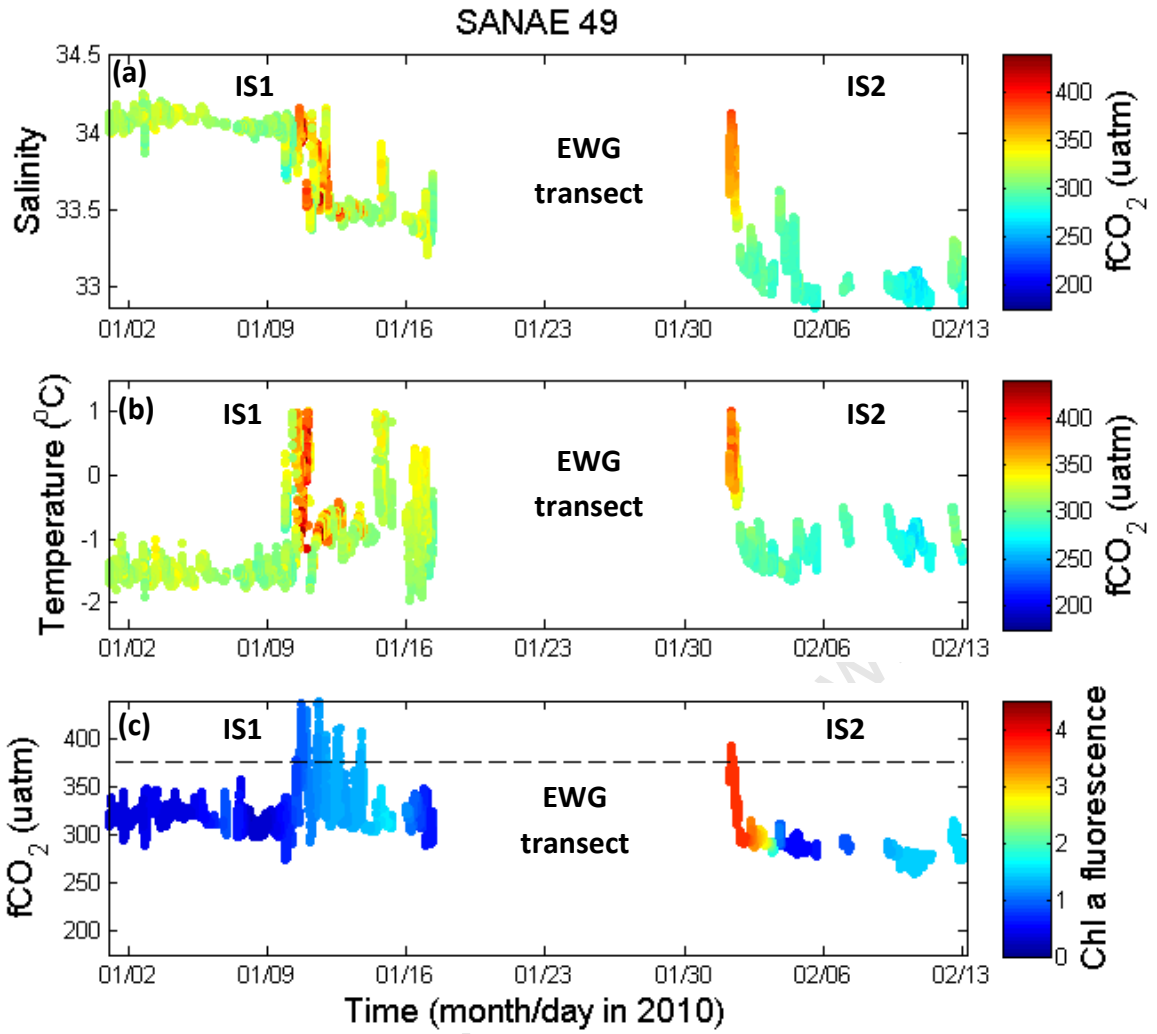

Figure 15. (a) Sea surface salinity with fCO_2 in colour, **(b)** Sea surface temperature with fCO_2 in colour and **(c)** Sea surface fCO_2 with Chlorophyll a fluorescence in colour and with mean atmospheric fCO_2 of 376µtm shown by the dashed black line, during SANAE 49 IS1 and IS2, with the gap due to spatial data collected in the EWG from the 17th-31st January 2010.

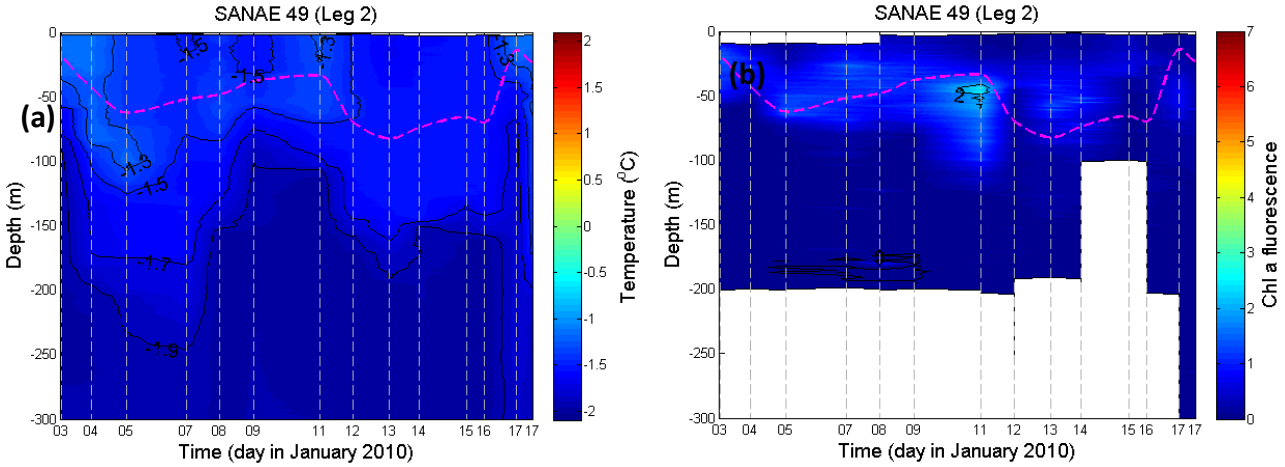

Figure 16. IS1 from the 3rd -19th January 2010 showing CTD data in the upper 300m for **(a)** temperature and **(b)** chlorophyll *a* fluorescence, dashed grey lines indicate CTD stations and dashed pink contour represents the mixed layer depth (MLD) calculated from temperature.

TA decreased at the ice shelf as summer progressed from early January (IS1) to February (IS2) and as SSS decreased through dilution from sea ice melt (Figure 18a). Mean TA during IS1 and IS2 was 2297.7 and 2265.8 respectively (Table 7). DIC decreased throughout the ice shelf period from early January to mid-February, with a mean DIC during IS1 and IS2 of 2165.6 and 2124.6µmol/kg respectively (Table 7). $[CO_3^{2-}]$ was supersaturated during IS1 and IS2 and showed a slight increase from IS1 (mean $[CO_3^{2-}]$ of 100.3µmol/kg) to IS2 (mean $[CO_3^{2-}]$ of 104.9µmol/kg), but was on average lower than the previous year (Table 7), with $[CO_3^{2-}]$ fluctuating around 100µmol/kg (Figure 18c). $[CO_3^{2-}]$ decreased to a minimum of 79µmol/kg between the 11th and 15th of January during IS1 where fCO_2 became supersaturated, the MLD increased and chlorophyll *a* fluorescence was very low (Figures 15c,16,18c). The Revelle Factor was relatively constant during IS1 and IS2 with the exception of a higher peak between the 11th and 15th of January during IS1 where the Revelle Factor increased to 17 due to an increase in DIC (Figures 18b,19a). Ω_{arag} was > 1, showing a slight increasing trend from a mean value during IS1 of 1.51 to a mean value during IS 2 of 1.59 (Table 7). Ω_{arag} reached a minimum of 1.16 during IS1on the 11th January, where DIC was at a maximum (Figure 19b). pH increased slightly throughout the ice station investigation, from a mean value of 8.11 during IS1 to 8.14 during IS2 (Figure 19c).

Mean surface water fCO_2 at both IS1 and IS2 was 20-30µatm higher than the mean fCO_2 recorded in the EWG where sea ice melt was relatively early (Table 7). The MLD was deeper during IS1 than in the EWG, fluctuating around 50m during IS1 and around 25m in the EWG, suggesting that in the EWG there was a more stratified water column and thus less light limitation than at the ice shelf, leading to higher primary production (Figures 15,17). In the EWG, the mean TA and DIC were lower than at the mean TA and DIC during IS1, while the mean $[CO_2^{3-}]$ and Ω_{arag} were both higher in the EWG than the mean $[CO_2^{3-}]$ and Ω_{arag} during both IS1 and IS2 (Table 7).

All available ice shelf surface data was averaged to get a monthly mean TA and DIC for January and February, with winter conditions estimated from SANAE 50 CTS's (Table 3), (Figure 20a). In the EWG data was collected only during January and thus a mean summer TA and DIC was calculated. The seasonal evolution of Ω_{arag} at the ice shelf shows that Ω_{arag} increased from winter (Ω_{arag}=1.34) to January (Ω_{arag}=1.49) and reached a maximum in early February (Ω_{arag}=1.55), with a decrease in both TA and DIC from winter through to late

summer in early February (Figure 20a). Salinity normalised TA (nTA) and DIC (nDIC) show the seasonal evolution of Ω_{arag} at the ice shelf in the absence of dilution, which decreases both TA and DIC (Figure 20b). Without the effects of dilution, Ω_{arag} reaches a maximum in February of approximately 1.8. The influence of dilution on Ω_{arag} was much higher at the ice shelf than in the EWG, although dilution resulted in Ω_{arag} in the EWG decreasing by approximately 0.1 from 1.7 to 1.6 (Figure 20). The effects of photosynthesis on TA could not be investigated as there was not sufficient nitrate data. The uptake of NO_3^- during photosynthesis decreases the H^+ ions in the surrounding water, increasing the TA, which is probably the cause of the increase in nTA as nDIC is decreased (seen in Figure 20b).

Table 7. Mean values of total alkalinity (TA, µmol/kg), dissolved inorganic carbon (DIC, µmol/kg) carbonate ion concentration (CO_3^{2-}) and aragonite saturation state (Ω_{arag}) for the first ice station (IS1), the second ice station (IS2) and the Eastern Weddell Gyre (EWG) during SANAE 48 and 49.

	Mean values for IS1				Mean values for IS2				Mean values for EWG			
Cruise	TA	DIC	CO_3^{2-}	Ω_{arag}	TA	DIC	CO_3^{2-}	Ω_{arag}	TA	DIC	CO_3^{2-}	Ω_{arag}
SANAE 48	2289.3	2105.8	130.1	1.97	2284.0	2117.1	119.8	1.91	2298.9	2170.6	98.2	1.48
SANAE 49	2297.7	2165.6	100.3	1.51	2265.8	2124.6	104.9	1.59	2292.8	2144.3	110.2	1.66

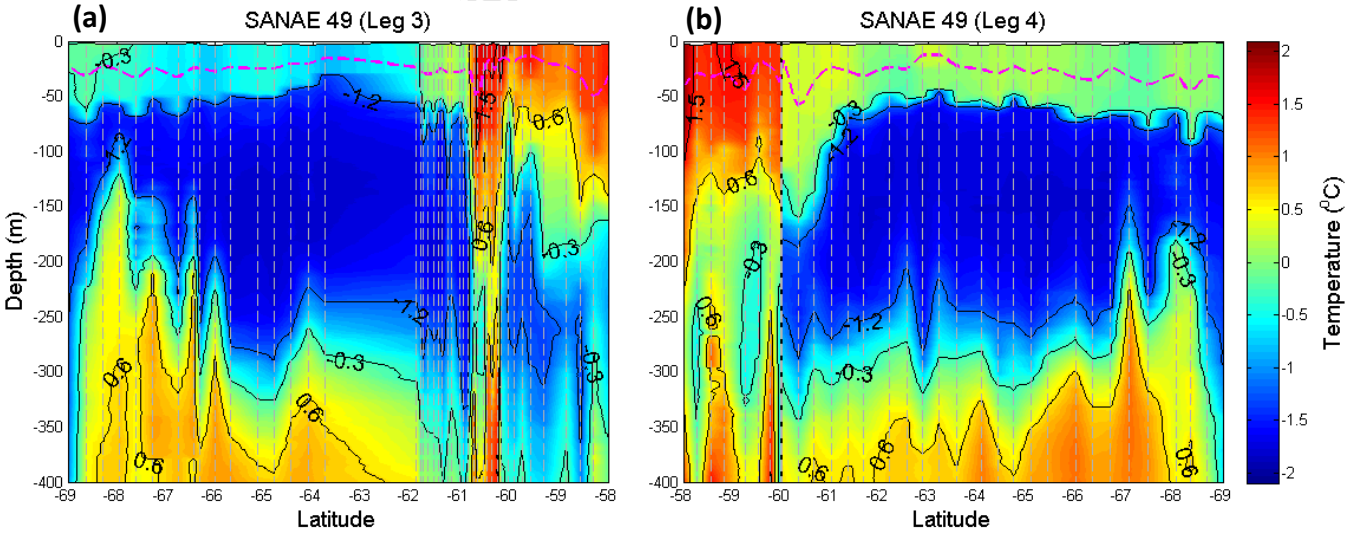

Figure 17. Eastern Weddell Gyre CTD and UCTD temperature data in the upper 400m for **(a)** leg 3 from 26th to 31st January 2010 and **(b)** leg 4 from 1st to 8th February 2010, dashed grey lines indicate CTD and UCTD stations and the dashed pink contour represents the mixed layer depth (MLD) calculated from temperature.

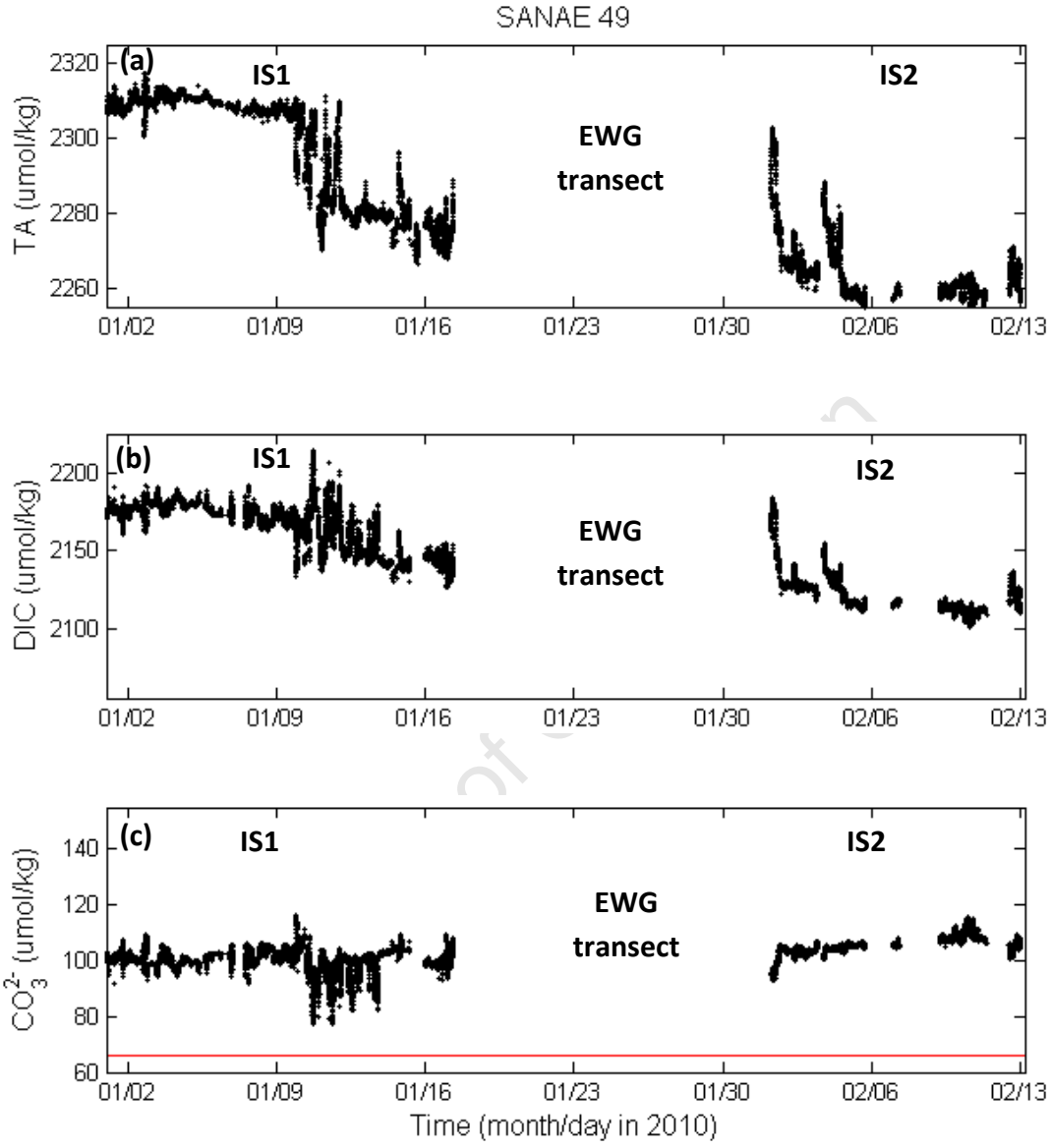

Figure 18. (a) Total alkalinity (TA), **(b)** dissolved inorganic carbon (DIC), **(c)** carbonate ion concentration (CO_3^{2-}) with a red line indicating the carbonate ion concentration below which aragonite becomes undersaturated (66µmol/kg), during SANAE 49 IS1 and IS2, with the gap due to spatial data collected in the EWG from the 17th-31st January 2010.

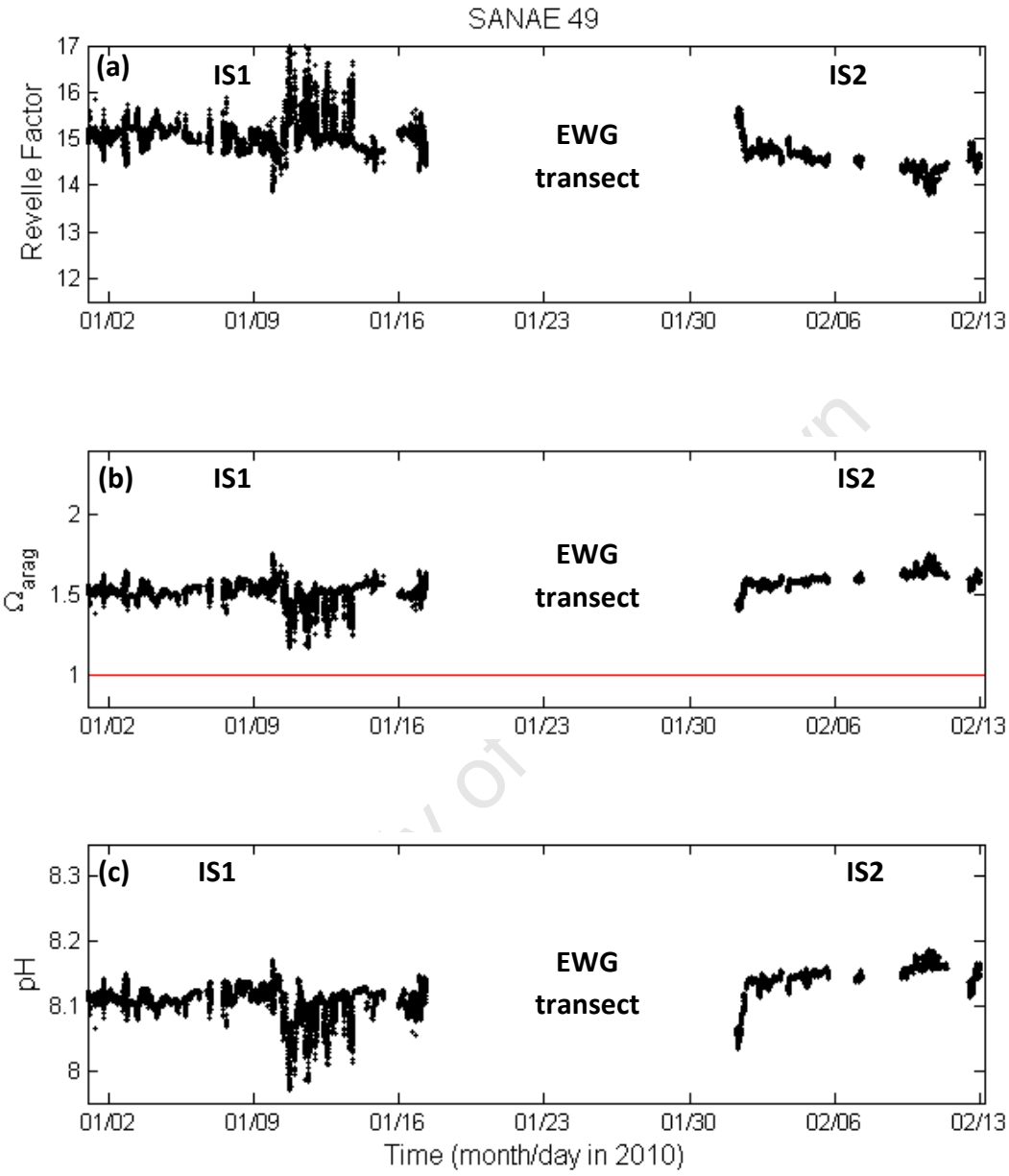

Figure 19. (a) Revelle Factor, **(b)** aragonite saturation state (Ω_{arag}) with a red line indicating the aragonite saturation horizon (Ω_{arag}=1), **(c)** pH, during SANAE 49 IS1 and IS2, with the gap due to spatial data collected in the EWG from the 17th-31st January 2010.

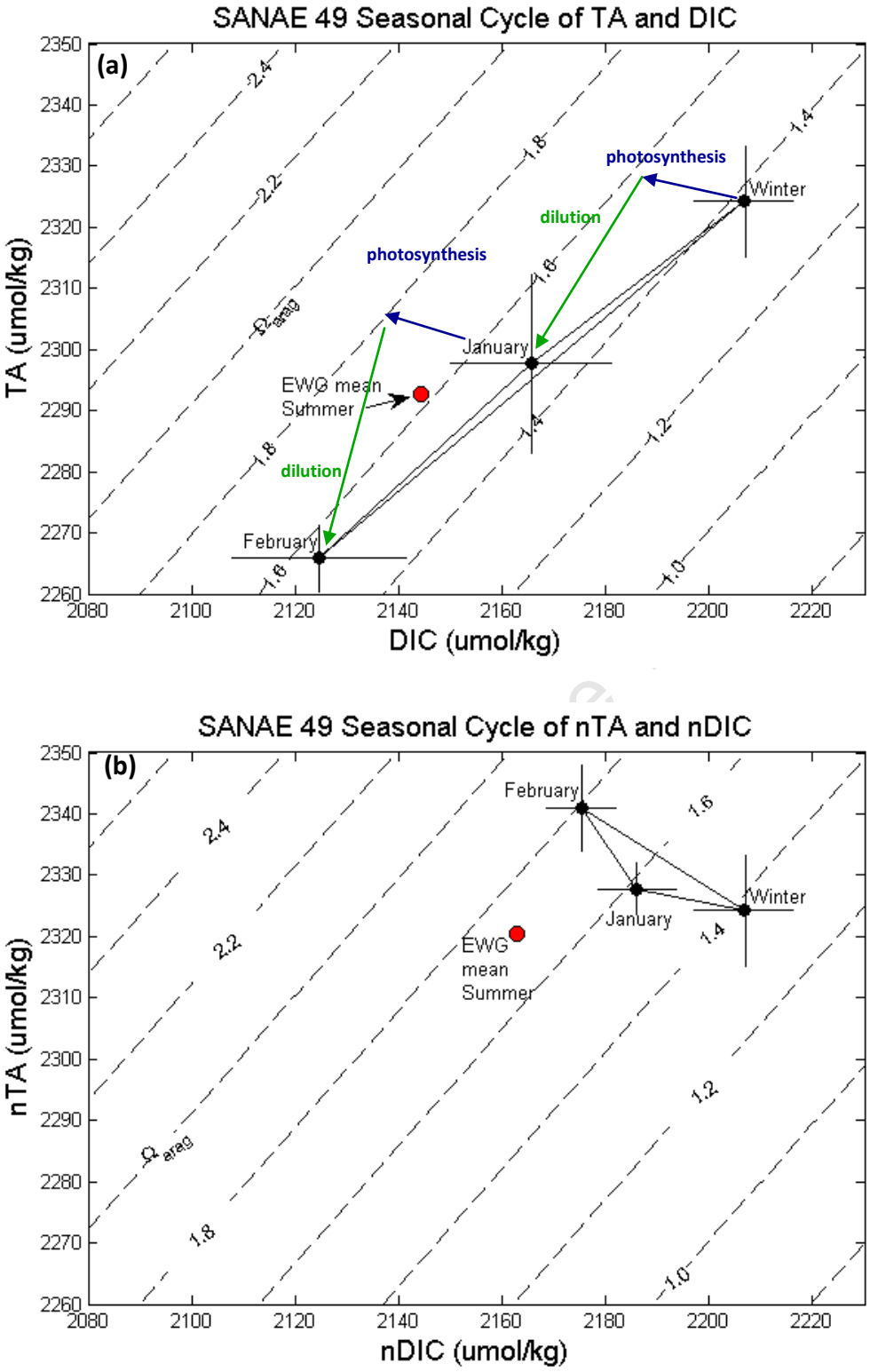

Figure 20. Seasonal evolution of **(a)** mean January 2010 and February 2010 total alkalinity (TA) and dissolved inorganic carbon (DIC) at the ice shelf with vectors indicating various processes that altered TA and DIC, as inferred from the salinity normalised TA (nTA) and salinity normalised DIC (nDIC) below, with the mean summer EWG TA and DIC shown in red and **(b)** mean January 2010 and February 2010 nTA and nDIC at the ice shelf with the mean summer EWG nTA and nDIC shown in red. Winter surface water conditions have been estimated from SANAE 50 CTDs, contours show aragonite saturation state (Ω_{arag}) at -1°C and 33.86psu.

4.1.3 SANAE 50

The first ice shelf data was collected from the 20th to 30th December 2010, 1-2 weeks earlier than both the previous cruises. Sea ice melted very early during December 2010 and January 2011, both at the ice shelf and in the EWG, with the Antarctic ice shelf between 0-15°W becoming sea ice free by January 2011 (Figure 10). CTD and UCTD data was available during IS1, IS2 and in the EWG and has been plotted on the same scales as used for SANAE 49 and 51 to see the interannual variability in the underlying water properties. The Mixed Layer Depth (MLD) is shown on the CTD and UCTD contour plots to get an idea of the water column stratification, which is important in Marginal Ice Zones (MIZ) in relieving light limitation and facilitating phytoplankton blooms (Smith and Nelson, 1986).

Ice shelf water freshened during IS1, in December 2010, but was the saltiest water found throughout the entire study with a mean salinity of 34.2psu (Figure 21a,c), likely to be residual Winter Water (WW) which typically has high concentrations of CO_2 (fCO_2 > 375µatm) and salinities and temperatures of 34.2psu and -1.5 to -1.7°C respectively. A deep MLD suggests upwelling of WW during IS1 and weak stratification (Figure 22a,b). SSS decreased as summer progressed, with a mean SSS during IS2 of 34.01 (Table 8). SST was at a minimum of -1.89°C at the beginning of IS1, increasing through January and into February (Figure 21b). fCO_2 was undersaturated (below 376µatm, the mean atmospheric fCO_2) for most of IS1 and for all of IS2, although surface chlorophyll *a* fluorescence was relatively low (Figure 21c). Below the surface during both IS1 and IS2, CTD data showed subsurface phytoplankton blooms, between 10-35m depth (Figure 22a,c). Chlorophyll *a* fluorescence increased where the MLD decreased, coinciding well with low surface fCO_2 regions (Figure 21c,22a,c). During IS1 fCO_2 increased to above 400µatm on the 24th and 25th December 2010, which corresponded to a period of increased SSS, low SST and chlorophyll *a* fluorescence and a deepening of the MLD.

Table 8. Mean values of sea surface salinity (SSS, psu), sea surface temperature (SSS, °C) and fCO_2 (µatm) for the first ice station (IS1), the second ice station (IS2) and the Eastern Weddell Gyre (EWG) during SANAE 48, 49 and 50.

	Mean values for IS1			Mean values for IS2			Mean values for EWG		
Cruise	SSS	SST	fCO_2	SSS	SST	fCO_2	SSS	SST	fCO_2
SANAE 48	33.68	-1.02	231.0±26	33.48	-1.96	241.9±19	33.90	-0.93	335.9±20
SANAE 49	33.85	-1.16	322.8±22	33.14	-0.99	293.9±25	33.89	0.50	315.2±46
SANAE 50	34.20	-0.99	309.4±41	34.01	-0.04	241.9±39	33.89	-0.10	340.6±30

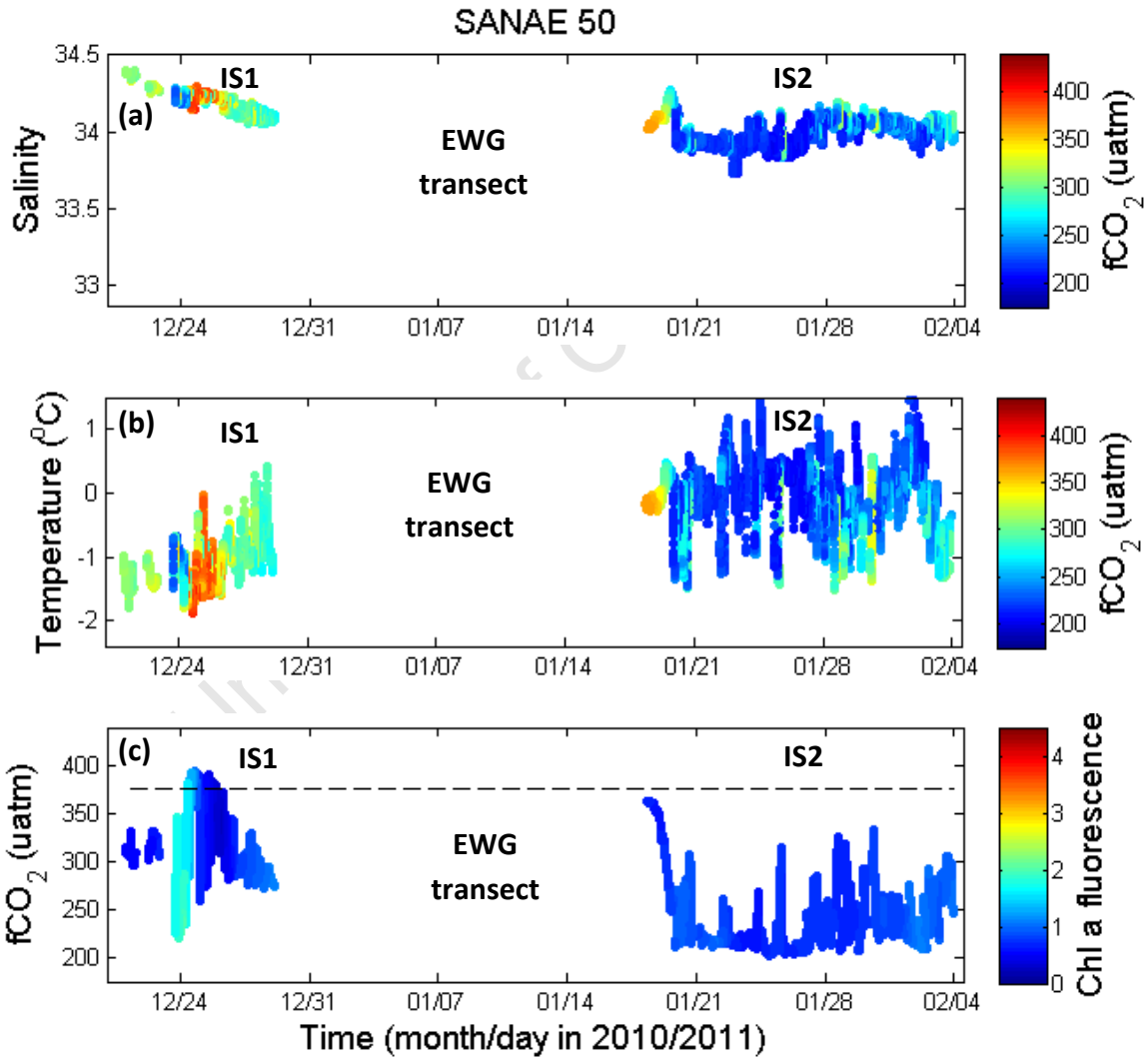

Figure 21. (a) Sea surface salinity with fCO_2 in colour, **(b)** Sea surface temperature with fCO_2 in colour and **(c)** Sea surface fCO_2 with Chlorophyll a fluorescence in colour and with mean atmospheric fCO_2 of 376µtm shown by the dashed black line, during SANAE 50 IS1 and IS2, with the gap due to spatial data collected in the EWG from the 2nd -19th January 2011.

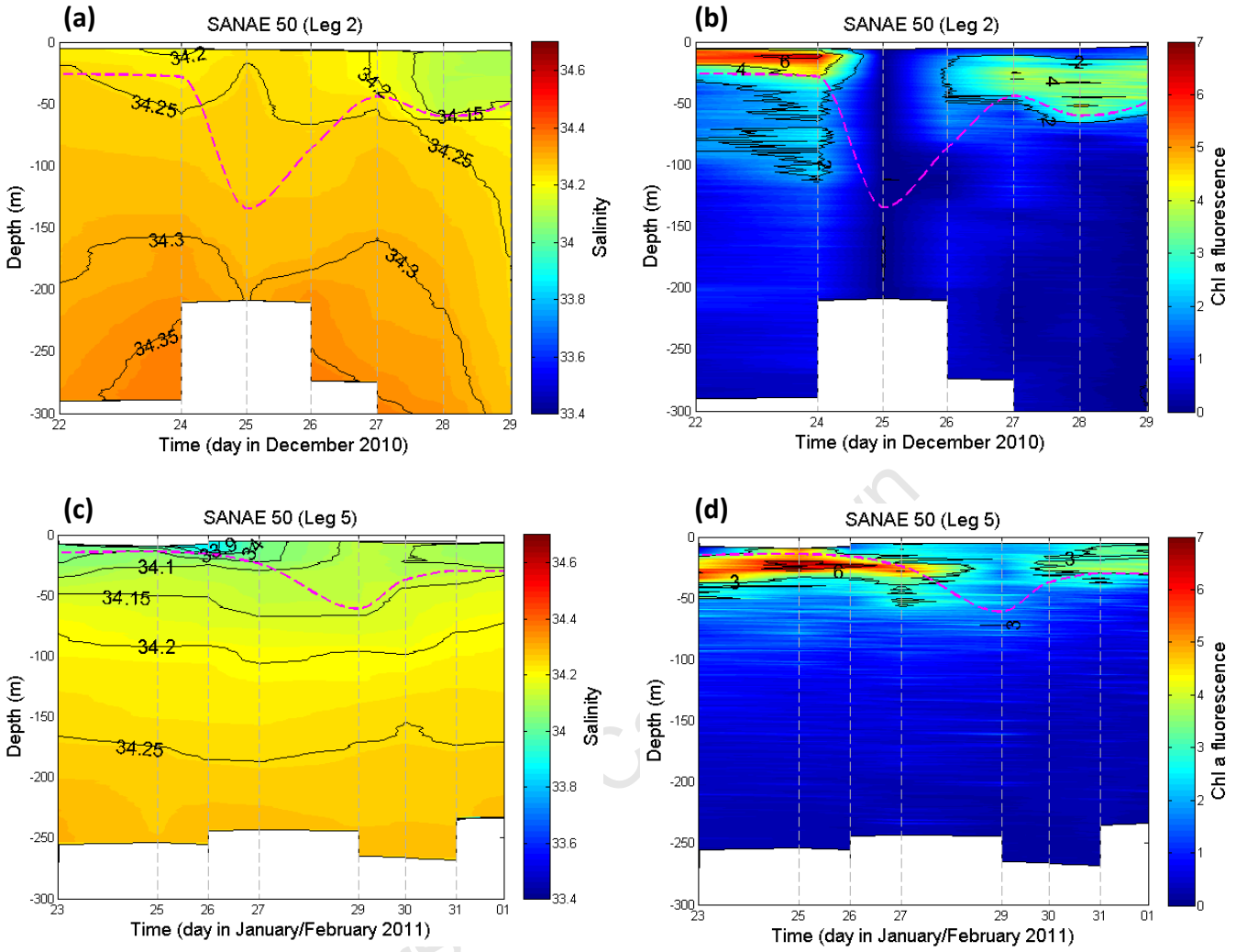

Figure 22. IS1 from the 22nd to 29th December 2010 showing CTD data in the upper 300m for **(a)** salinity and **(b)** chlorophyll *a* fluorescence, and IS2 from the 23rd January to 1st February 2011 showing CTD data in the upper 300m for **(c)** salinity and **(d)** chlorophyll *a* fluorescence, dashed grey lines indicate CTD stations and dashed pink contour represents the mixed layer depth (MLD) calculated from density.

TA decreased at the ice shelf as summer progressed from December 2010 (IS1) to January and early February 2011 (IS2) and as SSS decreased through dilution from sea ice melt (Figure 24a). TA was relatively high throughout the summer period, with a mean TA of 2313.3µmol/kg during IS1 and 2300.0µmol/kg during IS2 (Table 9). DIC at the ice shelf decreased from December to January and early February with a mean DIC during IS1 and IS2 of 2169.3 and 2112.4µmol/kg respectively (Table 9). The mean DIC during SANAE 50 IS1 was higher than the mean DIC during IS1 of both the previous years and the mean DIC was lower during SANAE 50 IS2 than during both the previous years (Table 9). $[CO_3^{2-}]$ was supersaturated during IS1 and IS2 but decreased to a minimum of 81µmol/kg during IS1 on the 25th December, where the MLD increased, chlorophyll *a* fluorescence was very low and fCO_2 was supersaturated (Figures 21c,22b,24c). $[CO_3^{2-}]$ was relatively high during IS2 where fCO_2 was low, with a mean $[CO_3^{2-}]$ concentration of 107.4 and 133.2µmol/kg during IS1 and IS2 respectively (Table 9). The Revelle Factor decreased from IS1 to IS2, fluctuating around 15 during IS1 and around 13 during IS2 (Figure 25a). Ω_{arag} was > 1, decreasing as summer progressed from IS1 to IS2, with a mean value of 1.62 during IS1 and 2.01 during IS2 (Table 9) Ω_{arag} reached a maximum of 2.4 during late January and early February 2011, the highest Ω_{arag} observed during all four years (Figure 25b). pH increased throughout summer, from a mean value of 8.13 during IS1 to 8.22 during IS2 (Figure 25c).

Mean surface water fCO_2 at both IS1 (309.4) and IS2 (241.9) was lower than the mean fCO_2 recorded in the EWG (340.6µtm), as was observed during SANAE 48 (Table 8). The MLD was shallower during IS1 and during IS2 than in the EWG, with the exception of an upwelling event during IS1 on the 25th December 2010, where the MLD decreased from 27-145m (Figures 22,23). During IS2 the MLD was mostly above 30m, while in the EWG the MLD fluctuated around 50m, suggesting a more stratified water column during IS2 than in the EWG. In the EWG, the mean TA, $[CO_3^{2-}]$ and Ω_{arag} were lower than at the mean TA, $[CO_3^{2-}]$ and Ω_{arag} during IS1 and IS2 (Table 9).

All available ice shelf surface data was averaged to get a monthly mean TA and DIC for December, January and February, with winter conditions estimated from SANAE 50 CTD's (Table 3), (Figure 26a). In the EWG data was collected only during January and thus a mean summer TA and DIC was calculated. The seasonal evolution of Ω_{arag} at the ice shelf shows that Ω_{arag} increased from winter (Ω_{arag}=1.34), to December (Ω_{arag}=1.58), to January

(Ω_{arag}=1.71) reaching a maximum during early February (Ω_{arag}=1.93), with a decrease in both TA and DIC from winter through to late summer in early February (Figure 26a). Salinity normalised TA (nTA) and DIC (nDIC) show the seasonal evolution of Ω_{arag} at the ice shelf in the absence of dilution, which decreases both TA and DIC (Figure 26b). Without the effects of dilution, Ω_{arag} reaches a maximum in February of approximately 2, about 0.08 higher than the mean February Ω_{arag} when dilution is not corrected for (Figure 26b). The influence of dilution on Ω_{arag} was slightly lower at the ice shelf than in the EWG, with dilution resulting in Ω_{arag} in the EWG decreasing by approximately 0.1 from 1.48 to 1.58 (Figure 26). The effects of photosynthesis on TA could not be investigated as there was not sufficient nitrate data. The uptake of NO_3^- during photosynthesis decreases the H^+ ions in the surrounding water, increasing the TA, which is likely the cause of the increase in nTA as nDIC is decreased as seen in figure 20b.

Table 9. Mean values of total alkalinity (TA, µmol/kg), dissolved inorganic carbon (DIC, µmol/kg) carbonate ion concentration (CO_3^{2-}) and aragonite saturation state (Ω_{arag}) for the first ice station (IS1), the second ice station (IS2) and the Eastern Weddell Gyre (EWG) during SANAE 48, 49 and 50.

	Mean values for IS1				Mean values for IS2				Mean values for EWG			
Cruise	TA	DIC	CO_3^{2-}	Ω_{arag}	TA	DIC	CO_3^{2-}	Ω_{arag}	TA	DIC	CO_3^{2-}	Ω_{arag}
SANAE 48	2289.3	2105.8	130.1	1.97	2284.0	2117.1	119.8	1.91	2298.9	2170.6	98.2	1.48
SANAE 49	2297.7	2165.6	100.3	1.51	2265.8	2124.6	104.9	1.59	2292.8	2144.3	110.2	1.66
SANAE 50	2313.3	2169.3	107.4	1.62	2300.0	2112.4	133.2	2.01	2294.8	2163.0	100.5	1.52

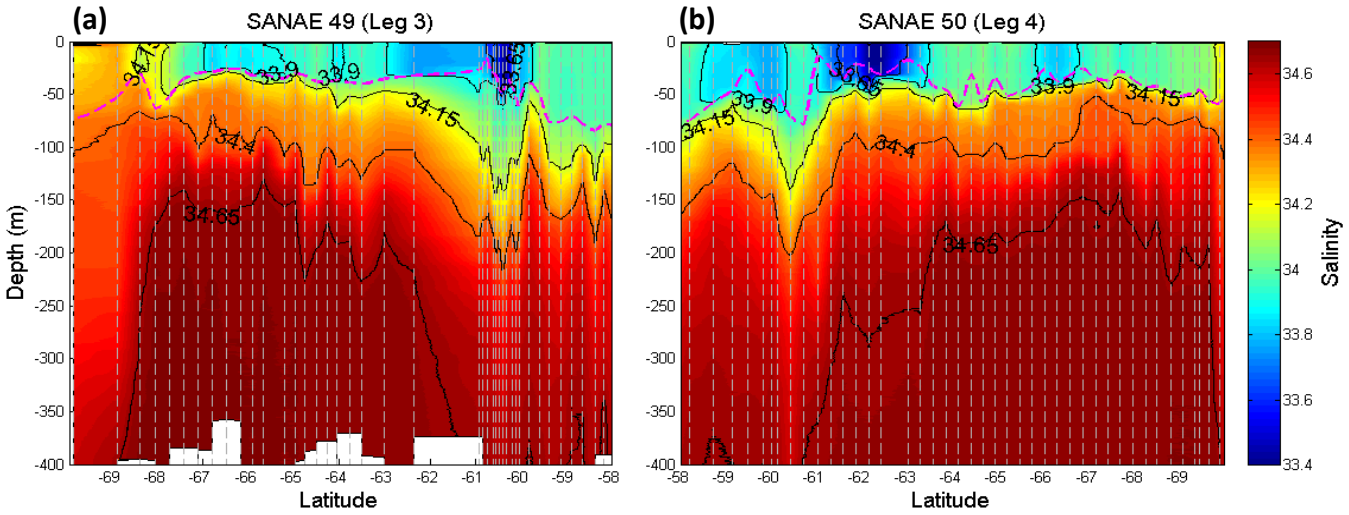

Figure 23. Eastern Weddell Gyre showing CTD and UCTD salinity data in the upper 400m for **(a)** leg 3 from 1st to 6th January 2011 and **(b)** leg 4 from 12th to 20th January 2011, dashed grey lines indicate CTD and UCTD stations and the dashed pink contour represents the mixed layer depth (MLD) calculated from density.

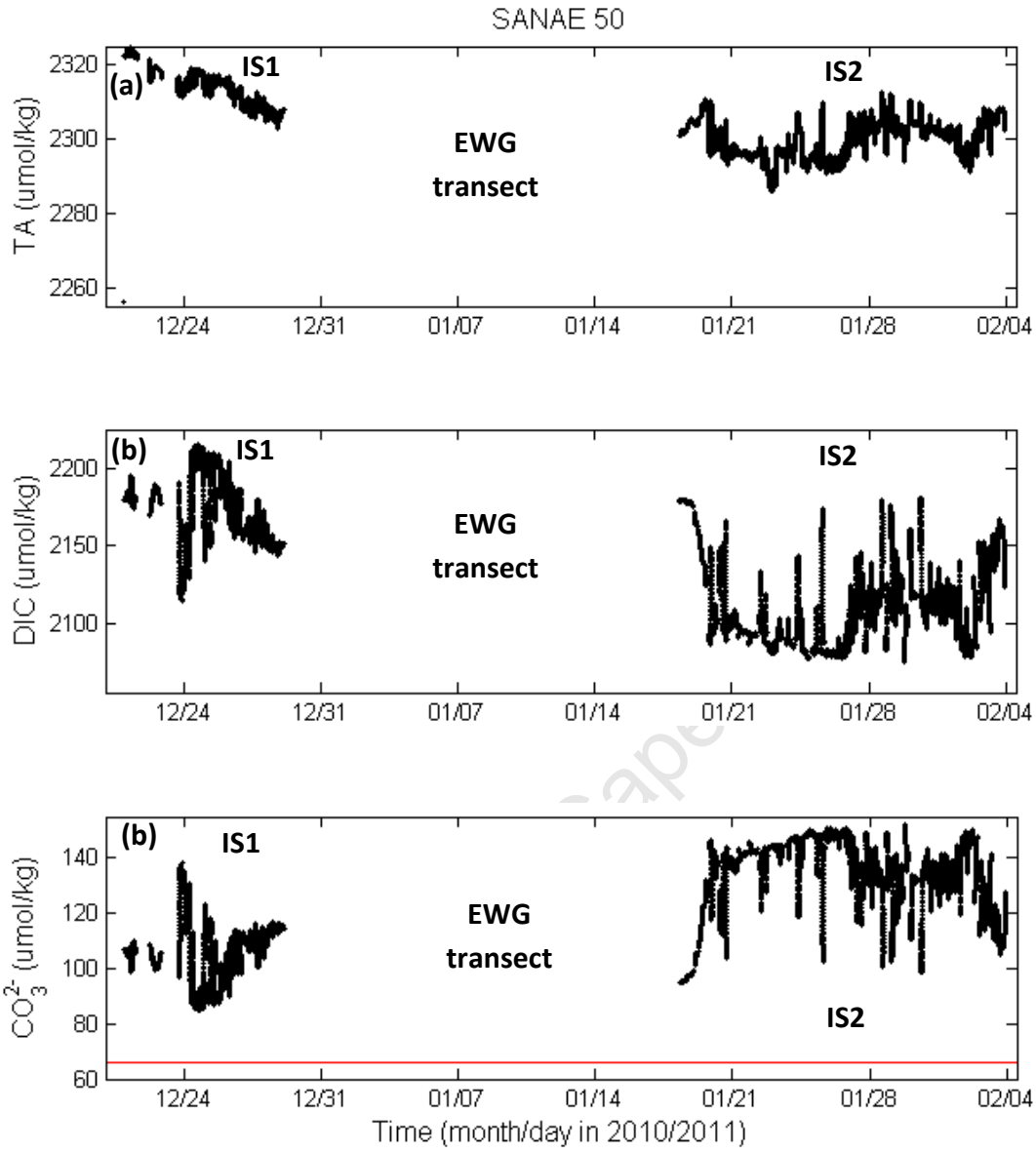

Figure 24. (a) Total alkalinity (TA), **(b)** dissolved inorganic carbon (DIC), **(c)** carbonate ion concentration (CO_3^{2-}) with a red line indicating the carbonate ion concentration below which aragonite becomes undersaturated (66µmol/kg), during SANAE 50 IS1 and IS2, with the gap due to spatial data collected in the EWG from the 1st to 20th January 2011.

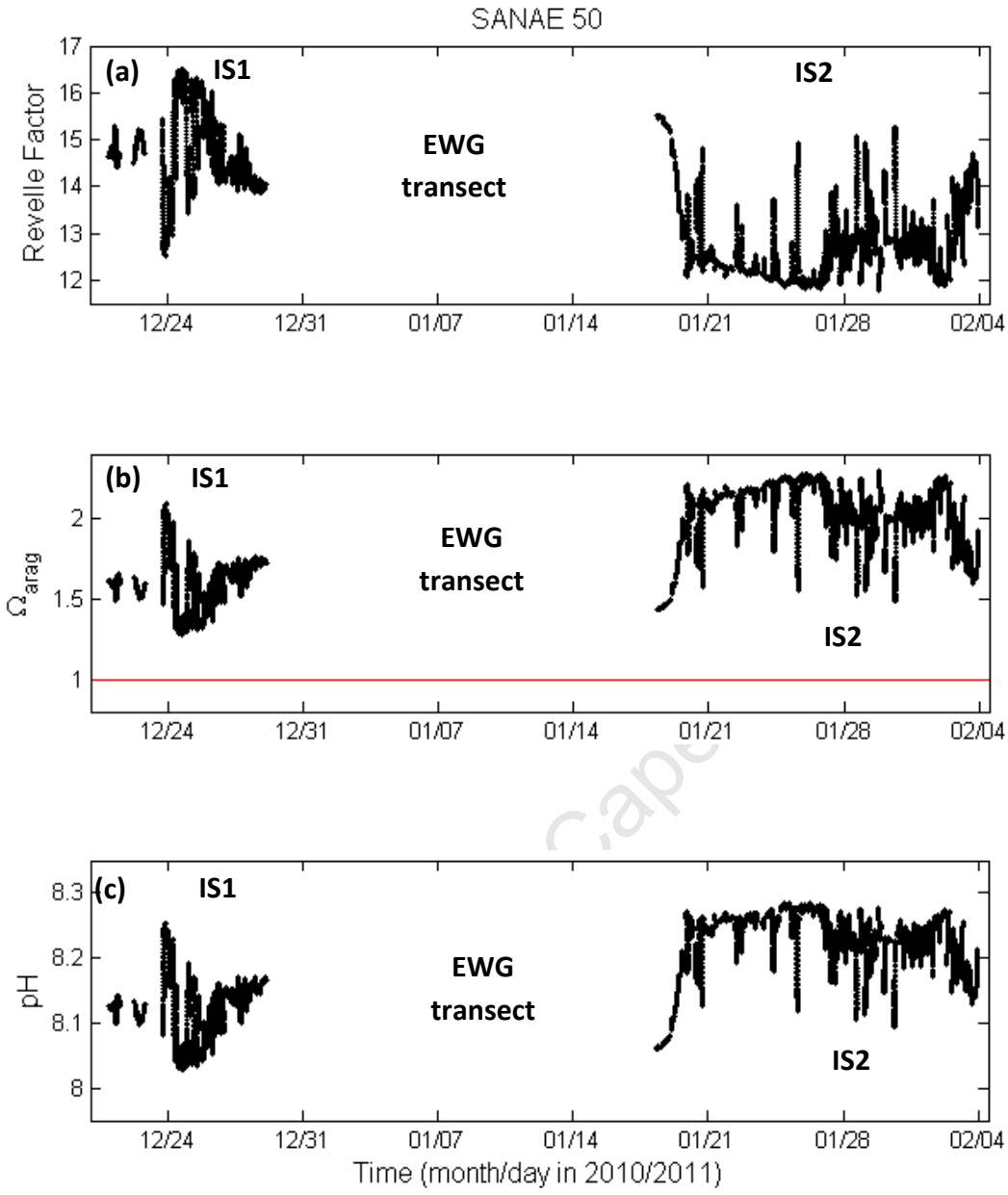

Figure 25. (a) Revelle Factor, **(b)** aragonite saturation state (Ω_{arag}) with a red line indicating the aragonite saturation horizon (Ω_{arag}=1), **(c)** pH, during SANAE 50 IS1 and IS2, with the gap due to spatial data collected in the EWG from the 1st to 20th January 2011.

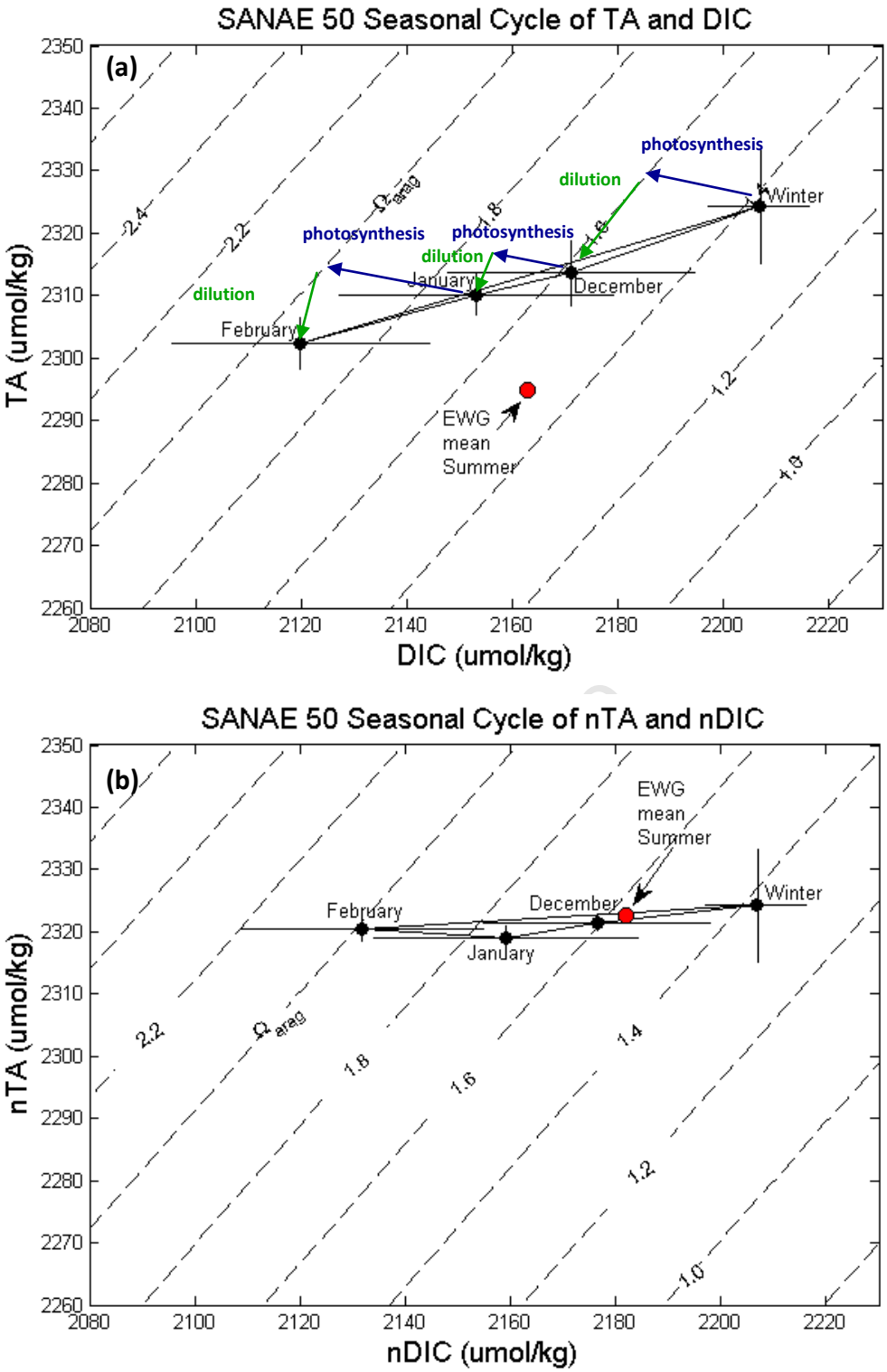

Figure 26. Seasonal evolution of **(a)** mean December 2010, January 2011 and February 2011 total alkalinity (TA) and dissolved inorganic carbon (DIC) at the ice shelf with vectors indicating various processes that altered TA and DIC, as inferred from the salinity normalised TA (nTA) and salinity normalised DIC (nDIC) below, with the mean summer EWG TA and DIC shown in red and **(b)** mean December 2010, January 2011 and February 2011 nTA and nDIC at the ice shelf with the mean summer EWG nTA and nDIC shown in red. Winter surface water conditions have been estimated from SANAE 50 CTDs, contours show aragonite saturation state (Ω_{arag}) at -1°C and 33.86psu.

4.1.4 SANAE 51

During SANAE 51 sea ice trapped in the sea water intake caused bubbles to interrupt the flow of the underway conductivity sensor during legs 2, 3 and 4, resulting in very spiky salinity data. The underway station Portasal salinity values have been interpolated for legs 3 and 4 but as there were no Portasal salinity samples taken during leg 2, the SSS data for leg 2 (the first part of IS1) will not be included in this study. The first ice shelf data was collected from the 28th December 2011 to the 9th January 2012, but due sea ice blocking the underway pCO2 system, surface IS1 data was only available from the 5th January 2012. In both December 2011 and January 2012 sea ice melted very late both at the ice shelf and in the EWG relative to the summers of 2009, 2010 and 2011 (Figure 10). CTD data was only available for IS1 and IS2 and has been plotted on the same scales as used for SANAE 49 and 50 to see the interannual variability in the underlying water properties. The Mixed Layer Depth (MLD) is shown on the CTD contour plots to get an idea of the water column stratification, which is important in Marginal Ice Zones (MIZ) in relieving light limitation and facilitating phytoplankton blooms (Smith and Nelson, 1986).

Ice shelf SSS followed a similar pattern to SSS during the previous year (SANAE 50). WW (S=34.2±0.11psu) was still present during IS1, where SSS was high ranging between 34-34.2psu (Figure 27a). During IS2 SSS was initially high (34.2psu), decreasing to 33.4psu and then increasing again towards the end of IS2 in early February (Figure 27a). SST increased as summer progressed from early January to early February, with a mean SST during IS1 and IS2 of -1.02 and -0.93°C respectively (Figure 27b, Table 10). fCO_2 was supersaturated, increasing above the mean atmospheric fCO_2 of 374µatm at all stations during IS1 and at the beginning and at the end of IS2 (Figure 27c). Where fCO_2 was supersaturated, chlorophyll *a* fluorescence was close to zero and, where CTD data was available at the beginning of IS2, the MLD was observed to be below 150m depth (Figures 27c,28). During IS2 fCO_2 decreased as chlorophyll *a* fluorescence increased and the MLD decreased to around 25m until the 3rd February 2012, after which fCO_2 increased to a maximum of 440µatm corresponding to a decrease in chlorophyll *a* fluorescence and SST and an increase in SSS (Figure 27). The mean fCO_2 was higher at both IS1 and IS2 during SANAE 51, where sea ice melt was very late, than during IS1 and IS2 of any of the previous three cruises (Table 10).

Table 10. Mean values of sea surface salinity (SSS, psu), sea surface temperature (SSS, °C) and fCO_2 (µatm) for the first ice station (IS1), the second ice station (IS2) and the Eastern Weddell Gyre (EWG) during SANAE 48, 49, 50 and 51.

	Mean values for IS1			Mean values for IS2			Mean values for EWG		
Cruise	SSS	SST	fCO_2	SSS	SST	fCO_2	SSS	SST	fCO_2
SANAE 48	33.68	-1.02	231.0±26	33.48	-1.96	241.9±19	33.90	-0.93	335.9±20
SANAE 49	33.85	-1.16	322.8±22	33.14	-0.99	293.9±25	33.89	0.50	315.2±46
SANAE 50	34.20	-0.99	309.4±41	34.01	-0.04	241.9±39	33.89	-0.10	340.6±30
SANAE 51	34.20	-1.69	385.4±5	33.90	-1.40	314.8±32	33.71	-0.62	325.1±42

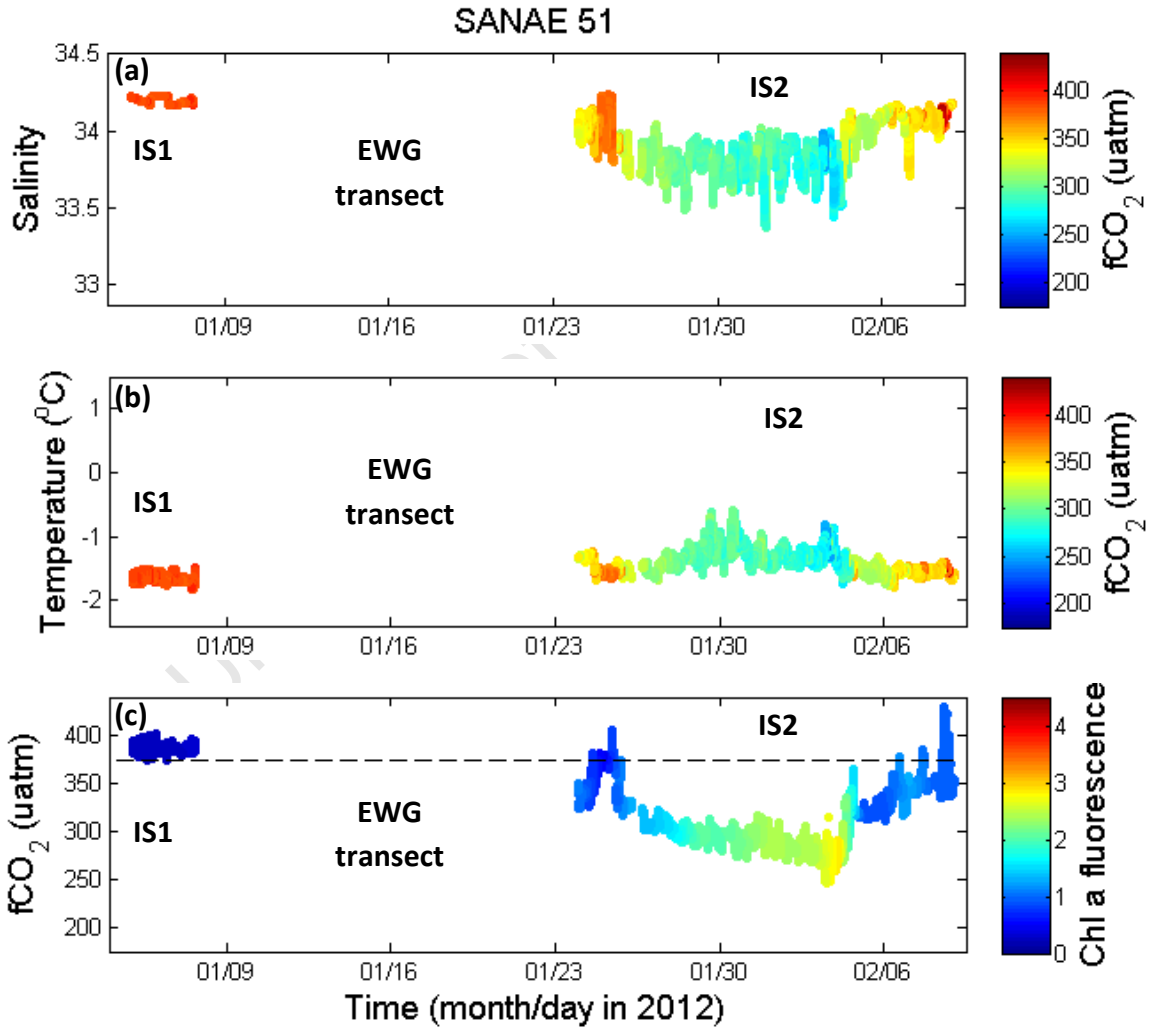

Figure 27. (a) Sea surface salinity with fCO_2 in colour, **(b)** Sea surface temperature with fCO_2 in colour and **(c)** Sea surface fCO_2 with Chlorophyll a fluorescence in colour and with mean atmospheric fCO_2 of 376µtm shown by the dashed black line, during SANAE 50 IS1 and IS2, with the gap due to spatial data collected in the EWG from the 8th -22nd January 2012.

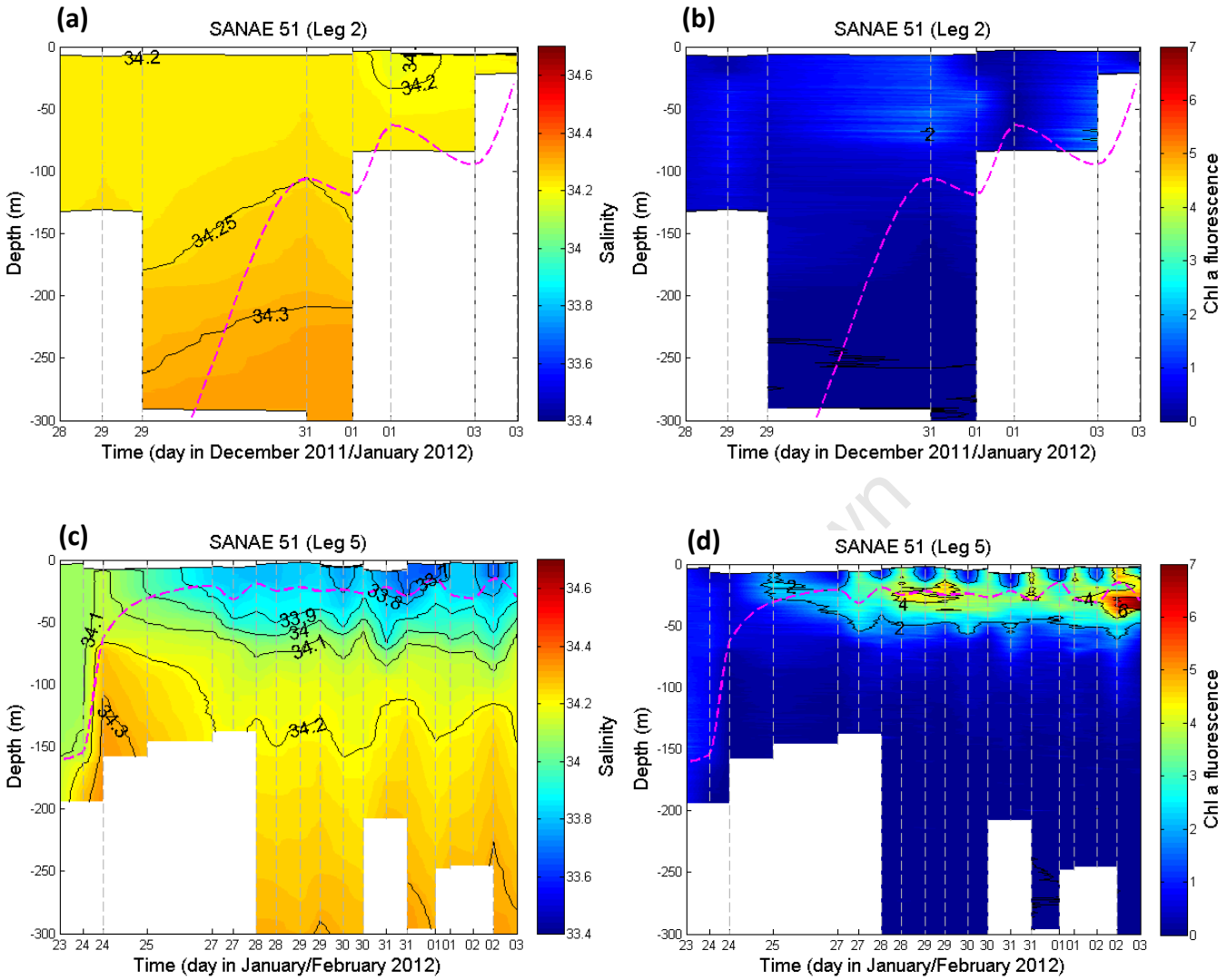

Figure 28. IS1 from the 28th December 2011 to 3rd January 2012 showing CTD data in the upper 300m for **(a)** salinity and **(b)** chlorophyll *a* fluorescence, and IS2 from the 23rd January to 3rd February 2012 showing CTD data in the upper 300m for **(c)** salinity and **(d)** chlorophyll *a* fluorescence, dashed grey lines indicate CTD stations and dashed pink contour represents the mixed layer depth (MLD) calculated from density.

TA decreased at the ice shelf as summer progressed from early January (IS1) to late January (IS2) and as SSS decreased through dilution from sea ice melt (Figure 29a). TA increased towards the end of IS2 in early February, as SSS increased. Mean TA during both IS1 (TA=2315.8µmol/kg) and IS2 (TA=2300.9µmol/kg) was higher than the mean TA at the ice shelf during the three previous years (Table 11). DIC during IS1 was relatively high, with a mean value of 2209.3µmol/kg which is 2.3µmol/kg higher than the mean Winter Water (WW) DIC estimated from SANAE 50 CTDs, and is below the WW DIC of 2220 µmol/kg found by Jones et al (2010). DIC then decreased during IS2 reaching a minimum of 2110.5µmol/kg on the 3rd February (Figure 29b). [CO_3^{2-}] was supersaturated during IS1 and IS2, but was on average lower during both IS1 and IS2 than during any of the other three years, with a mean [CO_3^{2-}] during IS1 and IS2 of 86.4 and 102.0µmol/kg respectively (Table 11) The Revelle Factor was very high during IS1 with a mean value of 16.3, after which it decreased during IS2 where chlorophyll *a* fluorescence increased and DIC decreased (Figure 30a). Ω_{arag} was > 1, with very low values of 1.34 observed during IS1 and at the end of IS2 where fCO_2 was supersaturated (Figure 30b). The mean Ω_{arag} during IS1 was 1.3 and during IS2 was 1.54, both lower than in all other years (Table 11). pH increased slightly as summer progressed from early January to early February, from a mean value of 8.04 during IS1 to 8.08 during IS2 (Figure 30c).

Mean surface water fCO_2 was highest during IS1 (385.4µatm) lower in the EWG (325.1µatm) and lowest during IS2 (314.8µatm), (Table 10). In the EWG, the mean TA and DIC were lower than at the mean TA and DIC during both IS1 and IS2, while the mean [CO_3^{2-}] and Ω_{arag} were very similar during IS2 and in the EWG, but were lower during IS1 (Table 11).

All available ice shelf surface data was averaged to get a monthly mean TA and DIC for January and February, with winter conditions estimated from SANAE 50 CTS's (Table 3), (Figure 31a). In the EWG data was collected only during January and thus a mean summer TA and DIC was calculated. The seasonal evolution of Ω_{arag} at the ice shelf shows that Ω_{arag} increased from winter (Ω_{arag}=1.34) to January (Ω_{arag}=1.4) to reach a maximum during early February (Ω_{arag}=1.51), with a decrease in both TA and DIC from winter through to late summer in early February (Figure 31a). Salinity normalised TA (nTA) and DIC (nDIC) show the seasonal evolution of Ω_{arag} at the ice shelf in the absence of dilution, which decreases both TA and DIC (Figure 31b). Without the effects of dilution, Ω_{arag} reaches a maximum in early

February of approximately 1.6. The influence of dilution on Ω_{arag} was slightly higher in the EWG than at the ice shelf. The summer increase in Ω_{arag} during SANAE 51 at the ice shelf likely due to primary production was small, with Ω_{arag} increasing from a winter value of 1.38 to a February value of 1.6 when the effect of dilution was corrected for (Figure 31b). In the EWG, dilution resulted in summertime Ω_{arag} decreasing by approximately 0.1 from 1.52 to 1.62 (Figure 31). The effects of photosynthesis on TA could not be investigated as there was not sufficient nitrate data. The uptake of NO_3^- during photosynthesis decreases the H^+ ions in the surrounding water, increasing the TA, which is likely the cause of the increase in nTA as DIC is decreased as seen in figure 31b.

Table 11. Mean values of total alkalinity (TA, µmol/kg), dissolved inorganic carbon (DIC, µmol/kg) carbonate ion concentration (CO_3^{2-}) and aragonite saturation state (Ω_{arag}) for the first ice station (IS1), the second ice station (IS2) and the Eastern Weddell Gyre (EWG) during SANAE 48, 49, 50 and 51.

	Mean values for IS1				Mean values for IS2				Mean values for EWG			
Cruise	TA	DIC	CO_3^{2-}	Ω_{arag}	TA	DIC	CO_3^{2-}	Ω_{arag}	TA	DIC	CO_3^{2-}	Ω_{arag}
SANAE 48	2289.3	2105.8	130.1	1.97	2284.0	2117.1	119.8	1.91	2298.9	2170.6	98.2	1.48
SANAE 49	2297.7	2165.6	100.3	1.51	2265.8	2124.6	104.9	1.59	2292.8	2144.3	110.2	1.66
SANAE 50	2313.3	2169.3	107.4	1.62	2300.0	2112.4	133.2	2.01	2294.8	2163.0	100.5	1.52
SANAE 51	2315.8	2209.3	86.4	1.3	2300.9	2165.6	102.0	1.54	2289	2154.2	101.9	1.54

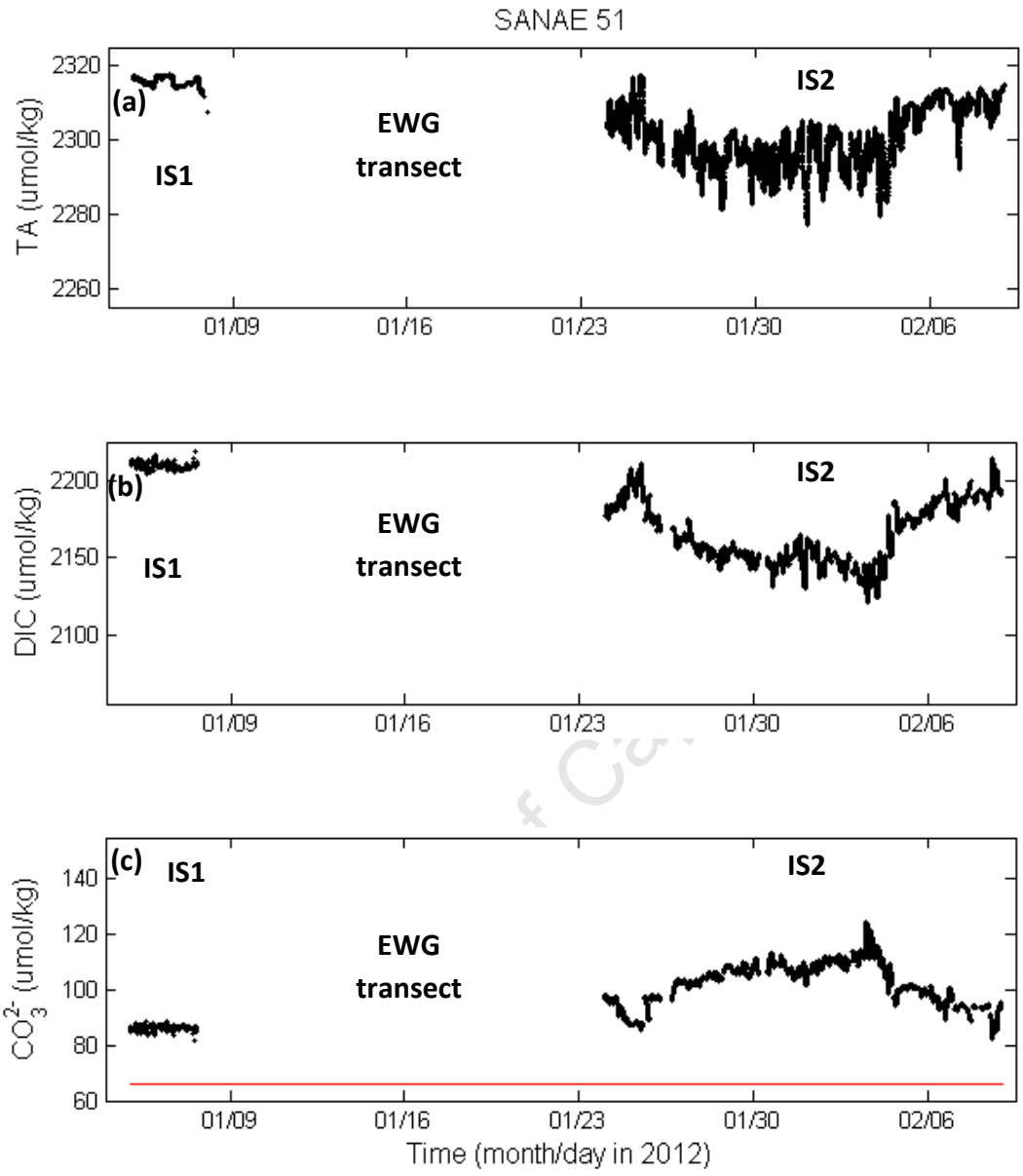

Figure 29. (a) Total alkalinity (TA), **(b)** dissolved inorganic carbon (DIC), **(c)** carbonate ion concentration (CO_3^{2-}) with a red line indicating the carbonate ion concentration below which aragonite becomes undersaturated (66µmol/kg), during SANAE 50 IS1 and IS2, with the gap due to spatial data collected in the EWG from the 8th -22nd January 2012.

.

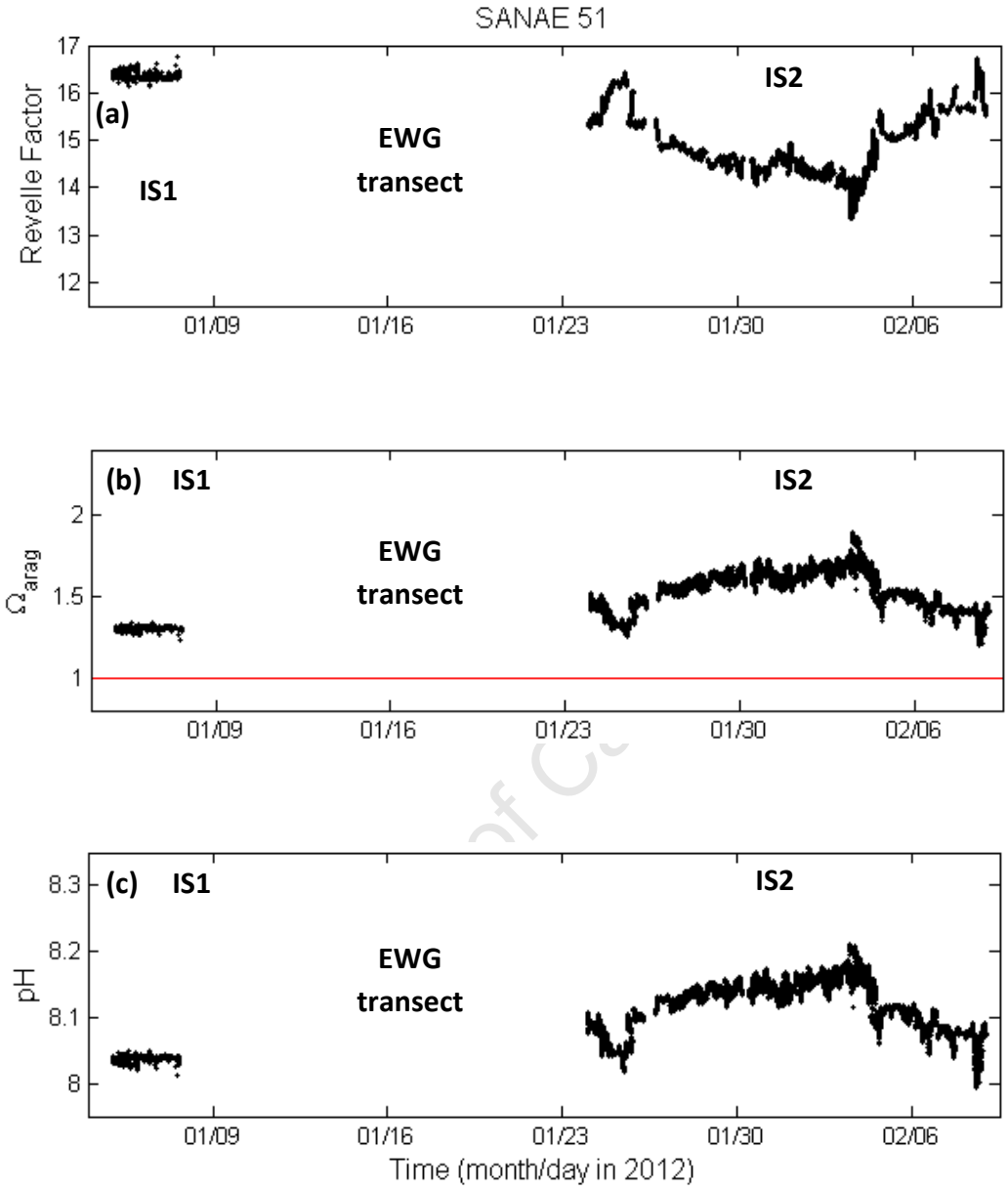

Figure 30. (a) Revelle Factor, **(b)** aragonite saturation state (Ω_{arag}) with a red line indicating the aragonite saturation horizon (Ω_{arag}=1), **(c)** pH, during SANAE 50 IS1 and IS2, with the gap due to spatial data collected in the EWG from the 8th -22nd January 2012.

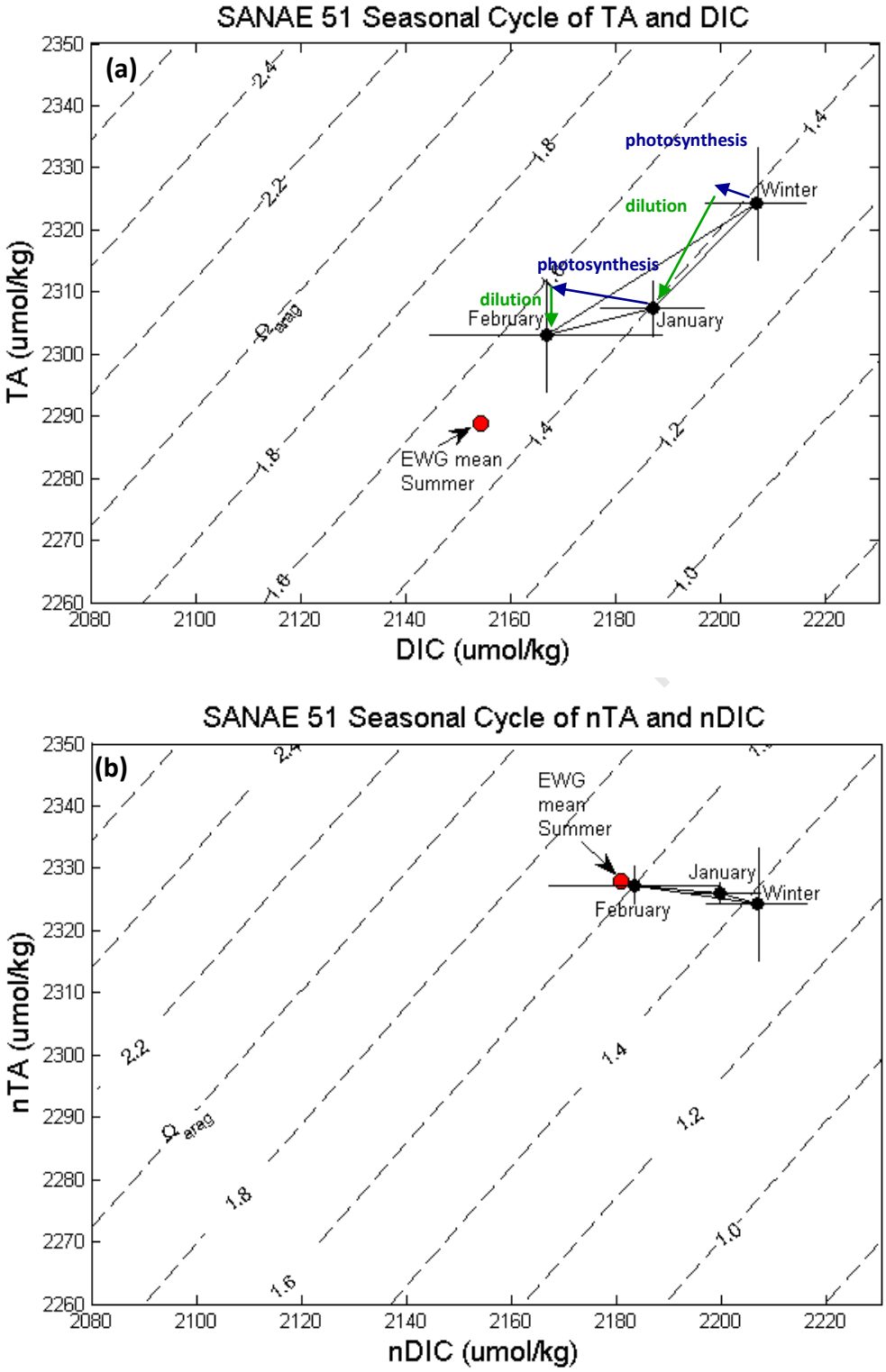

Figure 31. Seasonal evolution of **(a)** mean January 2012 and February 2012 total alkalinity (TA) and dissolved inorganic carbon (DIC) at the ice shelf with vectors indicating various processes that altered TA and DIC, as inferred from the salinity normalised TA (nTA) and salinity normalised DIC (nDIC) below, with the mean summer EWG TA and DIC shown in red and **(b)** mean January 2012 and February 2012 nTA and nDIC at the ice shelf with the mean summer EWG nTA and nDIC shown in red. Winter surface water conditions have been estimated from SANAE 50 CTDs, contours show aragonite saturation state (Ω_{arag}) at -1°C and 33.86psu.

4.1.5 Seasonality of carbonate ion concentration and aragonite saturation state at the ice shelf and in the EWG

Weekly mean [CO_3^{2-}] and Ω_{arag} at the Antarctic ice shelf (IS) and in the EWG for all four SANAE cruises have been plotted, to examine the variability of the seasonal cycle of Ocean Acidification. The Winter Water (WW) values are estimated from SANAE 50 CTD data, where WW is defined as the water below the surface where temperature is at a minimum (see section 3.4.1). The interannual variability of [CO_3^{2-}] and Ω_{arag} was higher at the ice shelf than in the EWG (Figure 32). The interannual variability in the phasing of sea ice melt was the major determinant of the extent of the summer increases in [CO_3^{2-}] at the IS, and to a lesser extent in the EWG (Figure 32). Years with early ice melt at the ice shelf such as 2009 (SANAE 48) and 2011 (SANAE 50) had higher variability of [CO_3^{2-}] and Ω_{arag} between the ice shelf region and the EWG, while years with later sea ice melt at the ice shelf such as 2010 (SANAE 49) and 2012 (2012) had less variability of [CO_3^{2-}] and Ω_{arag} between the ice shelf region and the EWG.

[CO_3^{2-}] and Ω_{arag} were lowest at the ice shelf during all weeks of SANAE 51 (when sea ice melt was very late) than during the other three years, with Ω_{arag} reaching a mean weekly minimum of 1.3 during SANAE 51 (Figure 32b). SANAE 49 had similarly low [CO_3^{2-}] and Ω_{arag} at the ice shelf during all weeks, where the timing of ice shelf ice thaw was also relatively late. The week with the highest mean Ω_{arag} was found at the ice shelf during the last week of January 2011 (SANAE 50) where sea ice melt was very early. Here mean Ω_{arag} was 2.13, while during January 2009, where ice shelf ice thaw was relatively early (SANAE 48), Ω_{arag} reached a weekly mean maximum of 2.1 (Figure 32).

The seasonal evolution of [CO_3^{2-}] and Ω_{arag} can be seen at the ice shelf during all years, where [CO_3^{2-}] and Ω_{arag} are lower during early summer (early January) and peak in the period between the 15th January and 4th February, after which they decrease (Figure 32). During SANAE 51 where sea ice melt was very late, early and late summer ice shelf [CO_3^{2-}] and Ω_{arag} were below or close to those of the estimated WW conditions, with only one week between the 29th January and 4th February 2012 where Ω_{arag} increased above 1.5 The lack of data in the EWG limits the ability to understand the seasonal cycle of $\Omega_{arag,}$ but the lack of interannual variability in Ω_{arag} in the EWG suggests that the phasing of sea ice melt does not play as strong a role in determining the interannual variability of Ω_{arag} in the EWG as it does at the ice shelf.

A dipole in $[CO_3^{2-}]$ and Ω_{arag} between the ice shelf and the EWG was seen during all years. Years with earlier ice shelf ice thaw had higher $[CO_3^{2-}]$ and Ω_{arag} at the ice shelf (SANAE 48 and 50) had lower $[CO_3^{2-}]$ and Ω_{arag} in the EWG (Figure 32). Years with later ice shelf ice thaw had lower $[CO_3^{2-}]$ at the ice shelf (SANAE 49 and 51) had higher $[CO_3^{2-}]$ in the EWG (Figure 32a). At the ice shelf during SANAE 49 and 51, weekly mean $[CO_3^{2-}]$ and Ω_{arag} were never above 108.7µmol/kg and 1.64 respectively, while during SANAE 48 and 50 all weekly mean ice shelf surface water $[CO_3^{2-}]$ and Ω_{arag} were always above 109.1µmol/kg and 1.65 respectively. $[CO_3^{2-}]$ and Ω_{arag} at the ice shelf during the lowest mean weeks of both SANAE 48 and 50 were higher than the $[CO_3^{2-}]$ and Ω_{arag} during the highest mean weeks of both SANAE 49 and 51. The opposite was found in the EWG, where weekly mean $[CO_3^{2-}]$ and Ω_{arag} were lower during SANAE 48 and 51, where EWG ice melt was relatively late, than during SANAE 49 and 50 where EWG ice melt was relatively early.

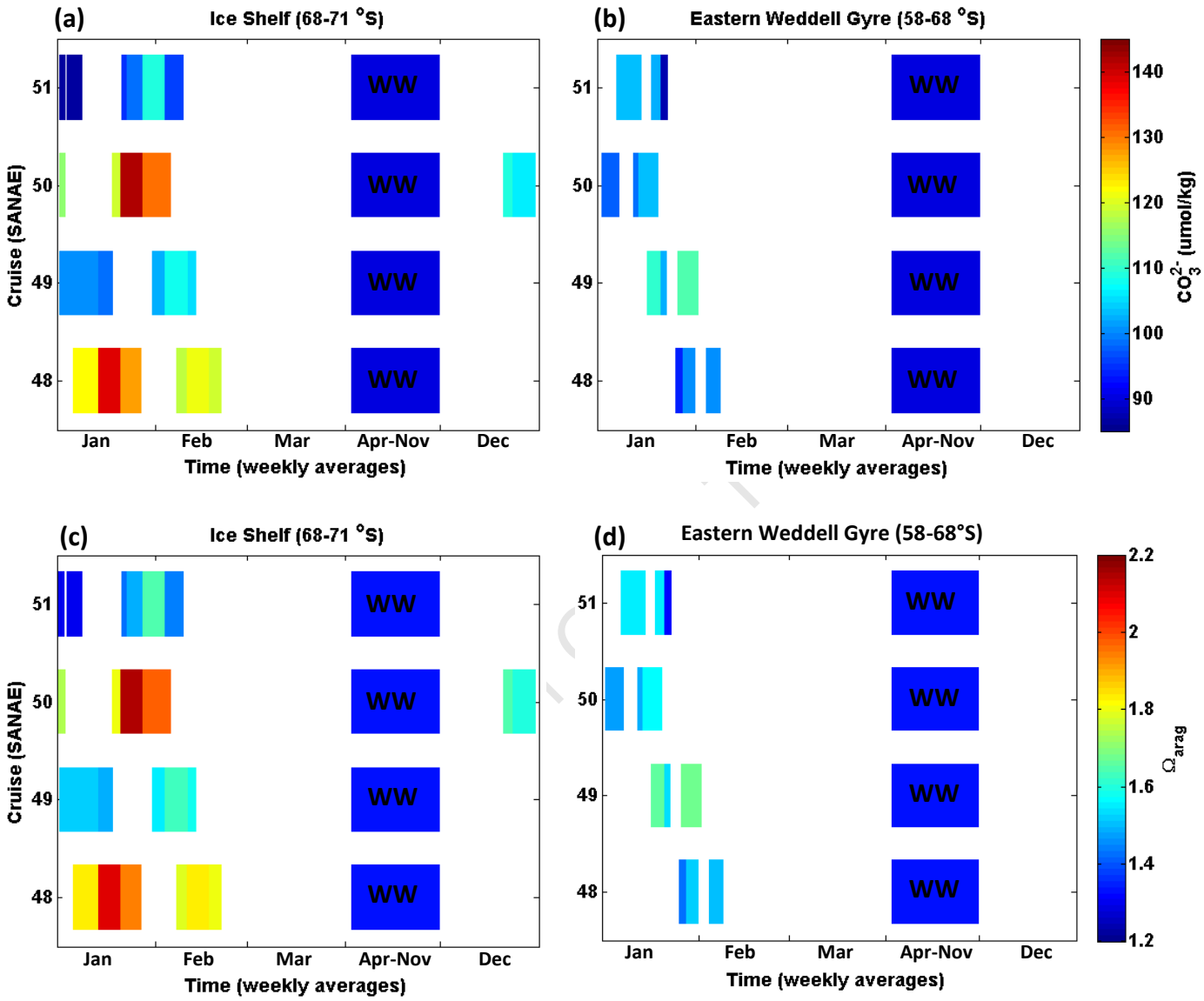

Figure 32. Weekly mean surface underway data for the Antarctic ice shelf (IS) and the Eastern Weddell Gyre (EWG) during the SANAE 48, 49, 50 and 51 cruises for carbonate ion concentration (CO_3^{2-}) at **(a)** the ice shelf and **(b)** the EWG, and for aragonite saturation state (Ω_{arag}) at **(c)** the ice shelf and **(d)** the EWG. The Winter Water (WW) values were estimated from the depth where potential temperature was at a minimum during the SANAE 50 CTDs.

4.1.6 Mean seasonal cycle of aragonite saturation state

All available ice shelf surface data for all years was averaged to get a monthly mean TA and DIC for December, January and February, with winter conditions estimated from SANAE 50 CTS's (Table 3), (Figure 33a). In the EWG data was collected only during January and thus a mean summer TA and DIC was calculated. The seasonal evolution of Ω_{arag} at the ice shelf shows that Ω_{arag} increased from winter (Ω_{arag}=1.34), to December (Ω_{arag}=1.58), to January (Ω_{arag}=1.62) and reached a maximum in early February (Ω_{arag}=1.69), with a decrease in both TA and DIC from winter through to summer in early February (Figure 33a).

The two first order mechanisms that change TA and DIC that will be analysed in this study are production and dilution, with production decreasing DIC and increasing TA and dilution decreasing both TA and DIC. Production decreased DIC and increased TA which increased the Ω_{arag}, while dilution decreased both TA and DIC, decreasing the $\Omega_{arag.}$ Salinity normalised TA (nTA) and DIC (nDIC) show the seasonal evolution of Ω_{arag} at the ice shelf in the absence of dilution, which decreases both TA and DIC (Figure 33b). Without the effects of dilution, Ω_{arag} reaches a maximum in February of approximately 1.85, suggesting that dilution decreased the summer Ω_{arag} increases by approximately 0.16. Dilution had a greater effect on reducing Ω_{arag} at the ice shelf than in the EWG. The mean seasonal decrease in Ω_{arag} during summer was greater at the ice shelf than in the EWG (Figure 33). At the ice shelf Ω_{arag} increased from winter to February by approximately 0.31, while in the EWG Ω_{arag} increased from winter to summer by approximately 0.13.

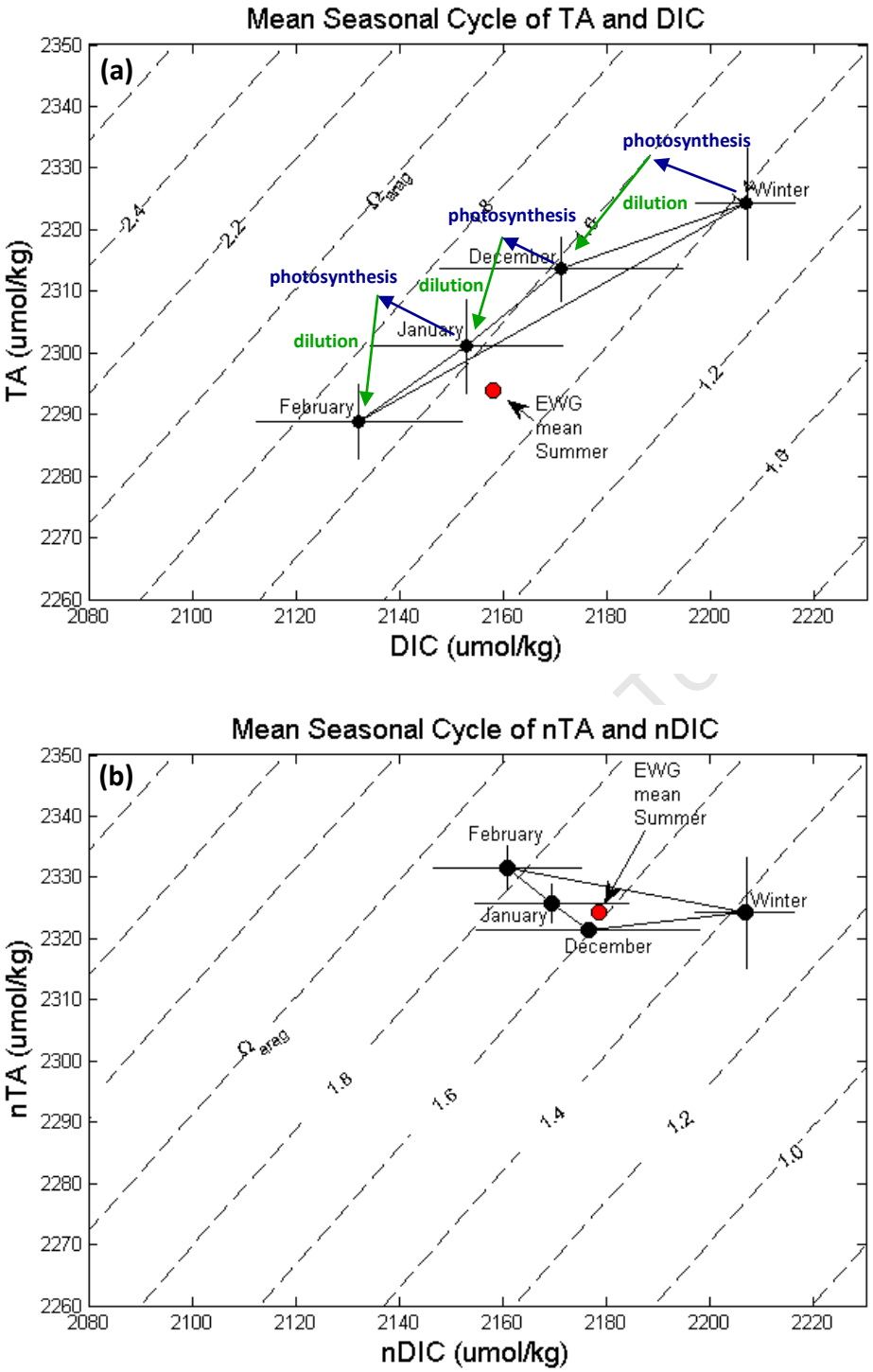

Figure 33. Seasonal evolution of **(a)** mean January and February total alkalinity (TA) and dissolved inorganic carbon (DIC) at the ice shelf with vectors indicating various processes that altered TA and DIC, as inferred from the salinity normalised TA (nTA) and salinity normalised DIC (nDIC) below, with the mean summer EWG TA and DIC shown in red and **(b)** mean January and February nTA and nDIC at the ice shelf with the mean summer EWG nTA and nDIC shown in red. Winter surface water conditions have been estimated from SANAE 50 CTDs, contours show aragonite saturation state (Ω_{arag}) at -1°C and 33.86psu.

4.2 Aragonite saturation states predicted for the future

A simplified sensitivity test was conducted to determine at what surface water fCO_2 would Ω_{arag} decrease below 1, and what the Ω_{arag} would be if surface water fCO_2 was doubled, a likely scenario for the end of this century (Steinacher et al., 2009). Assumptions were made that atmospheric CO_2 will increase according to the IPCC 92a scenario (IPCC, 2007), that the surface water fCO_2 will remain in equilibrium with atmospheric fCO_2 and that SST, SSS, nutrients and seasonality of the Antarctic ice shelf and EWG will remain unchanged during this century (Orr et al., 2005; McNeil and Matear, 2008).

Three years were chosen to represent three future surface water scenarios at the ice shelf and in the EWG: Early sea ice thaw (SANAE 50), Late sea ice thaw (SANAE 51) and 'Normal' sea ice thaw (SANAE 49). When surface water fCO_2 was increased by 160µatm, Ω_{arag} decreased below 1 at the ice shelf during all three future summer surface water scenarios (Figure 34). An atmospheric CO_2 increase of 160µatm is predicted to occur by 2054 under the IPCC 92a scenario (Steinacher et al., 2009). At the ice shelf, Ω_{arag} fluctuated between 0.95-1.50, 0.89-1.41, and 0.91-1.33 during the Early, "Normal" and Late sea ice melt scenarios respectively (Figure 34). The predicted mean Ω_{arag} at the ice shelf for the year 2054, was highest (Ω_{arag}=1.23) when sea ice melt was early and lowest when sea ice melt was late (Ω_{arag}=1.08), (Table 12). In the EWG, "Normal" ice melt conditions resulted in the highest mean summer Ω_{arag} (Ω_{arag}=1.18), while both Early and Late sea ice thaw had a summer Ω_{arag} of 1.10 (Table 12). At the ice shelf, mean pH was lowest (pH=7.95) during the Late sea ice thaw scenario, while in the EWG the lowest mean pH was found when sea ice thaw was early.

Doubled surface water fCO_2 resulted in the overall mean Ω_{arag} at both the ice shelf and in the EWG decreasing below 1 (Table 12). In water where $\Omega_{arag} < 1$ the aragonite shells of aragonite calcifying organisms will dissolve. The only time that the mean Ω_{arag} was above 1 was during the Early sea ice thaw scenario at the ice shelf (Table 12). The overall mean pH predicted for the end of this century was calculated to be 7.85 at the ice shelf and 7.83 in the EWG, approximately 0.25 and 0.27 pH units respectively below the current surface water pH of 8.10 (Royal-Society, 2005).

All three ice thaw scenarios were combined to get a predicted mean December, January and February Ω_{arag} for the middle of this century (fCO_2 increased by 160µatm) and for the end of this century (fCO_2 doubled). Winter conditions were estimated from SANAE 50 CTS's (Table 3) where the winter fCO_2 was increased by 160µatm (mid-century scenario) or doubled (end-of century scenario), (Figure 35). In the EWG data was collected only during January and thus a mean summer TA and DIC for the two future fCO_2 increase scenarios was calculated.

When surface water fCO_2 was increased by 160 µatm, the seasonal evolution of Ω_{arag} at the ice shelf showed that Ω_{arag} increased from winter (Ω_{arag}=1.03) to December (Ω_{arag}=1.12) to January (Ω_{arag}=1.7) to reach a maximum during early February (Ω_{arag}=1.18), with a decrease in both TA and DIC from winter through to late summer in early February (Figure 35). In the EWG the summer increase in Ω_{arag} was less, with mean summer Ω_{arag} in the EWG of approximately 1.1. When surface water was doubled, mean Ω_{arag} never increased above 1, the aragonite saturation horizon (Figure 35). Summer primary production (if unchanged from present levels) would have increased the Ω_{arag} from a winter minimum of approximately 0.78 to a summertime maximum during early February of 0.95.

Table 12. Mean aragonite saturation state (Ω_{arag}) and mean pH at the ice shelf and in the EWG for the three future surface water scenarios (Early ice thaw, Normal ice thaw and Late ice thaw), with surface water fCO_2 increased by 160µtm (predicted by IPCC92a for the year 2054) and with surface water fCO_2 doubled (predicted by IPCCa92a for the year 2100).

	With fCO_2 predicted for 2054				With fCO_2 predicted for 2100			
	Ice Shelf		EWG		Ice Shelf		EWG	
Summer Scenario	Ω_{arag}	pH	Ω_{arag}	pH	Ω_{arag}	pH	Ω_{arag}	pH
Early ice thaw	1.28	8.01	1.10	7.93	1.03	7.90	0.85	7.81
Normal ice thaw	1.09	7.96	1.18	7.96	0.87	7.85	0.94	7.85
Late ice thaw	1.08	7.95	1.10	7.95	0.79	7.80	0.86	7.83
Mean	1.15	7.97	1.13	7.95	0.90	7.85	0.88	7.83

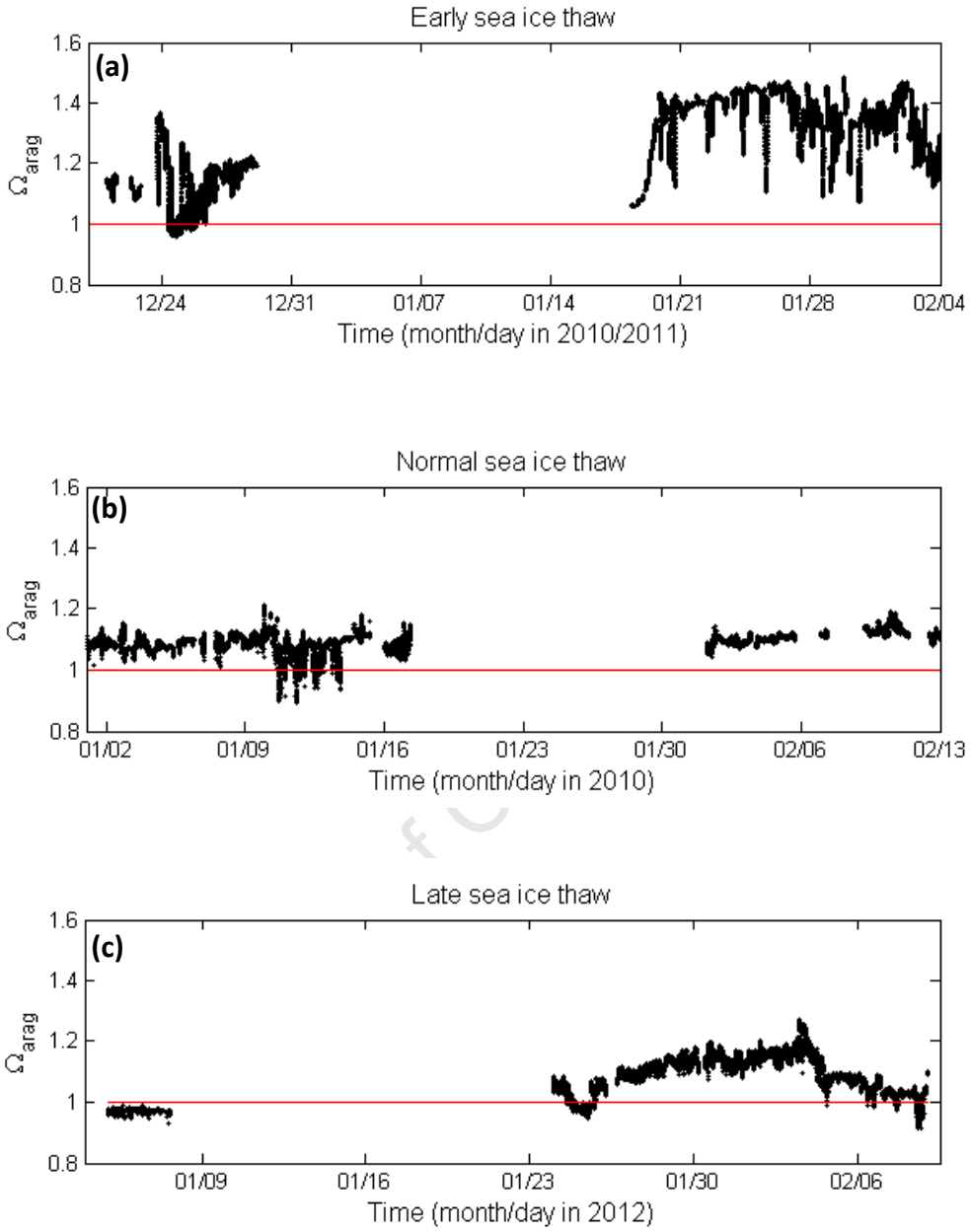

Figure 34. Predictions of the aragonite saturation state (Ω_{arag}) at the ice shelf with fCO_2 increased by 160µatm for three future sea ice scenarios, **(a)** Early sea ice thaw, **(b)** Normal sea ice thaw, **(c)** Late sea ice thaw, with a red line indicating the aragonite saturation horizon (Ω_{arag}=1).

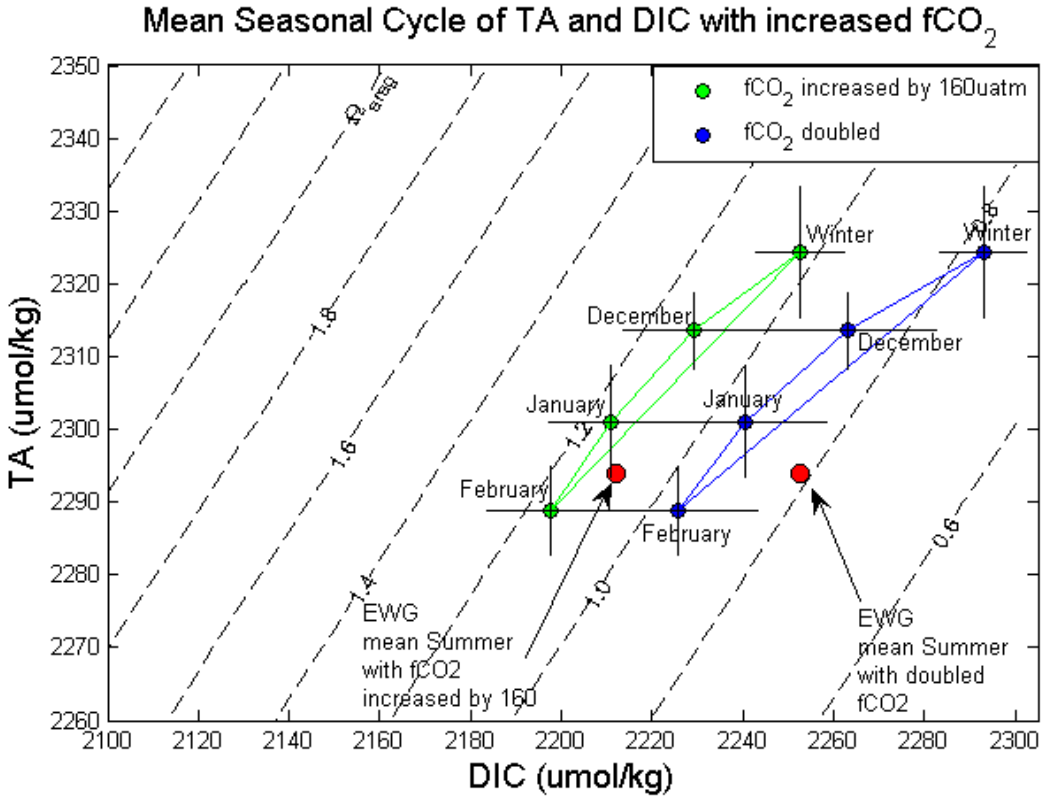

Figure 35. Surface water fCO_2 was increased by 160µatm (green) and surface water fCO_2 was doubled (blue) while TA was unchanged from present conditions, to analyse the possible seasonal cycle of Ω_{arag} as fCO_2 increases during this century. Seasonal evolution of mean January and February total alkalinity (TA) and dissolved inorganic carbon (DIC) at the ice shelf , with the mean summer EWG TA and DIC shown in red. Winter surface water conditions have been estimated from SANAE 50 CTDs, contours show aragonite saturation state (Ω_{arag}) at -1°C and 33.86psu.

5. Discussion

The seasonal cycle is the dominant mode of variability that couples climate forcing mechanisms to ecosystem variability in production (Thomalla et al., 2011) It is therefore important to understand the climate influence on the seasonal cycle and how it might influence ecosystem phenology and productivity, which, in turn, affect ocean biogeochemistry. In order to predict the trends and understand the effects of Ocean Acidification on marine ecosystems, regional scale ecosystem response to variability in the seasonal cycle need to be understood. Recent studies in both the Arctic Ocean (Steinacher et al., 2009; Yamamoto et al., 2012) and the Antarctic Ocean (McNeil and Matear, 2008) have highlighted the importance of the seasonal cycle in hastening the onset of surface water Ocean Acidification.

Coupled ocean-atmosphere modelling and empirical data studies suggest that surface waters in some regions of the Southern Ocean are likely to become undersaturated with aragonite (the less stable form of calcium carbonate) as early as the year 2030 (McNeil and Matear, 2008), by 2050 (Orr et al., 2005) or as late as the 22nd century when atmospheric CO_2 levels reach 1200µatm (Feely et al., 2004). The processes that influence the trends in Ocean Acidification within the Southern Ocean are complex due to the combination of seasonal variability, very low surface temperatures, sea ice, upwelling processes and high Revelle Factors (Orr et al., 2005; Sabine et al., 2004). McNeil and Matear (2008) show that there is large spatial and seasonal variability of carbonate ion concentration in the Southern Ocean, and highlight the need for a more robust understanding of how changes in the seasonal variability influences carbonate conditions that could become detrimental for marine calcifiers. Surface water aragonite undersaturation ($\Omega_{arag} < 1$) will not only result in the dissolution of aragonite shelled organisms such as the Thecosome Pteropods, but will also affect the ecosystem stability through calcifiers physiological adaptation to decreasing concentrations of carbonate ions (Fabry et al., 2008).

In the Southern Ocean *in situ* data is sparse and thus the current Ω_{arag} in most regions can only be estimated using models. This study shows that the seasonal cycle of sea ice thaw and summer primary production is important in increasing the summer surface water Ω_{arag} and creating a favourable habitat for Thecosome Pteropods. Interannual variability in the phasing

of sea ice thaw caused interannual variability in summer primary production and in the extent of the summer surface water increase in Ω_{arag}. Austral summer Ω_{arag} at the Antarctic ice shelf (71-68°S 4°E-13°W) and in the Eastern Weddell Gyre (EWG, 68-58°S 4°E-30°W) is currently above the level at which the mineral form of aragonite is thermodynamically stable ($\Omega_{arag} > 1$), (Figures 13b,19b,25b,30b). At the ice shelf during all four years, the photosynthetic uptake of CO_2 increased the carbonate ion concentration [CO_3^{2-}], from between 79-120µmol/kg when fCO_2 was high during early summer, to between 100-145µmol/kg when fCO_2 had decreased by mid-January/early February (Figures 14b,19b,24b,29b). At the Antarctic ice shelf, interannual variability in the timing of sea ice thaw saw years with early sea ice melt (such as 2009 and 2011) having higher Ω_{arag} than years with late sea ice melt (such as 2010 and 2012), (Figures 10,32c). While all years showed supersaturated Ω_{arag} ($\Omega_{arag} > 1$), the timing and extent of the summer Ω_{arag} increase differed interannually, being primarily affected by sea ice thaw, dilution and primary production. We also examined how the surface water Ω_{arag} would be affected by increased fCO_2 conditions predicted to occur through the 21st century (IPCC, 2007), assuming that climate change drivers that affect primary production and sea ice thaw remain unchanged.

5.1 Seasonal cycle of Ocean Acidification at the Antarctic ice shelf and in the Eastern Weddell Gyre

Productivity and hence carbon dynamics in much of the Southern Ocean, especially the marginal ice zone (MIZ) are characterised by a strong seasonal cycle (Thomalla et al., 2011). Within the Eastern Weddell Gyre (EWG) of the Southern Ocean, the seasonal cycle of water masses has been well documented (Carmack and Foster, 1975; Foldvik et al., 1985). Winter storms cause DIC-rich Weddell deep water (WDW) to be upwelled within the EWG (Gordon et al., 1981; Gordon and Huber, 1990). WDW is the source water to the Weddell Sea and mixes with the surrounding, cooler shelf water to become Modified Weddell Deep Water (MWDW) and eventually after heat loss through mixing, Winter Water (WW) with characteristic near freezing temperatures and salinities of between 34.20-34.52psu (Foster and Carmack, 1976a; Jones et al., 2010; Orsi et al., 1993; Whitworth and Nowling, 1987). Much of this characteristically very cold and high DIC WW is capped by sea ice during winter which limits gas exchange with the atmosphere (Hoppema et al., 1999; Takahashi et al., 1993). In winter and early summer before the development of spring phytoplankton blooms, supersaturated CO_2 conditions in WW have been documented, with surface water

fCO_2 reaching levels of 400µatm (Takahashi et al., 1993) and 375µatm (Bakker et al., 1997). Bakker et al (2008) found a surface water ΔfCO_2 (w-a) of up to 40µatm in some regions of the Weddell Gyre. During summer, sea ice melt freshens and warms WW, stratifying the upper layers of the water column and decreasing the Mixed Layer Depth (MLD), forming a less dense layer of Summer Surface Water (SSW) above the cooler and more saline WW (Carmack and Foster, 1975). It is this seasonal ice melt that drives water column stratification through the formation of shallow mixed layers (Smith and Nelson, 1985) and increased iron supply (Martin, 1990; Geibert et al., 2010), relieving light and iron limitation that are critical to the development of phytoplankton blooms which decrease surface water fCO_2 and increase $[CO_3^{2-}]$.

Examination of the surface water biogeochemistry during the four Antarctic ice shelf summers, shows a pattern of higher fCO_2 in early summer (late December and early January) and a decrease in surface water fCO_2 as summer progresses (late January and early February), (Figures 11c,15c,21c,27c). Increases in chlorophyll *a* fluorescence were indicative of phytoplankton blooms, which correlated well to periods of low fCO_2 during all years at the ice shelf. Surface water salinity and thus stratification at the ice shelf is primarily controlled by sea ice processes. A shallower mixed layer depth (MLD) and low SSS were observed to result in increased chlorophyll *a* fluorescence and decreased fCO_2 at the ice shelf during SANAE 49, 50 and 51, where CTD data was available (Figures 16,22,28). This suggests that sea ice melt decreased SSS, forming a stratified upper water column with shallow MLD's, where sufficient light and iron could facilitate high levels of primary production. This highlights the importance of summer sea ice thaw in stratifying the water column which initiates summer phytoplankton blooms, decreasing surface water DIC and increasing the Ω_{arag}, and thus limiting the dissolution of calcifiers (Figures 14,20,26,31).

Many studies have investigated the summer photosynthetic fCO_2 drawdown in the Southern Ocean (Metzel et al., 2006; Takahashi et al., 1993) and in different Southern Ocean regions such as Prydz Bay (Gibson and Trull, 1999), the Ross Sea (Arrigo et al., 2007; Sweeney, 2003), downstream of South Georgia (Jones et al., 2012) and the Weddell Gyre (Bakker et al., 1997; Bakker et al., 2008; Jones et al., 2010; Hoppema et al., 1995; Hoppema et al., 2000). All these studies highlight the importance of spring/summer phytoplankton blooms, initiated through ice-melt induced water column stratification (Smith and Nelson, 1986), in

decreasing the surface water fCO_2, creating an oceanic sink region for atmospheric CO_2 and increasing the $[CO_3^{2-}]$.

Changes in sea ice cover were found to be closely linked to interannual variability in annual production in a study by Arrigo et al (2008) in the Southern Ocean, where the Antarctic sea ice area typically increases from March to September and decreases from October to February (Kimura and Wakatsuchi, 2011). The timing of sea ice melt was found to be a major driver of interannual variability in surface water properties, carbon characteristics and primary production within the Ross Sea (Arrigo et al., 2007). Arrigo et al (2007) showed that inter-annual sea ice cover in the Ross Sea during a six year study (1997-2003) was highly variable, with three years displaying normal springtime sea ice retreat and three years showing late sea ice melt. Primary production was found to be higher during the years with normal sea ice melt than during the years with late sea ice melt, suggesting a positive relationship between early sea ice melt and increased primary production.

Thomalla et al (2011) show that in the Southern Ocean MIZ, the first and second weeks of December are the critical period for the initiation of phytoplankton blooms, and thus early sea ice melt in December would be favourable for increased primary production, as was observed in this study during SANAE 50 (Figure 22b,d). During the SANAE 51 where sea ice melt was very late, the summer bloom initiation occurred in mid-January, meaning that the phytoplankton had a shorter, less favourable summer period. Towards the end of summer (late January/February) the heat flux has decreased sufficiently so that if sea ice melt is late there will be less light available for photosynthesis and thus December bloom initiation is critical (Thomalla et al., 2011).

In this study, the interannual timing of sea ice thaw varied considerably, with very early sea ice thaw conditions during SANAE 50 (2010/2011) and very late sea ice melt conditions during SANAE 51 (2012), (Figure 10). As found in Arrigo et al (2007), this study showed years with relatively summer early sea ice thaw (SANAE 48 and 50) to have lower surface water fCO_2 and higher $[CO_3^{2-}]$ at the Antarctic ice shelf, while years with relatively later summer sea ice thaw (SANAE 49 and 51) to have higher surface water fCO_2 and lower $[CO_3^{2-}]$ (Table 10,11). This suggests that during January 2009 and 2011 (SANAE 48 and 50) early sea ice thaw during the critical first weeks of December stratified the upper water column, supporting increased primary production. Decreased SSS and increased chlorophyll

a fluorescence at the ice shelf during SANAE 48 and 50 confirm the presence of SSW (Figures 11a,c,21a,b,c,22). During SANAE 50, underway surface chlorophyll *a* fluorescence was almost zero but CTD data showed that just below the surface chlorophyll *a* fluorescence increased, suggesting that a thin layer of less dense, warmer water had capped the productive SSW. Late sea ice thaw as seen during SANAE 49 and 51 would suggest denser SSW at the ice shelf, a less stratified water column with a deeper MLD resulting in light limitation, and thus lower primary production and lower [CO_3^{2-}] at the ice shelf, as was observed (Figures 15a,c,16,27a,c,28, Table 11). Both these years had relatively high concentrations of DIC during IS1 where the MLD was usually below 50m, with the highest DIC of 2210µmol/kg found during January 2012 where sea ice still covered most of the Antarctic coastline between 0-10°W (Figure 10). By IS2 DIC had decreased in both SANAE 49 and 51 with an increase in chlorophyll *a* fluorescence and a decrease in the MLD (Figure 28,d, Table 11).

From these four years it can be seen that there were two contrasting sea ice and subsequent surface water fCO_2 scenarios at the ice shelf, which had a direct effect on the surface water [CO_3^{2-}] and Ω_{arag}. The first scenario being early sea ice thaw, with a longer summer period of ice-free, fresh summer surface water (SSW) and higher Ω_{arag}, as seen during SANAE 50 (2011). The second scenario is when there is late sea ice thaw, which shortens the summer season, with only around a month in which surface waters are ice free and sea ice melt induced water column stability can allow for the development of phytoplankton blooms, as seen during SANAE 51 (2012).

Ocean Acidification is more sensitive to changes in fCO_2 in regions with higher Revelle Factors than in regions with lower Revelle Factors (Egleston et al., 2010). The Revelle Factor describes how the oceanic fCO_2 changes for a given change in DIC, where the oceanic capacity for CO_2 uptake is inversely proportional the Revelle Factor (Sabine et al., 2004). The Revelle Factor tells us the sensitivity of fCO_2 to changes in TA and DIC, where $Revelle\ Factor \approx \frac{3 \cdot TA \cdot DIC - 2 \cdot DIC^2}{(2 \cdot DIC - TA)(TA - DIC)} \approx \frac{DIC}{CO_3^{2-}}$ (Sarmiento and Gruber, 2006). An increase in DIC will result in an increase in the Revelle Factor, while an increase in TA decreases the Revelle Factor. An overall mean summer surface water Revelle Factor of 14.3 was calculated for all years combined during this study which is below the average surface water Revelle Factor for the Southern Ocean of approximately 15 (Sabine et al., 2004). This is due to the data for this study being collected during summer when primary production decreased the

surface water DIC and thus decreased the Revelle Factor. A below average Revelle Factor during summer suggests that the Ω_{arag} will be less affected by variations in fCO_2, while during winter, where WW had a mean Revelle Factor of 15.85±0.45 (Table 3) and early summer when the Revelle Factor was high (> 15) a small increase in fCO_2 will result in a much greater decrease in Ω_{arag}.

All years during this study showed that the summer photosynthetic CO_2 uptake decreased DIC and therefore the Revelle Factor and increased [CO_3^{2-}], Ω_{arag}, and pH in the SSW, creating favourable summertime conditions for marine calcifying organisms. The interannual variability in the timing of sea ice thaw resulted in the two years with early sea ice thaw (SANAE 48 and 50) having higher Ω_{arag} and lower Revelle Factors at the Antarctic ice shelf than the two years where sea ice thaw was later (SANAE 49 and 51). The mean Ω_{arag} at IS2 during both SANAE 48 and 50 was above 1.9 due to the undersaturated fCO_2 conditions (Table 11). A minimum Ω_{arag} of 1.16 was observed on the 11th January 2010, during SANAE 49 (Figure 19b). This low Ω_{arag} was linked to high Revelle Factors of around 17 (Figure 19a) and a deepening in the MLD (Figure 16) limiting light availability for primary production, likely to have been caused by upwelling and mixing processes at the ice shelf. At the beginning and end of summer during the SANAE 51 ice shelf stations, Ω_{arag} was also very low, reaching minimum values of 1.23 and 1.2 during IS1 and IS2 respectively (Figure 30b). This suggests that the Ω_{arag} in the WW during the winter of 2011 was around 1.2 and that summer productivity reduced the surface water fCO_2 and increased the Ω_{arag} during January and February, decreasing the possibility of pteropod shell dissolution. A recent study by Bednarsek et al (2012) showed that live SO pteropods began to experience shell dissolution in waters with $0.98 > \Omega_{arag} > 1.12$. Therefore even if the pteropods are able to calcify in waters where $\Omega_{arag} < 1$ (Roleda et al., 2012) their rate of calcification may not be sufficient to stop dissolution of their shells from occurring.

Natural seasonal variation is believed to either amplify (Orr et at., 2005; Steinacher et al., 2009; Yamamoto et al., 2012) or mitigate Ocean Acidification (McNeil and Matear, 2008). To understand the seasonal variability of Ω_{arag}, we need to look at the processes that control Ω_{arag} and how they are affected by variability in the seasonal cycle. Carbonate ion concentration in the oceans is controlled by changes in TA and DIC (see eq. 2.2.14), where higher TA increases [CO_3^{2-}] and higher DIC decreases [CO_3^{2-}] (Sarmiento and Gruber, 2006).

The formation and dissolution of $CaCO_3$ minerals changes TA and DIC in a ratio of 2:1. Variations in $CaCO_3$ were previously thought to be solely due to marine calcifying organisms, but are now also believed to be influenced by sea ice formation and melting (Bakker et al., 2008; Jones et al., 2010). Recent sea ice research has shown that during sea ice formation, CO_2 is more efficiently rejected than TA, leading to higher concentrations of TA relative to DIC in the sea ice compared to the surrounding sea water (Rysgaard et al., 2012). The ratio of TA:DIC within sea ice has been found to be as high as 2:1, indicating that natural $CaCO_3$ is formed in sea ice, which has been confirmed by the discovery of ikaite crystals ($CaCO_3 \bullet 6H_2O$) in both southern and northern hemisphere sea ice (Dieckmann et al., 2008, 2010; Rysgaard et al., 2012). How the precipitation and release of ikaite crystals affects the surface ocean carbonate chemistry in the Southern Ocean is complex and remains poorly understood. During sea ice melt in spring and summer, $CaCO_3$ minerals within the melting ice should increase the TA and DIC and decrease the fCO_2 of the surface mixed layer. A TA and DIC increase in the summer surface layers of the WG was not observed during previous studies (Bakker et al., 2008; Jones et al., 2010) but rather a decrease of TA and DIC in a 2:1 ratio was found, confirming the complexity of this natural process. TA in this study was calculated using an empirical second order linear regression equation for the Southern Ocean region according to Lee et al (2006), where SSS and SST are used to estimate TA. Due to this, any ikaite mineral dissolution processes or calcification processes causing variability in TA and DIC (which are considered a second order effort compared to variations in TA and DIC through primary production and dilution) would not have been observed.

The extent to which calcifiers shells and skeletons are affected by increasing CO_2 depends upon the $CaCO_3$ saturation state (Ω), (Fabry et al., 2008), where $\Omega_{arag} \approx [CO_3^{2-}]/[CO_3^{2-}]_{sat}$. An $\Omega_{arag} < 1$ results in the dissolution of aragonite calcifier shells. Ocean $[CO_3^{2-}]$ can be approximated as [TA - DIC] (eq. 2.2.14) and therefore an increase in TA will result in an increase in $[CO_3^{2-}]$ and in an increase in Ω_{arag} (Sarmiento and Gruber, 2006). Ω_{arag} was found by Yamamoto et al (2012) in the Arctic Ocean, to decrease predominantly due to increased oceanic CO_2 uptake from the atmosphere and to a lesser extent from dilution as a result of freshwater input, and to increase due to primary production, warming of the surface water (as gas solubility decreases with increasing temperature (Takahashi et al., 1993)) and due to transport of carbon out of the surface water layers. For the purpose of this study we have separated the mechanisms that control variations in TA and

DIC into first order and second order mechanisms. The first order mechanisms that will be investigated are production and dilution. Production decreases DIC and increases TA in a 117:16 ratio due to the uptake of CO_2 and H^+ ions during photosynthesis (Sarmiento and Gruber, 2006; Zeebe and Wolf-Gladrow, 2001). Dilution occurs in MIZ primarily due to sea ice melt and results in a decrease in both TA and DIC (Yamamoto et al., 2012). The second order mechanisms that influence the $[CO_3^{2-}]$ through variations in TA and DIC are the air-sea flux of CO_2 gas (only affects DIC) and the precipitation and dilution of mineral $CaCO_3$, which changes TA and DIC in a ratio of 2:1 (Zeebe and Wolf-Gladrow, 2001). Although the second order mechanisms are important, in this study we will focus on the first order mechanisms as they appeared to be the dominant controlling mechanisms of the interannual seasonal variability in Ω_{arag} at the ice shelf.

Surface water Ω_{arag} was increased primarily through primary production decreasing DIC and was mainly decreased through the reduction of TA by dilution from sea ice melt (Figures 14,20,26,31). Winter Ω_{arag} has been estimated from SANAE 50 CTD's where winter water (WW) is defined as the water below the surface where potential temperature is at a minimum as in Jones et al (2010), (Table 3). From winter to summer both TA and DIC decreased in all years, resulting in an increase in Ω_{arag}. In the Southern Ocean winter upwelling causes an increase in surface water TA and DIC as deeper waters have accumulated TA from the dissolution of $CaCO_3$ and DIC-rich Circumpolar Deep Water (Key et al., 2004; Whitworth and Nowling, 1987). Thus in winter, surface water TA and DIC are high, causing Ω_{arag} to reach a winter seasonal minimum, as seen during this study and in McNeil and Matear (2008). Summer production in the stratified surface layers decreases DIC, increasing the Ω_{arag} (Figure 33). Salinity normalised TA (nTA) and DIC (nDIC) show that in the absence of dilution, production would have resulted in a likely increase in the overall mean Ω_{arag} by approximately 0.45, from a winter Ω_{arag} of 1.38 to a summer Ω_{arag} of 1.83. Dilution decreased the increase in Ω_{arag} from winter to summer by approximately 0.31, resulting in a summer maximum Ω_{arag} in early February of 1.69 (Figure 33). Surface water Ω_{arag} in the EWG was less influenced by the interannual variability in the seasonal cycle than Ω_{arag} at the ice shelf (Figure 32b,c).

SANAE 48 (2009) was the only year where the Ω_{arag} was higher in January than in February, as January TA and DIC concentrations were higher and lower respectively than in February (Figure 14). All other years showed increasing Ω_{arag} from winter through summer, with early

February having the highest Ω_{arag} (Figure 20,26,31). The formation of stratified layer of SSW by February (late summer) facilitated primary production, decreasing fCO_2 and increasing $\Omega_{arag,}$ thus creating favourable conditions for marine calcifying organisms. All years show that small variations in DIC resulted in variations in $\Omega_{arag,}$ while small and even large (SANAE 49, Figure 20a) variations in TA had a much lesser effect on $\Omega_{arag.}$ This is important for Ocean Acidification in the future, where some studies suggest that summer surface water TA will decrease during this century, due to increased stratification limiting the upwelling of deeper waters with higher concentrations of TA from calcium carbonate dissolution, and due to increased sea ice melt as SSTs increase, resulting in higher levels of TA dilution (Doney, 2006; Yamamoto et al., 2012). Future DIC is predicted to increase as a result of increasing air-sea CO_2 exchange as anthropogenic CO_2 increases (Yamamoto et al., 2012). A further concern is that if production decreases with climate change through increased stratification limiting the upwelling of nutrients (Steinacher et al., 2010), dilution may result in rapidly decreasing the Ω_{arag} below the winter minimum without the primary production contribution to remove surface water CO_2 and increase Ω_{arag}.

This study shows that the ice shelf and the EWG are two separate systems, with surface water Ω_{arag} the ice shelf being much more sensitive to variations in the timing of sea ice melt than surface water Ω_{arag} in the EWG. During years with early sea ice melt in the EWG (SANAE 49 and 50) weekly mean Ω_{arag} in the EWG was mostly higher than the weekly mean Ω_{arag} during years where ice melt in the EWG was later (SANAE 48 and 51). Weekly mean ice shelf Ω_{arag} was never below 1.6 during SANAE 48 and 50 where ice shelf sea ice melt was early, while Ω_{arag} during these two years in the EWG was much lower never going above 1.56. Conversely, during SANAE 49 and 51 where ice shelf ice melt was late, weekly averaged Ω_{arag} was lower at the ice shelf (below 1.45) than in the EWG, where weekly averaged Ω_{arag} increased to around 1.6 (Figure 32). During SANAE 48 and 50, weekly averaged $[CO_3^{2-}]$ was always above 105µmol/kg, the average $[CO_3^{2-}]$ in the Southern Ocean (Orr et al., 2005), while during SANAE 49 and 51 the opposite was found, with ice shelf weekly average $[CO_3^{2-}]$ being close to or below 105µmol/kg. This highlights the importance of understanding regional scale carbonate processes especially in ice shelf regions where the phasing of sea ice thaw is critical.

In summary, interannual variability in the timing of the summer sea ice thaw was the major driver of the interannual variability of summertime surface water Ω_{arag}. Relatively early sea

ice thaw resulted in increased primary production, decreased surface water fCO_2 and increased Ω_{arag}, while the opposite was observed for late sea ice thaw. Surface water Ω_{arag} was at a minimum during winter and increased through summer, reaching a maximum during late January/early February during all years. Production was the major driver of the summer increase in Ω_{arag}, with dilution of TA from sea ice melt dampening the summer Ω_{arag} increase. All years showed increased summertime Ω_{arag} highlighting the importance of seasonal phytoplankton blooms in decreasing the possibility that marine calcifiers may experience shell dissolution which would likely have knock-on effects for the ice shelf ecosystem.

5.2 Ecosystem implications of carbonate ion variability

Ocean Acidification will affect the process of calcification, as calcifying organisms precipitate calcium carbonate minerals through the reaction of calcium and carbonate ions (Royal-Society, 2005). There are contrasting views on whether calcification is possible in waters where the carbonate saturation state (Ω) is < 1 (Roleda et al., 2012), but there is agreement that in water where $\Omega < 1$, dissolution of shells and skeletons is likely (Fabry et al., 2008). Comeau et al (2010) showed that when fCO_2 was experimentally increased, the Arctic aragonite calcifying Pteropod, *Limacina helicina* was still able to calcify even when Ω_{arag} decreased below 1, although calcification rates did decrease as Ω_{arag} decreased. A recent study by Bednaršek et al (2012) showed that live pteropods showed shell dissolution in Antarctic surface waters where $0.98 > \Omega_{arag} > 1.12$. All surface waters during our study showed supersaturated aragonite conditions at the Antarctic ice shelf and in the EWG, with $\Omega_{arag} > 1$. Aragonite calcifiers such as pteropods, would have likely not experienced shell dissolution at the ice shelf during the summers of 2009 (Figure 13b), 2010 (Figure 19b), 2011 (Figure 25b) and 2012 (Figure 30b). Winter Water (WW) conditions observed during SANAE 50 ($\Omega_{arag}=1.34\pm0.07$) suggest that during winter surface water Ω_{arag} was > 1 and therefore aragonite calcifiers would have likely not been detrimentally affected by low Ω_{arag} during winter.

Although calcification was possible and dissolution was unlikely during all years due to the Ω_{arag} being > 1, the physiological implications of calcification in water where carbonate ion concentrations are low come into effect well before the $\Omega_{arag} = 1$, which impacts on the entire ecosystem (Fabry et al, 2008; Royal-Society, 2005; Orr et al., 2005). Laboratory Ocean

Acidification experiments (Riebesell et al., 2000) as well as paleoceanographic studies (Barker and Elderfield, 2002) show a positive correlation between increased [CO_3^{2-}] and calcification rates, and a negative correlation between decreased [CO_3^{2-}] and calcification rates. This means that as [CO_3^{2-}] decreases, calcification will become increasingly difficult requiring a greater proportion of energy, and could negatively affect calcifiers, their predators and ecosystems before undersaturation is reached (Fabry et al, 2008; Royal-Society, 2005). When [CO_3^{2-}] decreases, calcifying organisms concentrate an increasing proportion of their energy on the process of calcification, therefore neglecting other vital processes such as growth and reproduction (Seibel et al, 2012). So, in waters where Ω_{arag} is close to but > 1, calcifying organisms may experience significantly decreased growth and reproductive success, impacting the balance of the ecosystem, even though calcification is still thermodynamically stable. Due to the physiological and ecosystem implications of Acidification coming into effect before the Ω_{arag} decreases < 1, Ocean Acidification effects on ecosystem processes will likely be a concern in the near future, before the aragonite saturation horizon reaches the surface (Fabry et al, 2008; Royal-Society, 2005; Orr et al., 2005).

The seasonally driven Antarctic ecosystem is home to many endemic species (Griffiths, 2010). Aragonite-calcifying pelagic gastropod molluscs, known as Thecosome (shelled) pteropods, are prominent components of polar ecosystems (Comeau et al., 2009, 2010; Hunt et al., 2008, 2010). These zooplankton are an important link in the Antarctic trophic structure as both predators and prey, grazing on smaller diatoms, copepods and phytoplankton while being prey items for the larger Gymnosome (naked) pteropods, zooplankton, fish, whales and some sea birds (Hunt et al., 2008; Karnovsky et al., 2008). Pteropod life cycles are poorly understood with only a few studies of both the Arctic and Antarctic pteropods (Hunt et al., 2008). Literature suggests that Antarctic pteropods survive for 1-2 years, having two generations per life cycle (Hunt et al., 2008; Kobayashi et al., 1974; Seibel and Dierssen, 2003). The spawning events are during spring and late summer, with young juveniles or larvae having to survive overwinter surface water conditions (Hunt et al., 2008). The most dominant Southern Ocean Thecosome pteropod is *Limacina helicina,* a bipolar species believed to be particularly vulnerable to ocean acidification (Hunt et al., 2010). Sediment traps in the Southern Ocean show that just below the aragonite saturation horizon pteropod shells (predominantly *Limacina helicina*) showed signs of partial dissolution and pitting (Honjo et al., 2004), indicating the sensitivity of pteropods to low [CO_3^{2-}].

In this study, two contrasting extreme summer sea ice melt scenarios were observed, early sea ice melt (2011) and late sea ice melt (2012). The timing of sea ice melt had a direct effect on the surface water biogeochemistry and would have therefore affected the Antarctic ice shelf and EWG ecosystems. A schematic of the contrasting sea ice conditions and the subsequent ecosystem implications can be seen in figure 36 showing how the interannual variability in the timing of sea ice melt may have trade-offs for the Antarctic ecosystem. Seasonal sea ice creates a critical habitat for sea ice algae and Antarctic krill, both of which play important roles in the Antarctic ecosystem (Brierly et al, 2002; Smetacek and Nicol, 2005; Thomas and Dieckmann, 2010). Sufficient winter sea ice is essential for the survival of sea ice algae that support Antarctic krill (Atkinson et al., 2004). Atkinson et al (2004) showed a positive relationship between sea ice extent and krill density in the Southern Ocean, thought to be due to higher levels of sea ice algae or possibly increased protection from the sea ice. Krill are critical species in the Southern Ocean ecosystem, being key to an energy efficient food web, an important prey source for albatross, penguins, seals and whales (Atkinson et al, 2004). Thus during years with late sea ice melt such as SANAE 51 (2012), there would likely be persistency of sea ice algae, krill and their predators (Figure 35a). The opposite is true for the calcifying pteropods, which rely on sufficient summer sea ice melt in initiating summer phytoplankton blooms to increase the Ω_{arag}. Pteropods rely on phytoplankton as a source of food as well as to decrease surface water fCO_2 and increase Ω_{arag}, and thus during early sea ice melt when primary production is higher, pteropods densities will likely increase. Although years with earlier sea ice melt seem to favour the survival of calcifying organisms such as pteropods, they are likely to be less favourable to the Southern Ocean krill population.

This highlights the importance of the timing and extent of sea ice melt in increasing the summer Ω_{arag} to a level where pteropods do not experience shell dissolution, and are able to grow and reproduce. As atmospheric and hence surface water fCO_2 increases due to anthropogenic activities, the seasonal summer fCO_2 decrease and subsequent Ω_{arag} increase may become the only time in which pteropods will be able to survive. In the next few decades, even if summer biological drawdown of CO_2 increases Ω_{arag} to levels where dissolution does not occur, the winter increase in fCO_2 and subsequent decrease in Ω_{arag} to levels of undersaturation will likely be detrimental to the pteropod population due to their overwintering lifestyles, leading to their northward migration or decline (McNeil and Matear, 2008). We will now examine two such future surface water CO_2 increase scenarios.

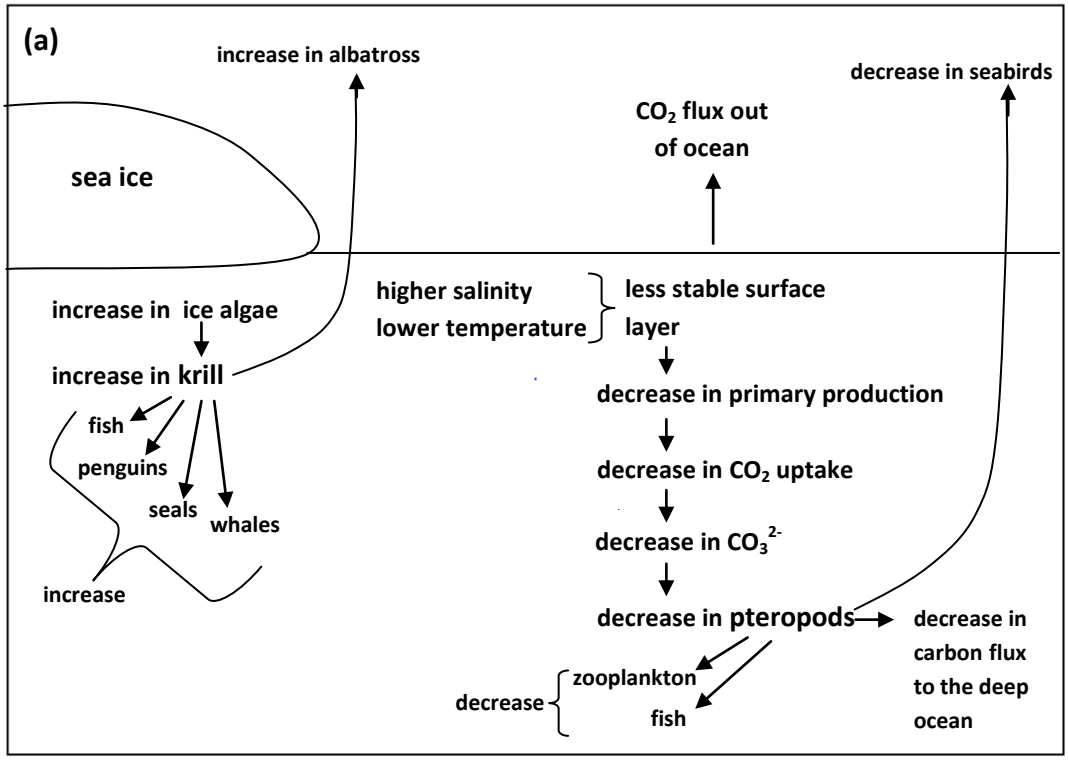

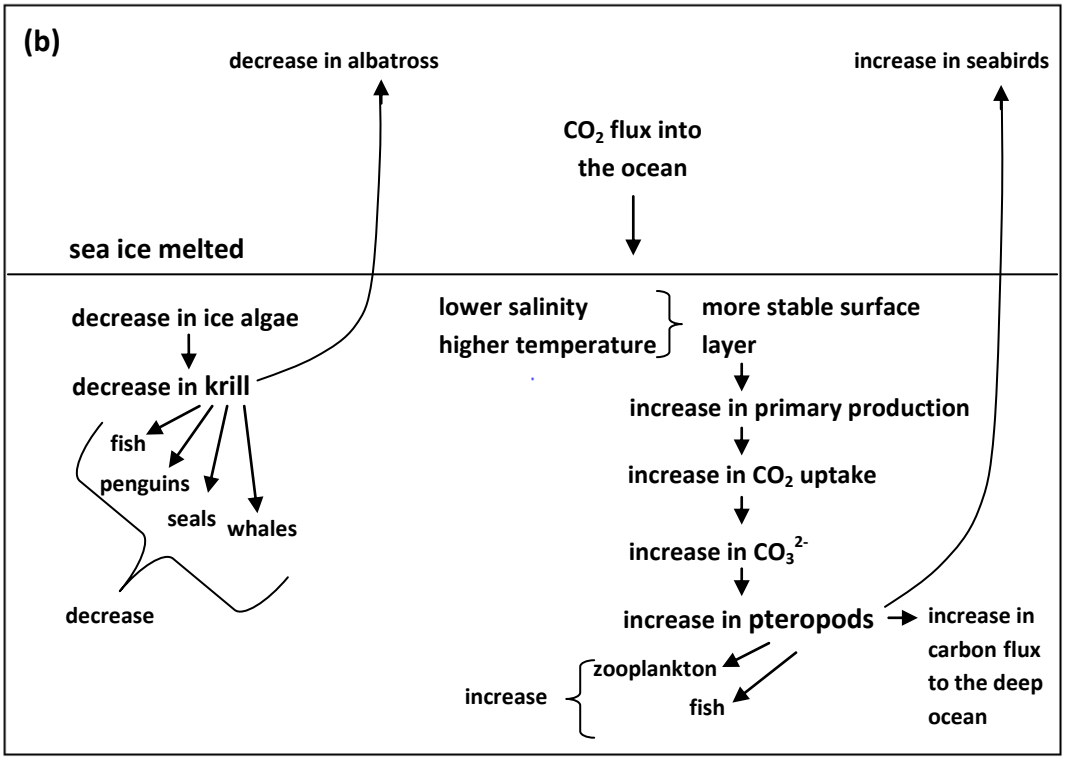

Figure 36. Schematic representation of two Austral summer scenarios for the Antarctic Ice shelf region with **(a)** being when there is low summer sea ice melt and **(b)** being when there is high summer sea ice melt

5.3 Outlook Scenarios for the 21st Century

As increased anthropogenic CO_2 enters the surface waters during this century, the concentration of DIC in the surface waters will increase causing a decrease in the oceans buffering capacity and resulting in higher sensitivity to local variability of DIC and TA (Egleston et al., 2010). This will likely result in local seasonal variations in Ω_{arag} which are mainly controlled by summertime primary production and dilution, being considerably amplified (Egleston et al., 2010). Increasing anthropogenic CO_2 will affect the oceans in two ways: the first is through climate change, causing ocean warming, sea ice melt and changes in ocean stratification and the second is through the process of Ocean Acidification (the chemical reaction of CO_2 with H_2O to increase the H^+ ions and decrease the CO_3^{2-} ions) (McNeil and Matear, 2007; Steinacher et al., 2009). In the Arctic Ocean, climate change effects have been shown to amplify the process of Ocean Acidification, through increased oceanic CO_2 uptake, as sea ice cover retreats, as well as through the decrease in $[CO_3^{2-}]$ by the increased addition of fresh water through sea ice melt (Steinacher et al., 2009; Yamamoto et al., 2012). Increasing sea surface temperatures as a result of climate change have been shown to increase surface water $[CO_3^{2-}]$ through solubility-driven CO_2 out-gassing due to gas being less soluble in warmer water (McNeil and Matear, 2007; Orr et al., 2005). In the Antarctic Ocean, future changes in surface water $[CO_3^{2-}]$ as a result of increased flux of atmospheric CO_2 into the surface waters and due to the upwelling of DIC-rich WDW, are predicted to more than offset the increase in $[CO_3^{2-}]$ as a result of ocean warming (McNeil and Matear, 2007).

McNeil and Matear (2008) looked at future Southern Ocean surface water $[CO_3^{2-}]$ and pH with various atmospheric fCO_2 increases scenarios, neglecting the impacts of climate change on Ocean Acidification. Orr et al (2005) show that variations in $[CO_3^{2-}]$ due to variations in temperature are very small, while Gruber (2011) suggest that SST's in the Southern Ocean are not likely to change much during this century. Here we examine future changes in Ocean Acidification assuming that TA remains constant and that climate change effects are negligible, as in Orr et al (2005).

Carbonate ion concentration in modern day surface Southern Ocean waters has already been reduced since preindustrial times by 18µmol/kg (Orr et al., 2005), and is predicted to decrease below the level at which the mineral form of aragonite is stable (66µmol/kg) within

the next few decades (McNeil and Matear, 2008; Orr et al., 2005). In this study, three years were chosen to represent three future sea ice melt and surface water scenarios at the ice shelf and in the EWG: Early sea ice thaw (eg: SANAE 50), Late sea ice thaw (eg: SANAE 51) and Normal sea ice thaw (eg: SANAE 49). Surface water fCO_2 was increased by 160µatm, while TA, SST and SSS were unchanged, to calculate a possible surface water Ω_{arag} state for the year 2054 (Figure 34). The Intergovernmental Panel on Climate Change (IPCC) have put forth two atmospheric CO_2 increase scenarios: the IS92a 'continuously increasing' scenario where atmospheric CO_2 reaches 788µatm by the year 2100, and the S650 'stabilization' scenario where by 2100 atmospheric CO_2 concentrations reach 563µatm. As current atmospheric CO_2 levels are approximately 392ppmv (Tans and Keeling, 2011), it follows that an increase of 160ppmv increase would increase atmospheric CO_2 levels to around 550ppmv. Under the IPCC IS92a scenario, atmospheric CO_2 concentration is predicted to reach 552ppm by the year 2054 - the middle of this century (Steinacher et al., 2009). If this IPCC prediction is accurate, our study suggests that by 2054 the Antarctic ice shelf surface waters between 4°E and 14°W will experience periodic intra-seasonal aragonite undersaturated conditions during the summer (Figure 34). With surface water fCO_2 increased by 160µatm, the highest mean Ω_{arag} at the ice shelf of 1.28 was found during the Early ice thaw scenario, while the Late ice thaw scenario resulted in the lowest mean Ω_{arag} at the ice shelf of 1.08 (Table 12). In the EWG, the mean Ω_{arag} was highest (Ω_{arag}=1.18) during the "Normal" ice thaw scenario than during both the Early and Late ice thaw scenarios (Table 12). As we saw in section 5.1, the summer surface water Ω_{arag} was likely to be controlled mainly by primary production and dilution through sea ice melt. Early sea ice thaw resulted in increased production and thus in a higher surface water Ω_{arag} (Figure 34a). This may be the true under the present climate conditions, but in the future where increased stratification is predicted to decrease upwelling, limiting the supply of nutrients to surface water and decreasing primary production, in combination with possible increased dilution from sea ice melt (Steinacher et al., 2010), the seasonal summertime increase in Ω_{arag} will likely become smaller.

The predicted aragonite undersaturation of the ice shelf and EWG surface waters by the year 2054 agrees well with Orr et al (2005), where 13 ocean-carbon models were used to predict aragonite undersaturation in Southern Ocean surface waters to occur by the year 2050. McNeil and Matear (2008) using an empirical data analysis show the Antarctic ice shelf and the EWG will likely experience winter aragonite undersaturation by the year 2030, 30 years before the annual average Southern Ocean aragonite undersaturation is predicted to occur.

They propose that early aragonite undersaturation will likely occur between 65 and 70°S in the winter months, due to the winter upwelling of DIC-rich sub-surface waters in this latitudinal band.

As a direct result of increased bicarbonate ions and decreased carbonate ions due to an increase in surface water fCO_2, the mean surface water pH decreased below 8 at both the ice shelf and in the EWG during all ice thaw scenarios, except during the Early ice thaw scenario at the ice shelf where the mean pH was 8.01 (Table 12). The overall mean of 7.97 is slightly more than a 0.1 decrease from the current average surface water pH of 8.1 (Royal-Society, 2005).

This study also shows that the Southern Ocean seasonality will influence future surface water Ω_{arag} at the Antarctic ice shelf and in the EWG, resulting in periodically supersaturated summertime surface water Ω_{arag} conditions (Figure 34). Early sea ice melt may prolong summertime surface water aragonite undersaturation ($\Omega_{arag} < 1$) at the ice shelf, but will likely be less effective in the EWG where seasonal variability had less of an effect on surface water Ω_{arag} (Figure 32c). If the surface water CO_2 remains in equilibrium with atmospheric CO_2 (as assumed in Orr et al., 2005) our study shows wintertime and periodic summertime aragonite undersaturation of the Antarctic ice shelf and EWG surface waters by the middle of this century, reinforcing model predictions by McNeil and Matear (2008) and Orr et al (2005). If the CO_2 disequilibrium between the surface water and the atmosphere is taken into account, then surface water aragonite undersaturation will occur a few years later (McNeil and Matear, 2008). A lag between the upper ocean CO_2 levels and atmospheric CO_2 levels is likely, due to the finite rate of air-sea CO_2 exchange and because of mixing processes between the surface and deep oceans (McNeil and Matear, 2008).

The mean seasonal cycle of ice shelf surface water Ω_{arag} with increased fCO_2 shows that the mean Winter Ω_{arag} estimated from SANAE 50 CTD's will likely be just above 1 (Ω_{arag}=1.03) when surface water fCO_2 is increased by 160µatm (Figure 35). Although the mean Winter, December, January and early February Ω_{arag} is greater than 1, Ω_{arag} decreased below 1 during all ice thaw scenarios (Figure 34). The summer increase in Ω_{arag} through summer primary production (assumed to remain unchanged during this century) was very small, with Ω_{arag} increasing from a winter value of approximately 1.03 to an early February value of approximately 1.16 (Figure 35). In the EWG the summer increase in Ω_{arag} was less, with a

mean summer Ω_{arag} of approximately 1.1 (Figure 35). If summertime primary production decreases during this century, as is likely (Steinacher et al., 2010), then the summer surface water increase in Ω_{arag} will likely decrease, resulting in summer Ω_{arag} of below 1.16, which will likely induce physiological stress on pteropods growth and reproductive success, with severe ecosystem implications. Summer surface water conditions at the ice shelf by the middle of this century, were observed to be more favourable for the pteropods than summer surface water conditions in the EGW, where summertime Ω_{arag} is lower (Figure 35). Thus the ice shelf may become a narrow habitat for pteropods in the future where possibly between 68° and 58°S, surface water Ω_{arag} may become undersaturated slightly earlier.

The aragonite undersaturation of the Southern Ocean surface waters within this century is almost unquestionable, but the year in which undersaturation will likely occur is still under much debate, as future atmospheric CO_2 predictions rely on IPCC carbon-climate models. The IPCC atmospheric CO_2 increase scenarios depend on many factors such as economic growth, variations in carbon sinks and climate and ecosystem feedbacks in a changing climate, all of which are currently estimated with much uncertainty (Canadelle et al., 2007; Fabry et al., 2008; IPCC, 2007; Le Quéré et al., 2009)

The consequences of future aragonite undersaturation of the Antarctic ice shelf and EWG surface waters for the Antarctic pteropods and the Antarctic marine ecosystem are serious (Fabry et al., 2008; Guinotte and Fabry, 2008; Orr et al., 2005). Due to the overwintering life cycles of pteropods, they will likely need to adapt to the possible wintertime aragonite undersaturation within the next two decades (Hunt et al., 2008; McNeil and Matear, 2008). Fabry et al (2008) hypothesise that as the surface water Ω_{arag} approaches 1, Thecosome pteropods will either have to adapt to surviving in water where aragonite is undersaturated or confine their vertical and latitudinal distributions to areas where $[CO_3^{2-}]$ is higher such as the warmer waters North of the Polar Front (McNeil and Matear, 2008). A northward migration of the pteropods may induce additional stress, as the Antarctic pteropods are adapted to the low temperatures of the Polar region, and they may not be able to survive in warmer waters (Fabry et al., 2008). The Gymnosome pteropods, zooplankton, fish and seabirds that prey on Thecosome pteropods will also have to either adapt and find new prey species or migrate northward with the aragonite saturated surface waters and the pteropods. For the carnivorous pelagic fish, switching to other types of prey may be an easy option, which would in turn increase the pressure for food on juvenile fish (Fabry et al., 2008). For Gymnosome

pteropods that prey only on Thecosome pteropods, this may not be an option which would result in them either following their prey northward or being unable to survive, which would have implications on the feeding diversity and trophic structure of the rest of the ice shelf and WEG ecosystems (Fabry et al., 2008).

Pteropods are not only important in the trophic structure of the ice shelf and the EWG, but also play a vital role in the transport of carbon out of the surface waters, through the sinking of their aragonite shells (Fabry et al., 2008; Hunt et al., 2008). A decrease in the production and export of $CaCO_3$ from the surface waters to the deep sea will increase the concentrations of both TA and DIC in the surface water. This will have contrasting effects on the surface water Ω_{arag} as increases in TA increase Ω_{arag} while increases in DIC decrease Ω_{arag} (Sarmiento and Gruber, 2006). The increase in TA will slow the process of Ocean Acidification by neutralising the bicarbonate ions, but increasing DIC will likely amplify the effects of anthropogenic CO_2 increase and climate change, possibly decreasing the oceanic CO_2 sinks further.

Seasonal summertime primary production may help to create favourable surface water Ω_{arag} in a higher CO_2 world. Early sea ice melt would result in higher primary production and hence in lower surface water fCO_2 and increased Ω_{arag}. Along with increased sea ice melt ocean stratification is predicted to increase, decreasing TA, nutrients and primary production in the surface waters (Gruber, 2011; Steinacher et al., 2010). This would suggest the although early sea ice melt currently favours the increase in Ω_{arag}, when surface water fCO_2 increases to levels where the Ω_{arag} is decreased below saturation (predicted within the next 2-4 decades), neither pteropods nor krill are likely to survive at the Antarctic ice shelf and in the EWG unless they are able to adapt rapidly to the changing conditions.

Doubled surface ocean fCO_2 (simulated to occur by the end of this century) resulted in mean surface water aragonite undersaturation during both the "Normal" and Late sea ice thaw scenarios at both the ice shelf and in the EWG (Table 12). During the Early sea ice thaw scenario, the mean ice shelf Ω_{arag} was just above saturation (Ω_{arag}=1.03), while in the EWG mean Ω_{arag}=0.85. WW fCO_2 was estimated to be 369.36±25.75µatm, which, when doubled (738µatm) reaches the predicted atmospheric fCO_2 level for the year 2090 under the IPCC IS92a atmospheric increase scenario (Steinacher et al., 2009). Thus our study suggests that by the end of this century surface waters at the Antarctic ice shelf and in the EWG will likely be

undersaturated with aragonite (Table 12). This prediction agrees with model the predictions of Orr et al (2005), who show that all Southern Ocean surface waters will likely become undersaturated with aragonite by 2100, with surface water pH dropping to 7.8 (McNeil and Matear, 2008).

As a direct result of increased bicarbonate ions and decreased carbonate ions due to an increase in surface water fCO_2, the mean surface water pH decreased below 7.9 during all sea ice thaw scenarios (Table 12) The overall mean pH when surface fCO_2 was doubled was calculated to be 7.85 at the ice shelf and 7.83 in the EWG, approximately 0.25 and 0.27 units respectively below the current surface ocean pH of 8.1 (Royal-Society, 2005). This agrees well with the predictions of McNeil and Matear (2008), where they show that Southern Ocean surface water pH will likely decline by 0.3 pH units by the year 2100, with seasonality possibly resulting in a wintertime pH decrease of 0.3 pH units by the year 2080.

The mean seasonal cycle of ice shelf surface water Ω_{arag} with doubled fCO_2 shows that the mean Ω_{arag} during winter, December, January and February will likely be below 1 (Figure 35). The summer increase in Ω_{arag} through summer primary production (assumed to remain unchanged during this century) increased Ω_{arag} by approximately 0.17, from an estimated winter value of 0.87 to a summer maximum during early February of 0.95 (Figure 35). In the WEG surface water Ω_{arag} was also below 1 throughout summer, with a smaller summer Ω_{arag} increase than at the ice shelf. This suggests that by the end of this century, summer phytoplankton blooms will not be sufficient to increase the mean summer surface water Ω_{arag} to a level where calcification is thermodynamically possible.

.

6. Conclusion

The seasonality driven summer increase in Ω_{arag} at the Antarctic ice shelf and in the Eastern Weddell Gyre (EWG) is critical for the survival of the aragonite-calcifying Thecosome Pteropods. Winter upwelling of DIC-rich WDW water combined with low winter primary production will likely hasten the onset of surface water aragonite undersaturation as predicted by McNeil and Matear (2008). High latitude oceanic regions such as the Antarctic ice shelf and the Eastern Weddell Gyre of the Southern Ocean will probably experience periodic surface water aragonite undersaturation within this century, possibly as early as the year 2054.

Natural seasonal variations in Ω_{arag} at the ice shelf and in the EWG were primarily as a result of changes in DIC through primary production and in TA through dilution from sea ice melt, both of which were affected by variability in the phasing of sea ice thaw. The intra-seasonal and inter-seasonal variability in Ω_{arag} was much greater at the ice shelf than in the EWG (Figure 32), indicating the sensitivity of the Antarctic ice shelf to seasonal variations in Ω_{arag}. Summer sea ice melt increased surface water stratification, relieving light and iron limitation and facilitating summer phytoplankton blooms and thus the summer increase in Ω_{arag}. Years with early sea ice melt at the ice shelf resulted in increased production and increased surface water Ω_{arag}. The opposite was observed for years with late sea ice melt, where production was decreased and the summer surface water Ω_{arag} increase was less. The summer increase in Ω_{arag} was observed to reach a maximum in all years during late January/early February when primary production was highest. All years showed an increase in surface water Ω_{arag} at the ice shelf as summer progressed, from a winter value of 1.34 to an overall mean early February value of 1.69 (Figure 33). Primary production decreased DIC, increasing Ω_{arag}, while dilution through summer sea ice melt decreased TA, decreasing Ω_{arag}, but to a lesser extent. The high interannual variability in Ω_{arag} at the ice shelf, highlights the importance of understanding regional scale carbon processes and how they are affected by the seasonal cycle.

Ecosystem implications of the seasonal minimum Ω_{arag} will likely be felt before aragonite undersaturation ($\Omega_{arag} < 1$) is reached. Calcification rates have previously been shown to have a positive correlation with increased [CO_3^{2-}] and a negative correlation with decreased [CO_3^{2-}

], suggesting that as [CO_3^{2-}] decreases, calcification will become increasingly difficult and could negatively affect calcifiers and ecosystems even before undersaturation is reached (Fabry et al, 2008; Riebesell et al., 2000; Royal-Society, 2005). Winter and early summer surface water Ω_{arag} were between 1.16-1.33, suggesting that small changes in the processes that control surface water Ω_{arag} (primary production, dilution, air-sea CO_2 flux and calcification) may result in periodic surface water aragonite undersaturation, with unknown consequences for the Thecosome Pteropods. Increased research is needed to determine if the Antarctic Thecosome Pteropods will be able to adapt to decreasing surface water Ω_{arag} or if they will migrate northwards to waters where Ω_{arag} is higher, with serious consequences for their predators and for the ecosystem (Fabry et al., 2008; McNeil and Matear, 2008).

This study shows that the summer surface water Ω_{arag} at the Eastern Weddell Gyre ice shelf will probably become periodically undersaturated with aragonite by the middle of this century, reinforcing model predictions by Orr et al (2005) and McNeil and Matear (2008). Periodic surface water aragonite undersaturation will be of serious concern for the Thecosome Pteropods that survive for 1-2 years and would therefore need to survive undersaturated wintertime conditions (Hunt et al., 2008). Pteropods are not only important in the trophic structure, but also in the export flux of carbon from surface to deeper waters (Honjo, 2004). The possible northward migration or decrease of pteropods at the ice shelf and in the EWG as Ω_{arag} decreases is predicted to affect the natural balance of the marine food web as well as the air-sea carbon flux, and is therefore a great concern.

Seasonality of the timing of sea ice melt, primary production, and upwelling processes at the Antarctic ice shelf and EWG are all of critical importance to pteropods and to the Antarctic ecosystem. There is a need for a more thorough understanding of the seasonal variability of this region, where detrimental carbonate conditions are likely to affect the ecosystem within the next few decades.

7. References

Abbasi, T. and Abbasi, S. A. (2011). Ocean Acidification: The Newest Threat to the Global Environment. *Critical Reviews in Environmental Science and Technology*, 41(18): 1601–1663.

Anderson, L. A. and Sarmiento, J. L. (1994). Redfeld ratios of remineralization determined by nutrient data analysis. *Global Biogeochemical Cycles*, 8(1): 65–80.

Andres, R. J., Fielding, D. J., Marland, G., Boden, T. A., Kumar, N. and Kearney, A. T. (1999). Carbon dioxide emissions from fossil-fuel use. *Tellus*, Ser. B, 51: 759–765.

Armstrong, J. L., Boldt, J. L., Cross, A. D., Moss, J. H., Davis, N. D., Myers, K. W., Walker, R. V., Beauchamp, D. A. and Haldorson, L. J. (2005). Distribution, size, and interannual, seasonal and diel food habits of northern Gulf of Alaska juvenile pink salmon, *Oncorhynchus gorbuscha*. *Deep Sea Research II*, 52: 247–265.

Arrhenius, S. (1896). On the infuence of carbonic acid in the air upon the temperature of the ground. *Philosophical Magazine and Journal of Science Series*, 5(41): 237–276.

Arrigo, K. R. (2005). Marine microorganisms and global nutrient cycles. *Nature*, 437: 349–55.

Arrigo, K. R. and Van Dijken, G. L. (2007). Interannual variation in air–sea CO_2 flux in the Ross Sea, Antarctica: a model analysis. *Journal of Geophysical Research*, 112: C03020, doi:10.1029/2006JC003492.

Arrigo, K. R., Van Dijken, G. L. and Bushinsky, S. (2008). Primary production in the Southern Ocean, 1997–2006, *Journal of Geophysical Research*, 113, C08004, doi:10.1029/2007JC004551.

Atkinson, A., Siegel, V., Pakhomov, E. and Rothery, P. (2004). Long-term decline in krill stock and increase in salps within the Southern Ocean. *Nature*, 432: 100–103.

Bakker, D. C E., De Baar, H. J. W. and Bathmann, U. V. (1997). Changes of carbon dioxide in surface waters during spring in the Southern Ocean. *Deep-Sea Research Part II*. 44: 91–127.

Bakker, D. C. E., Hoppema, M., Schröder, M., Geibert, W. and de Baar, H. J. W. (2008). A rapid transition from ice covered CO_2-rich waters to a biologically mediated CO_2 sink in the eastern Weddell Gyre. *Biogeosciences*. 5: 1205–1235.

Barker, S. and Elderfield, H. (2002). Foraminiferal calcification response to glacial-interglacial changes in atmospheric CO_2. *Science*, 297: 833–836.

Barker, S. and Ridgwell, A. (2012). Ocean Acidification. *Nature Education Knowledge*, 3(10): 21

Bednaršek, N., G. A. Tarling, D. C. E. Bakker, S. Fielding, E. M. Jones, H. J. Venables, P. Ward, A. Kuzirian, B. Lézé, and E. J. Murphy (2012a), Extensive dissolution of live pteropods in the Southern Ocean, *Nature Geoscience*, DOI: 10.1038/NGEO1635

Behrenfeld, M.J., O'Malley, R. T., Siegel, D. A., McClain, C. R., Sarmiento, J. L., Feldman, G. C., Milligan, A. J., Falkowski, P. G., Letelier, R. M. and Boss, E. S. (2006). Climate-driven trends in contemporary ocean productivity. *Nature*, 444: 752– 755.

Betts, R. A., Collins, M., Hemming, D. L., Jones, C. D., Lowe, J. A. and Sanderson, M. G. (2011). When could global warming reach 4◦C? *Philosophical Transactions of the Royal Society,* A 369: 67–84.

Brierley, A. S., Fernandes, P. G., Brandon, M. A., Armstrong, N. W., Mcphail, S .D., Stevenson, P., Pebody, M., Perrett, J., Squires, M., Bone, D. G. and Griffiths, G. (2002). Antarctic krill under sea ice: elevated Abundance in a narrow band just south of ice edge. *Science,* 295: 1890–1892.

Caldeira, K. and M. E. Wickett. (2003). Anthropogenic carbon and ocean pH. *Nature,* 425(6956): 365.

Callendar, G. (1938). The artificial production of carbon dioxide and its influence on temperature. *Quarterly Journal of the Royal Meteorological Society,* 64(275): 223–240.

Canadell, J. G., Le Quéré, C., Raupacha, M. R., Fielde, C. B., Buitenhuisc, E. T., Ciaisf, P., Conwayg, T. J., Gillettc, N. P., Houghtonh, R. A. and Marland, G. (2007). Contributions to accelerating atmospheric CO_2 growth from economic activity, carbon intensity, and efficiency of natural sinks. *Proceedings of the National Academy of Sciences USA,* 104(47): 18866–18870.

Carmack, E.C. (1977). Water characteristics of the Southern Ocean south of the Polar Front. In: Angel. M. (Ed.). A Voyage of Discovery, *Deep-Sea Research*, 24 (Supplementary).

Carmack, E. C. and Foster. T. D. (1975). On the flow of water out of the Weddell Sea. *Deep-Sea Research*. 22: 711–724.

Carmack, E.C. and Foster, T.D. (1977). Water masses and circulation in the Weddell Sea. In: *Polar Oceans, Proceedings of the Polar Oceans Conference, Montreal, 1974.* Dunbar, M.J. (Ed.). Arctic Institute of North America, Calgary, Canada: 151–165.

Comeau, S., Gorsky, G., Jeffree, R., Teyssie´, J. L. and Gattuso, J. P. (2009). Impact of ocean acidification on a key Arctic pelagic mollusc (*Limacina helicina*). *Biogeosciences,* 6: 1877–1882.

Comeau, S., Jeffree. R., Teyssie´, J. L., and Gattuso, J. P. (2010). Response of the Arctic Pteropod *Limacina helicina* to Projected Future Environmental Conditions. *PLoS ONE,* 5(6), e11362, doi:10.1371/journal.pone.0011362.

Deacon, G. E. R. (1937). The hydrology of the southern ocean. *Discovery Reports,* 15: 1-124.

Deacon, G. E. R. (1979). The Weddell Gyre. *Deep-Sea Research,* 26A: 981– 995.

Dickson, A. G. (1981). An exact definition of total alkalinity and a procedure for the estimation of alkalinity and total inorganic carbon from titration data. *Deep Sea Research Part A Oceanographic Research Papers,* 28(6): 609–623.

Dickson, A. G. and Millero, F. J. (1987). A comparison of the equilibrium constants for the dissociation of carbonic acid in seawater media. *Deep Sea Research*. 34: 1733–1743.

Dieckmann, G. S., Nehrke, G., Papadimitriou, S., Göttlicher, J., Steininger, R., Kennedy, H., Wolf-Gladrow, D. and Thomas, D. N. (2008). Calcium carbonate as ikaite crystals in Antarctic sea Ice. *Geophysical Research Letters,* 35, L08501, doi:10.1029/2008GL033540.

Dieckmann, G. S., Nehrke, G., Uhlig, C., Göttlicher, J., Gerland, S., Granskog, M. A. and Thomas, D. N. (2010). Brief Communication: Ikaite ($CaCO_3 \cdot 6H_2O$) discovered in Arctic sea ice,

The Cryosphere, 4: 227–230.

Doney, S. C. (2006). The dangers of ocean acidification. *Scientific American*, 294: 58–65.

Doney, S. C., Fabry, V. J., Feely, R. A. and Kleypas, J. (2009). Ocean Acidification: The Other CO_2 Problem. *Annual Review of Marine Science*, 1(1): 169–192.

Egleston, E. S., Sabine, C. L. and Morel, F. M. (2010). Revelle revisited: Buffer factors that quantify the response of ocean chemistry to changes in DIC and alkalinity. *Global Biogeochemical Cycles*, 24(1), GB1002.

Fabry, V. J., Seibel, B. A., Feely, R. A. And Orr, J. C. (2008). Impacts of ocean acidification on marine fauna and ecosystem processes. *ICES Journal of Marine Science*, 65: 414–432.

Feely, R. A., Sabine, C. L., Lee, K., Berelson, W., Kleypas, J., Fabry, V. J. and Millero, F. J. (2004). Impact of anthropogenic CO_2 on the $CaCO_3$ system in the ocean, *Science*, 305: 362–366.

Fetterer, Florence, K. Knowles, W. Meier, and M. Savoie. 2002, updated 2009. *Sea Ice Index*. [December and January 2008-2012]. Boulder, Colorado USA: National Snow and Ice Data Center.

Foldvik, A., Gammelsrod, T. and Torresen, T. (1985). Circulation and water masses on the southern Weddell Sea shelf. In: Jacobs, S.S. (Ed.). *Oceanology of the Antarctic Continental Shelf, Antarctic Research Series*. Washington, DC: American Geophysical Union. 43: 5 – 20.

Foster, T. D. and Carmack, E. C. (1976)a. Frontal mixing zone and Antarctic Bottom Water formation in the southern Weddell Sea. *Deep Sea Research.* 23: 301-317.

Foster, T. D. and Carmack, E. C. (1976)b. Temperature and Salinity Structure in the Weddell Sea. *Journal of Physical Oceanography.* 6: 36-44.

Frajka-Williams, E., Rhines, P. B. and Eriksen, C. C. (2009). Physical controls and mesoscale variability in the Labrador Sea spring phytoplankton bloom observed by Seaglider. *Deep Sea Research Part I: Oceanographic Research Papers*, *56*(12): 2144-2161.

Friedli, H., Lötscher, H., Oeschger, H Siegenthaler, U. and Stauffer, B. (1986). Ice core record of the C13/C12 ratio of atmospheric CO_2 in the past two centuries. *Nature*, 324: 237–238.

Friis, K., Kortzinger, A. and Wallace, D. W. R. (2003). The salinity normalization of marine inorganic carbon chemistry data, *Geophysical Research Letters*, 30(2), 1085, doi:10.1029/2002GL015898.

Geibert, W., Assmy, P., Bakker, D. C. E., Hanfland, C., Hoppema, M., Pichevin, L. E., Schröder, M., Schwarz, J. N., Stimac, I., Usbeck, R. and Webb, A. (2010). High productivity in an ice melting hot spot at the eastern boundary of the Weddell Gyre. *Global Biogeochemical Cycles*. 24, GB3007, doi:10.1029/2009GB003657.

Gibson, J. A. E. and Trull, T. (1999). Annual cycle of fCO_2 under sea-ice and in open ocean water in Prydz Bay, East Antarctica. *Marine Chemistry*. 66: 187–200.

Giddy, I. S., Swart, S. and Tagliabue, A. (2012). Drivers of non-Redfield nutrient utilization in the Atlantic sector of the Southern Ocean. *Geophysical Research Letters*, 39, L17604, doi:10.1029/2012GL052454.

Gloor, M., Gruber, N., Sarmiento, J. L., Sabine, C. L., Feely, R. A. and Roedenbeck, C. (2003). A first estimate of present and pre-industrial air-sea CO_2 fluxes patterns based on ocean interior carbon measurements and models, *Geophysical Research Letters*, 30(1), 1010, 10.1029/2002GL015594.

Goldman, J. C. and Brewer, P. G. (1980). Effect of nitrogen source and growth rate on phytoplankton-mediated changes in alkalinity. *Limnology and Oceanography*, 352-357.

Gordon, A. L. (1981). Seasonality of Southern Ocean sea ice. *Journal of Geophysical Research*, 86: 4193-4197.

Gordon, A. L. and Huber, B. L. (1984). Thermohaline stratification below the Southern Ocean sea ice. *Journal of Geophysical Research*, 89: 641–648.

Gordon, A.L. and Huber, B.A. (1990). Southern Ocean winter mixed layer. *Journal of Geophysical Research*. 95(C7): 11 655–11 672.

Gordon, A. L. and Huber, B. L. (1995). Warm Weddell deep water west of Maud Rise. *Journal of Geophysical Research*, 100: 13747–13753.

Gordon, A. L., Chen, C. T. A. and Metcalf, W. G. (1984). Winter Mixed Layer Entrainment of Weddell Deep Water. *Journal of Geophysical Research*, 89: 637-640.

Grasshoff, K.M., Ehrhardt, M., Kremling, K. (1983). Determination of urea (9.5). In: *Methods of seawater analysis*, 2nd edition. Verlag Chemie, Wienheim, Germany. pp. 158-162.

Griffiths, H. (2010) Antarctic Marine Biodiversity – What Do We Know About the Distribution of Life in the Southern Ocean? *PLoS ONE*, 5: e11683. doi:10.1371/journal.pone.0011683.

Gruber, N. (2011). Warming up, turning sour, losing breath: ocean biogeochemistry under global change. *Philosophical Transactions of the Royal Society A* 369: 1980–1996.

Guinotte, J. M. and Fabry, V. J. (2008). Ocean acidification and its potential effects on marine ecosystems. *Annals of the New York Academy of Sciences*, 1134: 320–342.

Hauck, J., Hoppema, M., Bellerby, R. G. J., Völker, C. and Wolf-Gladrow, D. (2010). Data- based estimation of anthropogenic carbon and acidification in the Weddell Sea on a decadal time scale. *Journal of Geophysical Research*, 115, C03004, doi:10.1029/2009JC005479.

Held, I. M. and Soden, B. J. (2000). Water Vapor Feedback and Global Warming. *Annual Review of Energy and the Environment*, 25(1): 441–475.

Hönisch, B., Hemming, N. G., Archer, D., Siddall, M, and McManus, J. F., (2009). Atmospheric carbon dioxide concentration across the mid-Pleistocene transition. *Science*, 324: 1551–1554.

Honjo, S. (2004). Particle export and the biological pump in the Southern Ocean. *Antarctic Science*, 16: 501–516.

Hoppema, M. (2004). Weddell Sea turned from source to sink for atmospheric CO_2 between pre-industrial time and present. *Global and Planetary Change*. 40: 219–231.

Hoppema, M., De Baar, H. J. W., Bellerby, R. G. J., Fahrbach, E. and Bakker, K. (2002). Annual export production in the interior Weddell Gyre estimated from a chemical mass balance of nutrients. *Deep-Sea Research Part II*, 49: 1675–1689.

Hoppema, M., Fahrbach, E., Schröder, M., Wisotzki, A. and De Baar, H. J. W. (1995). Winter – summer differences of carbon dioxide and oxygen in the Weddell Sea surface layer. *Marine Chemistry*, 51: 177–192.

Hoppema, M., Stoll, M. H. C. and De Baar, H. J. W. (2000). CO_2 in the Weddell Gyre and Antarctic Circumpolar Current: Austral autumn and early winter. *Marine Chemistry*, 72: 203–220.

Hunt, B. P. V., Pakhomov, E. A., Hosie, G. W., Siegel, V., Ward, P. and Bernard, K. (2008). Pteropods in Southern Ocean ecosystems, *Progress in oceanography*, 78(2): 193–221.

Hunt, B. P. V., Strugnell, J., Bednarsek, N., Linse, K., Nelson, R. J., Pakhomov, E., Seibel, B., Steinke, D. and Würzberg, L. (2010). Poles Apart: The ‘‘Bipolar’’ Pteropod species *Limacina helicina* is genetically distinct between the Arctic and Antarctic Oceans. *PLoS ONE*, 5(3): e9835. doi:10.1371/journal.pone.0009835.

Iglesias-Rodríguez, M. D., Brown, C. W., Doney, S. C., Kleypas, J., Kolber, D., Kolber, Z. and Falkowski, P. (2002). Representing key phytoplankton functional groups in ocean carbon cycle models: Coccolithophorids. *Global Biogeochemical Cycles*, 16(4): 1100, doi:10.1029/ 2001GB001454.

Iglesias- Rodríguez, M. D., Halloran, P. R., Rickaby, R. E. M., Hall, I. R., Colmenero-Hidalgo, E., Gittins, J. R., Green, D. R. H., Tyrrell, T., Gibbs, S. J., von Dassow, P., Rehm, E., Armbrust, E. V. and Boessenkoo, K. P. (2008). Phytoplankton calcification in a high CO_2 world. *Science* 320: 336–39.

IPCC (2007). Contribution of Working Groups I, II and III to the Fourth Assessment Report of the Intergovernmental Panel on Climate Change. In Core Writing Team, Pachauri, R. and Reisinger, A. editors, *IPCC Fourth Assessment Report*, number November, page 104. Geneva, Switzerland.
Jones, E. M., Bakker, D. C., Venables, H. J. and Watson, A. J. (2012). Dynamic seasonal cycling of inorganic carbon downstream of South Georgia, Southern Ocean. *Deep Sea Research Part II: Topical Studies in Oceanography*, *59*: 25-35.

Jones, E. M., Bakker, D. C. E., Venables, H. J., Whitehouse, M. J., Korb, R. E. and Watson, A .J. (2010). Rapid changes in surface water carbonate chemistry during Antarctic sea ice melt. *Tellus*, 62(B): 621–635.

Karnovsky, N. J., Hobson, K. A., Iverson, S. and Hunt, G. L. (2008). Seasonal changes in diets of seabirds in the North Water Polynya: a multiple-indicator approach. *Marine ecology progress series*, 357: 291–299.

Keeling, C. D., Whorf, T. P., Wahlen, M. and Van der Plicht, J. (1995). Interannual extremes in the rate of rise of atmospheric carbon dioxide since 1980. *Nature*, 375: 666–670.

Key, R. M. A., Kozyr, A., Sabine, C. L., Lee, K., Wanninkhof, R., Bullister, J. L., Feely, R. A., Millero, F. J., Mordy, C. and Peng, T.-H. (2004). A global ocean carbon climatology: results from Global Data Analysis Project (GLODAP). *Global Biogeochemical Cycles*, 18: 4031. doi:10.1029/ 2004GB002247.

Kimura, N. and Wakatsuchi, M. (2011). Large-scale processes governing the seasonal variability of the Antarctic sea ice. *Tellus A,* 63(4): 828-840.

Kobayashi, H. A. (1974). Growth cycle and related vertical distribution of the thecosomatous pteropod Spiratella "*Limacina*" *helicina* in the central Arctic Ocean. *Marine Biology,* 26: 295–-301.

Le Quéré, C., Raupach, M. R., Canadell, J. G., Marland, G., Bopp, L., Ciais, P., Conway, T. J., Doney, S. C., Feely, R. A., Foster, P., Friedlingstein, P., Gurney, K., Houghton, R. A., House, J. I., Huntingford, Chris., Levy, P. E., Lomas, M. R., Majkut, J., Metzl, N., Ometto, J. P., Peters, G. P., Prentice, I. C., Randerson, J. T., Running, S. W., Sarmiento, J. L., Schuster, U., Sitch. S., Takahashi, T., Viovy, N., van der Werf, G. R. and Woodward, F. I. (2009). Trends in the sources and sinks of carbon dioxide. *Nature Geosciences,* 2: 831–836.

Le Quéré, C., Rödenbeck, C., Buitenhuis, E. T., Conway, T. J., Langenfelds, R., Gomez, A., Labuschhagne, C., Ramonet, M., Nakazawa, T., Metzl, N., Gillett, N. and Heimann, M. (2007). Saturation of the Southern Ocean CO_2 Sink Due to Recent Climate Change. *Science.* 316: 1735–1738.

Lee, K., Tong, L. T., Millero, F. J., Sabine, C. L., Dickson, A. G., Goyet, C., Park, G. H., Wanninkhof, R., Feely, R. A. and Key, R. M. (2006). Global relationships of total alkalinity with salinity and temperature in surface waters of the world's oceans, *Geophysical Research Letters*, 33, L19605, doi:10.1029/2006GL027207.

Lenton, A., Metzl, N., Takahashi, T., Kuchinke M., Matear R. J., Roy T. and, Stewart C. (2012). Sutherland, Colm Sweeney, and Bronte Tilbrook. "The observed evolution of oceanic pCO_2 and its drivers over the last two decades." *Global Biogeochemical Cycles* 26(2): GB2021.

Lewis, E. And D.W.R. Wallace. (1998). CO2SYS-Program developed for the CO_2 system calculations. *Carbon Dioxide Information and Analysis Centre*. Report ORNL/CDIAC-105.

Lovenduski, N. S., Gruber, N., Doney, S. C. and Lima, I. D. (2007). Enhanced CO_2 outgassing in the Southern Ocean from a positive phase of the Southern Annular Mode. *Global Biogeochemical Cycles* 21, GB2026, doi:10.1029/2006GB002900.

Martin, J. H. (1990). Glacial-interglacial CO_2 change: The iron hypothesis. *Paleoceanography*, *5*(1): 1-13.

Maykut, G. A. (1985). The ice environment. In *Sea ice biota,* R. A. Horner, editor, pages 21-82. CRC press, Florida.

McNeil, B. I. and Matear, R. J. (2007). Climate change feedbacks on future oceanic acidification. *Tellus*, 59(B): 191–198.

McNeil, B. I. and Matear, R. J. (2008). Southern Ocean acidification : A tipping point at 450-ppm atmospheric CO_2. *PNAS*, 105(48): 18860–18864.

McNeil, B. I., Metzl, N., Key, R. M., Matear, R. J. and Corbiere, A. (2007). An empirical estimate of the Southern Ocean air-sea CO_2 flux. *Global Biogeochem Cycles,* 21, GB3011, doi:10.1029/ 2007GB002991.

Mehrbach, C., Culberson, C. H., Hawley, J. E. and Pytkowicz, R. M. (1973). Measurement of the apparent dissociation constants of carbonic acid in seawater at atmospheric pressure. *Limnology and Oceanography*, 18: 897–907.

Metzl, N., Brunet, C., Jabaud-Jan, A., Poisson, A. and Schauer, B. (2006). Summer and winter air–sea CO_2 fluxes in the Southern Ocean. *Deep-Sea Research*. I53: 1548–1563.

Millero, F. J., Graham, T. B., Huang, F., Bustos-Serrano, H. and Pierrot, D. (2006). Dissociation constants of carbonic acid in seawater as a function of salinity and temperature. *Marine Chemistry*, 100(1-2): 80–94.

Millero, F. J., Lee, K. and Roche, M. (1998). Distribution of alkalinity in the surface waters of the major oceans. *Marine Chemistry*, 60: 111 –130.

Monteiro, P. M. S., Schuster, U., Hood, M., Lenton, A., Metzl, N., Olsen, A., Rogers, K., Sabine, C., Takahashi, T., Tilbrook, B., Yoder, J., Wanninkhof, R. and Watson, A. J. (2010). A global sea surface carbon observing system: Assessment of changing sea surface CO_2 and air-sea CO_2 fluxes, in Proceedings of the *OceanObs'09*: *Sustained Ocean Observations and Information for Society* Conference, Venice, Italy, 21–25 September 2009, edited by J. Hall, D. E. Harrison, and D. Stammer, ESA Publishers, WPP-306, pp. XX–XX, European Space Agency, Paris.

Mosby, H.A. (1934). The waters of the Atlantic Antarctic Ocean. *Scientific Results of the Norwegian Antarctic Expedition 1927–1928*, 11: 1–131.

Mucci, A. (1983). The solubility of calcite and aragonite in seawater at various salinities, temperatures, and one atmosphere total pressure. *American Journal of Science*, 283: 780–99.

Nicholls, R. J., Marinova, N., Lowe, J. A., Brown, S., Vellinga, P., de Gusmão, D., Hinkel, J. and Tol, R. S. J. (2011). Sea-level rise and its possible impacts given a 'beyond 4°C world' in the twenty-first century. *Philosophical Transactions of the Royal Society*, *A* 369: 161–181.

Orr, J. C., Fabry, V. J., Aumont, O., Bopp, L., Doney, S. C., Feely, R. A., Gnanadesikan, A., Gruber, N., Ishida, A., Joos, F., Key, R. M., Lindsay, K., Maier-Reimer, E., Matear, R., Monfray, P., Mouchet, A., Najjar, R. G., Plattner, G.-K., Rodgers, K. B., Sabine, C. L., Sarmiento, J. L., Schlitzer, R., Slater, R. D., Totterdell, I. J., Weirig, M.-F., Yamanaka, Y. and Yool, A. (2005). Anthropogenic ocean acidification over the twenty-first century and its impact on calcifying organisms. *Nature*, 437(7059): 681–686.

Orsi, A. H., Nowlin Jr, W. D. and Whitworth III, T. (1993). On the circulation and stratification of the Weddell Gyre. *Deep-Sea Research I*, 40: 169-203.

Petit, J. R., Jouzel, J., Raynaud, D., Barkov, N. I., Barnola, J.-M., Basile, I., Bender, M., Chappellaz, J., Davisk, M., Delaygue, G., Delmotte, M., Kotlyakov, V. M., Legrand, M., Lipenkov, V. Y., Lorius, C., Pépin, L., Ritz, C., Saltzmank, E. and Stievenard, M. (1999). Climate and atmospheric history of the past 420,000 years from the Vostok ice core, Antarctica. *Nature*, 399: 429–436.

Pierrot, D., C. Neill, K. Sullivan, R. Castle, R. Wanninkhof, H. Lüger, T. Johannessen, A. Olsen, R.A. Feely and C.E. Cosca. (2009). Recommendations for autonomous underway pCO2 measuring systems and data reduction routines. *Deep-Sea Research Il.* 56: 512–522.

Redfield, A. C., Ketchum, B. H. and Richards, F. A. (1963). The influence of organisms on the compostion of seawater. In Hill, M. N., editor, *The Sea*, volume 2, pages 26-77. John Wiley and Sons.

Revelle, R. (1985). Introduction: The scientific history of Carbon Dioxide. In *The carbon cycle and atmospheric CO_2: natural variations Archean to present*, volume 1, pages 1-4.

Revelle, R. and Suess, H. (1957). Carbon dioxide exchange between atmosphere and ocean and the question of an increase of atmospheric CO_2 during the past decades. *Tellus*, 9(1): 18–27.

Riebesell, U., Zondervan, I., Rost, B., Tortell, P. D., Zeebe, R. E. and Morel, F. M. (2000). Reduced calcification of marine plankton in response to increased atmospheric CO_2. *Nature*, 407(6802): 364–7.

Roleda, M. Y., Boyd, P. W., and Hurd, C. L. (2012). Before Ocean Acidification: calcifier chemistry lessons1. *Journal of Phycology*, *48*(4): 840-843.

Rost, B and Riebesell, U. (2004). Coccolithophores and the biological pump: responses to environmental changes. In Thierstein, H. R, and Young, J. R., editors, *Coccolithophores—From Molecular Processes to Global Impact*, pages 76-99, Springer.

Royal-Society (2005). Ocean acidification due to increasing atmospheric carbon dioxide. *London: The Royal Society*, page 223 pp.

Rysgaard, S., Glud, R. N., Lennert, K., Cooper, M., Halden, N., Leakey, R. J. G., Hawthorne, F. C. and Barber, D. (2012) Ikaite crystals in melting sea ice – implications for *p*CO2 and pH levels in Arctic surface waters. *The Cryosphere Discuss*ions, 6: 1015–1035.

Sabine, C. L., Feely, R. A., Gruber, N., Key, R. M., Lee, K., Bullister, J., Wanninkhof, R., Wong, C. S., Wallace, D. W. R., Tilbrook, B., Millero, F. J., Peng, T.-H., Kozyr, A., Ono, T. and Rios, A. F. (2004). The oceanic sink for anthropogenic CO_2. *Science*, 305: 367–371.

Sackmann, B. S., Perry, M. J. and Eriksen, C. C. (2008). Seaglider observations of variability in daytime fluorescence quenching of chlorophyll-*a* in Northeastern Pacific coastal waters. *Biogeosciences Discussions*, *5*: 2839-2865.

Sarmiento, J. L. and Gruber, N. (2006). Ocean Biogeochemical Dynamics. Princeton University Press, Princeton.

Schiebel, R. (2002). Planktic foraminiferal sedimentation and the marine calcite budget. *Global Biogeochemical Cycles*, 16(4), 1065, doi:10.1029/2001GB001459.

Schlitzer, R. (2002). Carbon export fluxes in the Southern Ocean: results from inverse modelling and comparison with satellite-based estimates, *Deep-Sea Research Part II*, 49: 1623–1644.

Schmitz Jr, W. J. (1995). On the interbasin-scale thermohaline circulation. *Reviews of Geophysics*, 33: 151-173.

Schröder, M. and Fahrbach, E. (1999). On the structure and the transport of the eastern Weddell Gyre. *Deep-Sea Research Part II*, 46: 501–527.

Seibel, B. A. and Dierssen, H. M. (2003). Cascading trophic impacts of reduced biomass in the Ross Sea, Antarctica: Just the tip of the iceberg? *The Biological Bulletin*, 205(2): 93–97.

Seibel, B. A., Maas, A. E. and Dierssen, H. M. (2012). Energetic plasticity underlies a variable response to ocean acidification in the pteropod, *Limacina helicina Antarctica. PLoS ONE*, 7(4): e30464. doi:10.1371/journal.pone.0030464.

Shi, J., Cheng, Y., Jiao, Y. And Hou, J. (2011). Supercooled water in austral summer in Prydz Bay, Antarctica. *Chinese Journal of Oceanology and Limnology*, *29*(2): 427-437.

Siegenthaler, U. and Sarmiento, J. L. (1993). Atmospheric carbon dioxide and the ocean. *Nature*, 365: 119–125.

Sigman, D. M. and Boyle, E. A. (2000). Global/interglacial variations in atmospheric carbon dioxide. *Hemisphere*, 407(October): 859–869.

Smetacek, V. and Nicol, S. (2005). Polar ecosystems in a changing world. *Nature*, 437: 362–368.

Smith, W. O. and Nelson, D. M. (1986). Importance of ice edge phytoplankton production in the Southern Ocean. *Biogeosciences*, 36: 251–257.

Steinacher, M., Joos, F., Frölicher, T. L., Plattner, G.-K. and Doney, S. C. (2009). Imminent ocean acidification in the Arctic projected with the NCAR global coupled carbon cycle-climate model, *Biogeosciences*, 6: 515–533.

Steinacher, M., Joos, F., Frölicher, T. L., Bopp, L., Cadule, P., Cocco, V., Doney, S. C., Gehlen, M., Lindsay, K., Moore, J. K., Schneider, B. and Segschneider, J. (2010). Projected 21st century decrease in marine productivity: a multi-model analysis. *Biogeosciences* 7: 979–1005.

Sweeney, C. (2003). The annual cycle of surface water CO_2 and O_2 in the Ross Sea: A model for gas exchange on the continental shelves of Antarctica. In Dunbar, R. and DiTullio, G., editors, *Biogeochemistry of the Ross Sea, Antarctic Research Ser*ies, volume 78, pages 295– 312, AGU, Washington, D. C.

Takahashi, T., Broecker, W. S. and Langer, G. (1985). No Title. *Journal of Geophysical Research1*, 90: 6907–6924.

Takahashi, T., Olafsson, J., Goddard, J. G., Chipman, D. W. and Sutherland, S. C. (1993). Seasonal variation of CO_2 and nutrients in the high-latitude surface oceans: A comparative study. *Global Biogeochemical Cycles*, 7(4): 843–878.

Takahashi, T., Sutherland, S. C., Sweeney, C., Poisson, A., Metzl, N., Tilbrook, B., Bates, N. R., Wanninkhof, R., Feely, R. A., Sabine, C. L. and Others (2002). Global sea-air CO_2 flux based on climatological surface ocean pCO_2, and seasonal biological and temperature effects. *Deep Sea Research Part II: Topical Studies in Oceanography*, 49(9-10): 1601–1622.

Takahashi, T., Sutherland, S. C., Wanninkhof, R., Sweeney, C., Feely, R. A., Chipman, D. W., Hales, B., Friederich, G. E., Chavez, F., Sabine, C. L., Watson, A., Bakker, D. C. E., Schuster, U., Metzl, N., Yoshikawa-Inoue, H., Ishii, M., Midorikawa, T., Nojiri, Y., Kortzinger, A., Steinho_, T., Hoppema, M., Olafsson, J., Arnarson, T. S., Tilbrook, B., Johannessen, T., Olsen, A., Bellerby, R. G. J., Wong, C. S., Delille, B., Bates, N. R. and De Baar, H. J. W. (2009). Climatological mean and decadal change in surface ocean pCO_2, and net sea-air CO_2 flux over the global oceans. *Deep Sea Research Part II: Topical Studies in Oceanography*, 56(8-10): 554–577.

Tans, P. and Keeling, C. D. (2011). Trends in Atmospheric Carbon Dioxide. NOAA/ESRL and Scripps Institute of Oceanography, page http://www.esrl.noaa.gov/gmd/ccgg/trends/.

Thomalla, S. J., Fauchereau, N., Swart, S., and Monteiro, P. M. S. (2011). Regional scale characteristics of the seasonal cycle of chlorophyll in the Southern Ocean. *Biogeosciences*, 8: 2849–2866.

Thomas, D. N. and Dieckmann, G. S. (2010). *Sea Ice, 2nd edition*. Wiley-Blackwell, Oxford, U. K.

Tyndall, J. (1861). On the Absorption and Radiation of Heat by Gases and Vapours, and on the Physical Connexion of Radiation, Absorption, and Conduction. *Philosophical Transactions of the Royal Society*, 151(1861): 1–36.

Volk, T. and Hoffert, M. (1985). Ocean carbon pumps-Analysis of relative strengths and efficiencies in ocean-driven atmospheric CO_2 changes. In *The carbon cycle and atmospheric CO_2: natural variations Archean to present*, volume 1, pages 99–110.

Wanninkhof, R. and K. Thoning. (1993). Measurement of fugacity of CO_2 in surface water using continuous and discrete sampling methods. *Marine Chemistry*. 44: 189–205.

Watson, A. J. and J. C. Orr. (2003). Carbon dioxide fluxes in the global ocean. In: Fasham, M. J. R., editor, *Ocean Biogeochemistry: The Role of the Ocean Carbon Cycle in Global Change. pages* 123-144. Springer-Verlag, New York.

Weiss, R.F. (1974). Carbon dioxide in water and seawater: the solubility of a non- ideal gas. *Marine Chemistry*. 2: 203–215.

Weiss, R. and Price, B. A. (1980). Nitrous oxide solubility in water and seawater. *Marine Chemistry*, 8(4): 347–359.

Whitworth III, T. and Nowlin Jr. W. D. (1987). Water masses and currents of the Southern Ocean at the Greenwich Meridian. *Journal of Geophysical Research*. 92: 6462–6476.

Wolf-Gladrow, D., Zeebe, R. E., Klaas, C., Kortzinger, A. and Dickson, A. G. (2007). Total alkalinity: The explicit conservative expression and its application to biogeochemical processes. *Marine Chemistry*, 106(1-2): 287–300.

Yamamoto, A., Kawamiya, M., Ishida1, A., Yamanaka, Y. and Watanabe, S. (2012). Impact of rapid sea-ice reduction in the Arctic Ocean on the rate of ocean acidification. *Biogeosciences.* 9: 2365–2375.

Zeebe, R. E. (2012). History of Seawater Carbonate Chemistry, Atmospheric CO_2, and Ocean Acidification. *Annual Review of Earth and Planetary Sciences*, *40*: 141-165.

Zeebe, R. E. and Wolf-Gladrow, D. (2001). *CO_2 in seawater: equilibrium, kinetics, isotopes*, volume 65. Elsevier Science Ltd.

Zeebe, R. E., Zachos, J. C., Caldeira, K. and Tyrrell, T. (2008). Carbon emissions and acidification, *Science*, 321, 5885, doi:10.1126/science.1159124.

Ziveri, P., De bernardi, B., Baumann, K.-H., Stoll, H. M. and Mortyn, P. G. (2007). Sinking of coccolith carbonate and potential contribution to organic carbon ballasting in the deep ocean. *Deep-Sea Research Part II*, 54: 659–675.